2002

SPATIO-TEMPORAL VARIATION IN ACTIVATION INTERVALS DURING VENTRICULAR FIBRILLATION

Sachin Anil Moghe
University of Kentucky

ABSTRACT OF DISSERTATION

Sachin Anil Moghe

The Graduate School

University of Kentucky

2002

SPATIO-TEMPORAL VARIATION IN ACTIVATION INTERVALS DURING VENTRICULAR FIBRILLATION

ABSTRACT OF DISSERTATION

A dissertation submitted in partial fulfillment of the
requirements for the degree of Doctor of Philosophy in the
Graduate School
at the University of Kentucky

By
Sachin Anil Moghe

Lexington, KY

Director: Dr. Abhijit Patwardhan, Assistant Professor, Center for Biomedical Engineering
and Division of Cardiology

Lexington, KY

2002

ABSTRACT OF DISSERTATION

SPATIO-TEMPORAL VARIATION IN ACTIVATION INTERVALS DURING VENTRICULAR FIBRILLATION

Spatio-temporal variation in activation rates during ventricular fibrillation (VF) provides insight into mechanisms of sustained re-entry during VF. This study had three objectives related to spatio-temporal dynamics in activation rates during VF.

The first objective was to quantify spatio-temporal variability in activation rates, that is, in dominant frequencies, computed from epicardial electrograms recorded during VF in swine. Results showed that temporally and spatially, dominant frequencies varied as much as 20% of the mean dominant frequency, and the mean dominant frequencies increased during first 30 sec of VF. These results suggest that activation rates are non-stationary during VF.

The second objective of the study was to develop a new stimulation protocol for quantifying restitution of action potential duration (APD) by independently controlling diastolic intervals (DI). A property of cardiac cells that determines spatio-temporal variability in dominant frequencies is restitution of APD, which relates APD to the previous DI. Independent control of DI permits explicit determination of the role of

memory in restitution. Restitution functions quantified using mathematical models of activation and our stimulation protocol, showed significant hysteresis. That is, for a diastolic interval, the action potential durations were as much as 15% longer during periods when the DI were decreasing than when the DI were increasing. We verified the feasibility of implementing our protocol experimentally in isolated and perfused rat hearts with action potentials recorded using floating glass microelectrodes.

The third objective of our study was to verify that spatio-temporal variability in dominant frequencies during VF could be modified using spatially distributed pacing strength stimuli. Simulated VF was induced in 400x400 and 400x800 matrices of cells. Electrical function of cells was simulated using the Luo-Rudy model. Stimulators were arranged in the matrices such that there were 5 rows of line stimulators. Results showed that it was possible to modify activations in almost 54 % of the area and to modify spatio-temporal variability in activation during VF into a desired pattern by the use of synchronized pacing from multiple sites. These results support further exploration of distributed stimulation approach for potential improvements in defibrillation therapy.

KEYWORDS: Ventricular fibrillation, pacing, restitution, dominant frequency, time-frequency analysis.

Sachin Anil Moghe

March 20,2002

SPATIO-TEMPORAL VARIATION IN ACTIVATION INTERVALS DURING VENTRICULAR FIBRILLATION

By

Sachin Anil Moghe

Dr. Abhijit Patwardhan
(Director of Dissertation)

Dr. David Puleo
(Director of Graduate Studies)

March 20,2002

RULES FOR THE USE OF DISSERTATION

Unpublished dissertations submitted for the Doctor's degree and deposited in the University of Kentucky Library are as a rule open for inspection, but are to be used only with due regard to the rights of the authors. Bibliographical references may be noted, but quotations or summaries of parts may be published only with the permission of the author, and with the usual scholarly acknowledgements.

Extensive copying or publication of the dissertation in the whole or in part also requires the consent of the Dean of the Graduate School of the University of Kentucky.

DISSERTATION

Sachin Anil Moghe

The Graduate School
University of Kentucky
2002

SPATIO-TEMPORAL VARIATION IN ACTIVATION INTERVALS DURING VENTRICULAR FIBRILLATION

DISSERTATION

A dissertation submitted in partial fulfillment of the
requirements for the degree of Doctor of Philosophy in the
Graduate School
at the University of Kentucky

By
Sachin Anil Moghe

Lexington, Kentucky

Director: Dr. Abhijit Patwardhan, Assistant Professor, Center for Biomedical Engineering
and Division of Cardiology

Lexington, KY

2002

Acknowledgements

For all the work that led to this dissertation, I would like to thank Dr. Abhijit Patwardhan, my advisor. I began working with him in 1995 and through the past almost six and half years, it has been a wonderful and unforgettable experience. I appreciate his help in performing the elaborate animal experiments and more importantly in several of the exciting discussions we have had in the past six and half years. During these past years, his enthusiasm in the subject was always infallible. I would also like to thank Dr. Charles Knapp, Director of Center for Biomedical Engineering, for his time and advice. Next I wish to thank the other members of my Dissertation Committee, Dr. David Randall, Dr. Keith Rouch, Dr. William Abraham and the outside reader, Dr. Hassebrook, for their time.

This dissertation would not have been complete without the support of my wife, Smita Joshi. She displayed an enormous amount of courage and patience while inspiring me to complete my dissertation work, even though she had to stay in Chicago, IL (about 400 miles from Lexington) for her job while I was in Lexington, KY, during a crucial and significant part of my work. I would also like to thank, Fujian Qu, who was a Master's student in our laboratory, while I was working towards my dissertation. Fujian also provided invaluable help in performing the animal experiments.

TABLE OF CONTENTS

List of Tables

List of Figures

List of Files

MogheDis.pdf	2Mb
Movie1.avi	15Mb
Movie2.avi	15Mb
Movie3.avi	15Mb

Chapter One: Introduction

'The 2001 American Heart Association, Heart and Stroke Statistical Update' states, "While Ventricular Fibrillation is listed as the cause of relatively few deaths, the overwhelming number of sudden cardiac deaths from coronary heart disease (which are estimated at about 220,000 per year) are thought to be from ventricular fibrillation". Incidence of heart failure has increased remarkably in the United States for the past several years [Bonneux 94, Eckhardt 00, Higgins 00]. Heart failure in patients can result in two different fatal symptoms: cardiac deterioration with progressive pump failure or lethal arrhythmias [Eckhardt 00], the latter accounting for almost half of the deaths resulting from heart failure. The lethal arrhythmia is usually ventricular tachycardia degenerating into ventricular fibrillation (VF) within a short time. More often than not, the symptoms of VF are sudden and there is no prior warning. If VF is not terminated within the first few minutes of initiation, irreversible damage occurs to the heart. For individuals who survive episodes of VF, the options of preventive measure are drugs (such as Sotalol or Amiodarone) or implantable defibrillators. Drugs merely lower the chances of occurrence of VF but do not prevent or terminate VF if it occurs. On the other hand, defibrillators, either internal or external, do not lower the chances of occurrence of VF but are the best available solution to VF should one occur. Defibrillation is achieved by delivering a DC shock either across the heart or the thorax. When defibrillation therapy was first introduced almost 30 years ago, a monophasic pulse (i.e. a voltage changing in one polarity from zero to a positive value and back to zero) was used for defibrillation. Beginning 1994, biphasic waveform is widely used, which has a positive pulse for half the duration of the shock and a negative pulse for the other half duration of the shock. Improvements in shape and timing of the biphasic waveform continue to be made. However, it appears that any significant and dramatic improvement in defibrillation efficacy is not to be expected via the current methods of defibrillation shock delivery. The primary reason why defibrillation efficacy has remained largely invariant over the years is because the exact mechanisms of VF are not known. However, one characteristic that has been repeatedly observed during VF is the existence of several electrical wavefronts in the ventricles [Bayly 93, Rogers 99, Kim 97, Huang 98].

Whether these wavefronts are being spun off from a single wave within the myocardium [Karma 94] or whether they are individual waves i.e. those perpetuating from one another without a common source [Janse 95] is a question of debate and an active area of research.

In order to understand VF, it is important to understand the behavior of the activation wavefronts during VF. Activation wavefronts are electrical waves that travel in the heart. During sinus rhythm the activation wave is a one large electrical wave and therefore can be easily identified with an electrode placed at any point on the ventricle. During ventricular tachycardia the activation waves take the form of a reentrant wave. At any given time during tachycardia there may be one or more but not several reentrant waves. These reentrant waves, also known as spiral waves can be quite easily observed using optical mapping studies or epicardial electrodes, which record a sharp negative signal when an activation wave passes underneath it. The time instance at which the rate of change of voltage reaches a peak negative value is called the activation time and the interval between two such activation times is the activation interval (AI). The variability in activation intervals is a good indicator of how uniform the activations are in the tissue. This is evident by observing that the activation intervals during sinus rhythm are more or less constant over long periods of time and also over a large part of the ventricle. The spiral reentrant waves have a central core, which is excitable but is not excited; they also have a tail whose curvature depends on several factors. More importantly, activations recorded from various electrodes that lie at different locations within the spiral wavefront exhibit vastly different patterns depending on their location. In other words, the shape of the activations and the activation intervals reveal a lot of information about the underlying electrical activity. That is perhaps the reason why variability in activation intervals has been widely used to study VF also. Although several parameters viz. number of wavefronts, wavefront propagation velocity, area occupied with the wavefronts, and activation intervals have been used to quantify the behavior of VF, an overwhelmingly large number of studies use change in the activation intervals over time and space to study VF. For instance, change in mean activation interval was used as a measure to gain insight into maintenance of wavefronts during Procainamide induced VF [Kim 99], whereas, dominant frequency

(which is the inverse of activation interval) has been used to study the effect of global Ischemia on VF [Mandapati 98]. Studies by Cao et. al. [Cao 99] have found that varying the conduction velocity restitution creates a spatial variation in activation intervals, whereas the effective refractory period (ERP) restitution causes temporal variation in the activation intervals. This observation was used to explain wave-break [Cao 99]. This study along with the study of Choi et. al. [Choi 01] therefore suggests that variation in activation intervals leads to wavebreak during VF. Zaitsev et. al. [Zaitsev 00] have recorded activations from thousands of locations in a small slab of ventricle and computed dominant frequency maps. They found that the dominant frequencies in the adjacent regions were often in 1:2, 3:4, or 4:5 ratios. Based on these results they have suggested that stable higher frequency domains drive VF. A major limitation of this study is that it has used the electrograms recorded over 4 to 5 seconds to compute the dominant frequency. It would be better to use a much finer time resolution to quantify spatio-temporal changes in dominant frequencies. Thus, one reason to obtain information about the activation intervals is to further understand the mechanisms of VF in terms of whether one source drives VF or whether a number of sources contribute to sustain VF.

Another reason to study spatio-temporal behavior of activation intervals during VF is that it could provide information about the excitable gap during VF. There is a wide excitable gap that exists during sinus rhythm. A considerable excitable gap is also present during tachycardia. However, the quantification of excitable gap during VF is not determined as yet. For a long time, it was believed that there is no excitable gap present during VF, however, recent studies [Omichi 00] that recorded transmembrane voltages during VF clearly demonstrate the presence of an excitable gap. If the excitable gap were to be constant or if it were possible to predict the excitable gap, then termination of VF could be possible by appropriate pacing. However, excitable gap seems to vary substantially during VF and to this date it has not been possible to predict the excitable gap. Based on a previous study [Patwardhan 00] of ECGs in canines we hypothesized that activation intervals could be an indicator of the diastolic interval (DI) or the excitable gap. Using this basis, we have attempted to entrain VF in a computer model by using an arrangement of spatio-temporal distribution of stimulators. The goal is that even if we

are able to entrain VF for 4 or 5 cycles (and detect entrainment), termination of VF would be possible with a much smaller shock energy than what is required as of now.

That VF is easier to terminate if there are 'fewer' wavefronts has been demonstrated by several studies [Dorian 96, Dorian 97, Ujhelyi 99, Murakawa 97]. Evidence of excitable gap during VF has been demonstrated by KenKnight et. al. [KenKnight 95] by capturing a small region of ventricle using a single electrode. Pacing in left and right atria has been extensively demonstrated [Allessie 91, Kirchoff 93, Capuchi 99, Pandozi 97] but success in pacing ventricles has been limited [KenKnight 95, Newton 01]. We will use a novel scheme of having multiple stimulators distributed in space with the timing adjusted such that an organized wavefront will propagate in the tissue model.

An important property of the myocytes that links the variability in the activation intervals with variability in diastolic intervals is the restitution of the action potential duration (APD). Restitution curve describes how the APD depends on the previous DI. Restitution is also hypothesized to contribute a major role in the disintegration of electrical wavefronts and maintenance of VF. However, the same restitution curve which is applied to explain maintenance of VF, is measured under conditions where activation intervals are much longer than those observed during VF. Therefore we developed a new protocol to measure the restitution curve such that the restitution curve obtained using the new protocol is more relevant in situations such as VF. We implemented this new technique in a computer model. We also successfully attempted the technique in a rat cell.

This dissertation consists of three parts: 1) Quantification of spatial and temporal activation interval variability from swine ventricular epicardium during VF. 2) Use of the spatio-temporal distributed pacing to entrain activation intervals during simulated VF. 3) Quantifying restitution of APD via a new protocol using mathematical models, and verification of feasibility of the stimulation protocol using isolated and perfused rat hearts.

Chapter Two: Background

Dominant Frequency and Mechanism of VF

The exact mechanisms of VF remain unclear even after extensive investigations. There are three different hypotheses about how VF is maintained. One hypothesis states that activations during VF are spun off from a single dominant activation, known as the mother rotor. The mother rotor, also known as a scroll wave, is hypothesized to reside within the myocardial tissue transmurally [Karma 94]. Computer simulations using three-dimensional geometries of the heart have revealed patterns similar to those observed during real VF [Lee 01, Berenfield 98]. Experimentally, there is very little evidence for this hypothesis because recording activations transmurally is a difficult, although not an impossible task. There are two potential problems with recording transmurally: 1) recording from several electrodes to have a sufficient spatial resolution alters substantially what is to be measured, and 2) even if a wedge is made as in the case of study by Valderrabano et. al. [Valderrabano 01], it is still a 2-dimentional measurement so that a true 3-dimensional measurement is an extremely difficult task. The hypothesis of mother rotor implies that there is transmural reentry, however, a conclusion from the study of Valderrabano et. al. is that presence of transmural reentry is not absolutely necessary for maintaining VF. A second hypothesis is the multiple wavelet hypothesis of VF [Lee 96, Witkowski 98, Moe 64]. According to this hypothesis, VF is maintained by small individual activation wavefronts, which interact with each other and undergo transformations both in size, shape and direction of travel. Several investigators, who have performed optical mapping studies and confirm the existence of multiple rotors, favor this hypothesis. A third hypothesis suggests that it is not absolutely necessary to have multiple wavelets or a single rotor [Janse 95, Gray 95b]. A small number of rotors could drift within the heart and maintain VF.

There is ample evidence from both experimental as well as simulation studies that the activation intervals vary spatio-temporally [Choi 01]. One aspect common to all the hypothesized mechanisms of VF is the spatio-temporal variation in activation intervals. Drifting spiral waves have been shown to give rise to non-uniform spatio-temporal activations which have been attributed to: (1) global changes in the rate of

change of activations caused by a wave source moving away or towards the recording electrode [Gray 98], and (2) local changes in the amplitude of the spiral activity; the amplitude depending upon the proximity to the core [Davidenko 93]. Activation intervals during VF show spatio-temporal variability due to various reasons that include: (1) heterogeneity of ion channels, pumps and exchangers among different regions of the ventricle, (2) ischemia of cell injury contributing to changes in dynamics of membrane currents, (3) functional anisotropy of myocardium that includes spatio-temporal distribution of excitable gap, conduction velocity and refractory period, and (4) geometric structure and curvature of the electrical wavefront. Tissue mass also determines the complexity (and hence the variation) in activation intervals [Kim 97].

If a recording electrode is placed at any point on the ventricle, then it is observed that the voltage measured continuously at that location shows a sharp decrease when the wavefront passes underneath it which results in a peak in negative rate of change of voltage (dv/dt). The electrode is then said to have recorded an activation. The interval between two such activations is the activation interval.

More information about mechanisms of VF is being sought by studying spatio-temporal behavior of several parameters such as refractory period [Choi 01], spatial coherence [Fendelander 97], wavelength of the activation wave [Kwan 98], conduction velocity [Kwan 98], diastolic interval [Omichi 00] and number of wavefronts [Kim 99]. Of all these parameters, dispersion of refractory period has been determined to be a critical parameter for maintenance of VF [Choi 01, Kuo 83, Lammers 86]. Refractory periods can be measured by several different methods [Duytschaver 01], however, none of these methods can be used to measure refractory period directly during VF. Therefore, activation intervals which have been shown to be correlated with refractory periods [Lammers 86, Kim 96] can be used to quantify variability in refractory periods, as the activation intervals can be easily determined from electrograms from several locations simultaneously.

Spatio-temporal behavior of activation intervals has been used to infer and provide support for hypothesized mechanisms of VF. Zaitsev et. al. [Zaitsev 00] in their optical mapping study, computed dominant frequencies from transmembrane voltage recorded from several thousand locations in a small mass of tissue (3cmx3cm) and

found that the dominant frequencies remained constant for several seconds. Further, they also found that when the dominant frequencies were different, they were multiples of each other [Zatisev 00]. The authors concluded that there are small domains of tissue, which have a source at constant frequency that drives VF. In other words, the dominant frequency of this source is constant for a relatively long period of time (4-5 sec) and that there are similar domains adjacent to each other, each with a different driving frequency. It is important to realize that in the study, the investigators used a very small piece of tissue (3cmx3cm) to draw their conclusions. Therefore, it leaves open the question whether these results can be applied to VF in-vivo. Nevertheless, this study highlights the importance of measuring spatio-temporal dispersion of dominant frequency in understanding the mechanism of VF.

In order to study the mechanisms of VF, activations have been recorded using epicardial electrodes [Bayly 93, Kim 99, Huang 98] at hundreds of locations or using optical mapping at thousands of electrodes [Zatisev 00]. To determine activation intervals, electrograms are differentiated with respect to time (dv/dt) and the activation times are determined at time instances when dv/dt is less than –0.5mv/ms [KenKnight 95]. These studies have analyzed epicardial recordings for short periods of time (less than 5 sec at a time). To study evolutions of VF over long durations of time would require marking activations for long durations, which is a difficult and time consuming process. A few studies have used spectral analysis methods to compute the dominant frequency [Wang 98, Clayton 95, Zaitsev 00]. These investigators computed dominant frequencies using FFT of relatively long data segments (several seconds in duration) which causes temporal averaging of the dominant frequencies. The results of our previously reported study [Patwardhan 00] show that the dominant frequency during VF computed from ECGs, changes continuously during VF. This observation suggests that the dominant frequencies (and hence the activation intervals) recorded from epicardial electrograms are also likely to change continuously with time. The spectral methods used earlier will thus result in loss of information from a temporal perspective. Therefore, in this study we used a method based on time-frequency representation (TFR) of a signal to quantify spatio-temporal changes in dominant frequencies during VF. Using our method we were able to quantify changes in dominant frequency on a

beat-by-beat basis, something that has not been done before using spectral analysis methods.

Assessment of Restitution to Study Effects of Memory

Cardiac cells exhibit restitution, which specifies that when the DI of a cardiac cell is shortened, the APD also shortens [Boyette 80, Franz 88, Elharr 84]. It has been proposed that during VF, reentrant waves that are observed to break-up into smaller fragments, do so due to large oscillations in APDs, known as alternans. A functional block in the wave occurs at the location of alternans [Karma 94, Panfilov 98]. Critical to the occurrence of alternans is the condition that slope of the restitution curve has a region with slope >= 1 [Nolasco 68, Guevara 84]. Alternans can be considered as a precursor for the initiation and maintenance of VF [Qu 97]. Therefore, slope of the restitution curve is believed to play an important role in the maintenance of VF. A hypothesis, widely accepted by several investigators is that if the slope of the restitution curve is less than one, the reentrant wavefront is stable, whereas, if the slope of the restitution curve is greater than one, the reentrant wavefront becomes unstable and fragments into smaller reentrant waves [Qu 99]. This hypothesis is explained by using the schematic shown in Figure 1. The solid line in Figure 1(a) shows the restitution curve, which has a slope less than 1. The dotted line in the figure represents a constant cycle length (CL). Since APD=-DI+CL, this line has a slope of –1 (because CL=constant). When the spiral wave is stable, all the cells within the wave are operating at the intersection (I) of the two curves. When there is a perturbation such that a premature stimulus occurs, the DI is shorter than normal and the operating point now moves to P, the point that reflects the shortened DI. Since the APD of the cells is governed by the restitution curve, the APD for the DI corresponding to point P is the APD corresponding to point Q on the restitution curve. In order to maintain the cycle length, the DI during the next beat would be the DI corresponding to point R. This would result in the APD corresponding to point S and so on. Thus, the DI oscillates about the original operating point I until the DI returns back to its original value corresponding to I and the spiral wave reaches a stable operating point.

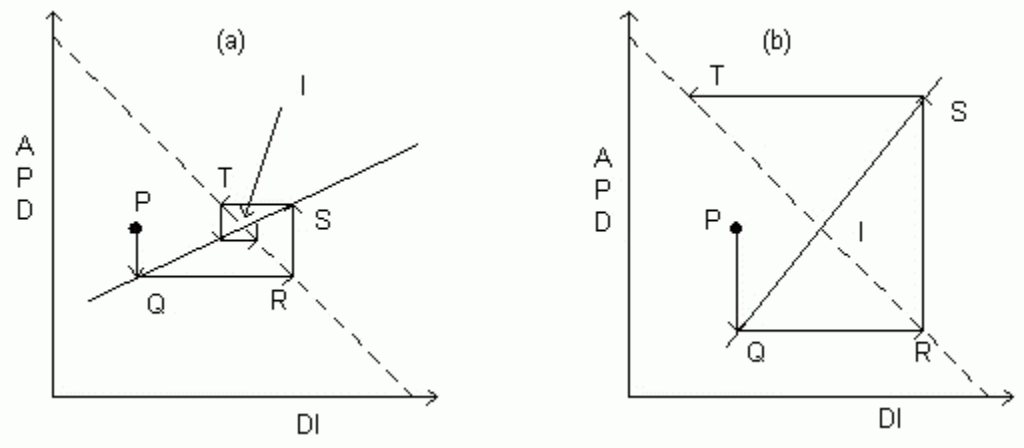

Figure 1. Slope of restitution curve (solid curve) affecting maintenance of VF. (a). Restitution curve with slope less than 1 illustrating a stable wavefront. (b). The restitution curve with slope greater than 1 leads to a wave break.

Figure 1(b) shows a restitution curve with slope greater than 1. As before, a perturbation caused the DI to be shorter at P. This results in the APD to be at a point corresponding to Q on the restitution curve. In order to maintain the CL constant, the DI during the next beat is longer and is given by the point corresponding to R. The APD corresponding to the point R is determined by point S on the restitution curve and so on. As a result of the oscillations between long and short DI, the APD begins to oscillate also to a point that the APD for a long DI becomes longer than the cycle length and a block occurs. Thus, the slope of the restitution curve is proposed to be an important factor in wave-break of spiral activation waves.

Restitution curve has been measured by what is known as the standard S1-S2 protocol [Gilmour 97, Riccio 99]. Basic pulses, about 20 in number, known as S1 are delivered at a constant basic cycle length (BCL) of about 300 ms. The BCL is the shortest cycle length at which no alteration of APD occurs. For example, in a canine purkinje muscle cell, a BCL of 300 ms would be typical [Koller 98]. Single test pulses (S2) are delivered at the end of delivering S1, and the S1-S2 coupling is progressively shortened in steps of 10-20 ms starting from the BCL until the premature pulse are blocked. The S1-S2 interval is then increased by 20 ms to restore capture and is subsequently shortened in 1-2 ms decrements until S2 is blocked. For each S1-S2 interval beginning from 300 ms the DI is computed from the transmembrane voltage corresponding to 90% repolarization (APD_{90}) of the action potential due to the S1

stimulus and the time instance of S2 delivery. The APD due to the S2 stimulus and the DI computed prior to S2 delivery constitute one point on the restitution curve.

Another protocol known as the dynamic protocol has been used by Koller et. al. in an attempt to address the APD dynamics during rapid pacing [Koller 98]. In this protocol, the cells were paced for 50 cycles at a BCL of 400 ms. Pacing was then stopped and the APD corresponding to 95% repolarization (APD_{95}) was measured. Pacing was restarted at a shorter BCL than before and APD_{95} was once again measured after the 50^{th} beat. The BCL was reduced in steps of 50 ms for BCL > 200ms and in decrements of 5-10 ms for BCL < 200ms. For BCL <250ms, alternans occurred and, therefore, for such cases pacing was interrupted once when the APD was long and once when the APD was short.

The relaxation properties of the cardiac I_{Na}, I_K (time-dependent potassium current) and I_{Ca}, which are the Na^+, K^+ and Ca^{2+} ionic currents largely determine the restitution properties of the cell [Luo 91, Shaw 97b]. These currents are dependent upon the time-dependent activation and inactivation of the gates. Incomplete recovery of these gates, as a premature stimulus is delivered, results in the restitution of the APD of the cell. If the recovery takes longer than the duration of one activation interval, then it is likely that previous history may have an effect. This issue of dependence of APD on the previous history of APDs and DIs has been termed as the 'memory' of the cardiac cell [Chiavlo 90, Otani 97]. The 'memory' can be imagined to be a term, which keeps track of the depolarized state of the tissue [Otani 97, Gilmour 97]. A mathematical model for memory term has been suggested by Otani [Otani 97] and Gilmour [Gilmour 97]. They suggest that during each infinitesimal time window Δt, an amount $V(t)*\Delta t$ is added to the memory, while simultaneously, the earlier memory decays exponentially with a time constant τ. Therefore, mathematically, the memory term can be explained as:

$$\Delta M/\Delta t = -M/\tau + V(t)$$

Here, V(t) is the membrane voltage at the time instant 't', and M is the memory term. Since the memory decays exponentially with a time constant τ, the action potentials, which are within the few τ units prior to the present action potential, would contribute heavily to the memory term. Let us consider memory with respect to the APD. A situation where there are several APDs with very short DI prior to each of them, would

contribute heavily to the memory term than the case where there are long DIs prior to each APD. The "single-memory" model of Otani and Gilmour et. al. suggest the following dependence of APD on the memory term (M).

$$APD(M)=APD_p \frac{1-\exp[(M-Mp)/Mapd]}{1-\exp(-Mp/Mapd)}$$

where APD_p=100, M_p=6000, M_{apd}=420 are constants. This model indicates that as the memory (M) increases, the APD decreases.

As explained earlier, ‘memory’ properties of cardiac cell refer to the dependence of APD on one or more previous DIs and APDs. If indeed there is memory, then using restitution curve by itself cannot be used to explain wave break as has been proposed and explained earlier in Figure 1. This is because the curve used to predict the APD from the previous DI is obtained during steady state with the activation history being very different from that during VF. To study the effect of memory in restitution, we developed a new method of stimulation, which was simulated using a model. In both the standard as well as dynamic protocols described earlier, the S1 stimuli are delivered at a constant BCL and therefore it is not possible to control the DI explicitly. The method developed by us to control DI explicitly is better than the standard or the dynamic protocol used to determine the restitution curve. In this study, we stimulated a cell and waited for a predetermined length of DI before delivering another stimulus. The DI sequences were pre-determined sequences of various combinations of increasing and decreasing DIs. Essentially, we changed the frequency with which the DIs changed, to study the behavior of restitution curve under fast and slow change of DI.

In order to verify that our approach of controlling DI is feasible experimentally, we conducted experiments using isolated hearts from rats. As our objective in this part of the study was to develop experimental methods and to demonstrate feasibility, we selected rats as an animal model. Transmembrane voltages were recorded using floating glass microelectrodes [Akiyama 81, Zhou 92, Omichi 00]. Our results show that an independent control of DI is possible and provide justification for further studies using rats and other species.

Simulation Study to Entrain VF

Currently, the only effective way to terminate VF is to deliver a large DC shock either through an implanted defibrillator or through an external device. A large DC shock is painful to the patient, causes myocardial damage and also drains the battery in the case of an internal defibrillator. Instead, if it were possible to terminate VF by using pacing strength stimuli, then defibrillation therapy could become much less painful than delivering large DC shocks. Pacing (and capture) is fairly easy during sinus rhythm but pacing (and capture) during VF is a difficult task since it is not possible to predict the excitable gap. In fact, whether there is an excitable gap during VF is in itself a question for debate. Some studies have suggested that the cells are activated as soon as they are repolarized [Opthof 98, Lammers 96] i.e. no excitable gap exists, whereas, others have suggested that an excitable gap exists [KenKnight 95, Omichi 00, Newton 01]. KenKnight et al. [KenKnight 95] have shown capture during VF from one site. In their study, pacing during VF was carried out using a single electrode at a cycle length equal to about the mean cycle length of the VF. This method of pacing resulted in capture of a small area, approximately $6cm^2$ of the myocardium. As expected, stimulating with only one electrode did not change the VF in the entire ventricle. Regional capture of atrial fibrillation has also been demonstrated by several studies [Capucci 99, Pandozi 97, Kirchoff 93]. In a study reported by Kirchoff et. al., a 4 cm diameter area of the atria was entrained using a single electrode [Kirchoff 93]. This is a relatively large area that can be entrained. Entrainment is also used extensively during tachycardia to identify areas of slow conduction. However, entrainment during VF is a particularly challenging issue because the temporal and spatial distribution of the excitable gap is unknown.

Since it is possible to terminate tachycardia by entrainment, and capture a fairly large area (4 cm diameter) in the atria using atrial fibrillation, we explored the possibility of entraining VF by capturing from multiple sites simultaneously. One of the objectives of such an entrainment was to achieve fewer activation wavefronts, as compared to those without intervention during VF. We will term this reduction in the number of propagating wavefronts as increased ‘organization’. (The term organization is not new with reference to VF. Although a universally accepted definition of ‘organization’ is not formed, investigators generally believe that ‘organization’ refers to the total number of

wavefronts existing during any time of VF. For example, a VF episode having fewer numbers of independent wavefronts is known to be more organized. Several studies have shown that organized VF is easier to terminate [Dorian 97, Murakawa 97, Hsia 96, Ujhelyi 99]. These previous studies suggest that the development of methods to entrain VF may also be useful in terms of defibrillation using lower energy shocks at the same efficacy of defibrillation, if not for termination of VF directly.

In order to demonstrate entrainment, we conducted a simulation study. In this study we explored approaches to convert VF into a single wavefront using a spatio-temporal distribution of stimulators. Pacing from a single site at a frequency slightly above the mean activation frequency at the site should enable us to capture a small area around the site. This technique has been used to demonstrate capture from a single site in the atria [Kirchoff 93]. Further, we have previously reported that in canines, the dominant frequency recorded in the ECGs is symmetrically distributed about the mean dominant frequency and have hypothesized that the excitable gap could be symmetrically distributed about the mean value [Patwardhan 00]. This hypothesis was based on the observation that the dominant frequency is shown to be correlated but not equal to the refractory period [Wang 98]. The distribution of excitable gap in time suggests that if pacing stimuli were delivered at a rate slightly faster than the mean VF activation interval, the probability that the pacing stimulus would occur during an excitable gap would exist, thus making it possible to capture from a single site. Our results of the canine study [Patwardhan 00] also show that at any time instant, the dominant frequencies can be different spatially. Therefore, if pacing stimuli were delivered from sites in the ventricles during VF, it should be possible to capture simultaneously from all the sites within a few cycles.

We used a scheme for entrainment of activations during simulations as described below. We started by inducing and establishing VF in a 400x400 matrix of cells. The spatial arrangement of stimulators was a square grid placed within the matrix of cardiac cells. The cell behavior was based upon the Luo-Rudy model of cardiac cell. All electrodes in a stimulator row were stimulated at the same time. As discussed above we hypothesized that within a few cycles these electrodes in the same row should produce a coherent wavefront which would travel towards and reach the next row of stimulating

electrodes. By estimating the time (based on conduction velocity) it would take for the wavefront to reach the next row of electrodes, the next row of electrodes would be stimulated at the same time. This scheme was repeated for all rows of stimulating electrodes. We varied parameters such as, the distance between the stimulators, strength of stimuli, area covered by the stimulators, the pacing cycle length to optimize capture, and the interval between two stimulators to assess the entrainment.

Chapter Three: Methods

Activation Interval Study

Data were collected from six swine of either sex weighting between 25-35Kg. All studies were approved by the Institutional Animal Care and Use Committee at the University of Kentucky. The animals were tranquilized with ketamine (22mg/kg) and acepromazine (1mg/kg). Anesthesia was induced and maintained using 30 mg/Kg of sodium pentobarbital as required. Animals were ventilated using room air supplemented with oxygen. Normal blood gases were maintained through the experiment. A midline thoracotomy was performed to expose the heart, which was suspended in a pericardial cradle. A custom made epicardial sock with 64 evenly placed electrodes was gently pulled over the heart. An endocardial lead electrode was placed at the right ventricular apex via the left jugular vein. A burst shock was used to induce VF. Defibrillation shocks were delivered between the apical coil electrode and a patch electrode sewn on the left chest wall of the animal. As soon as VF was induced, data were digitized at a sampling frequency of 1000 Hz for 35 sec using a 12-bit A/D converter. After 35 sec of VF, a DC shock was delivered to terminate VF. At least 10 minutes were allowed between trials of VF to allow for return of ionic status to baseline values. We recorded 28 trials of 35 seconds of VF in six animals.

Analysis Technique

We used an analysis technique based on the time-frequency representation of the signal. Smoothed-Pseudo Wigner Distribution (SPWD) was used to estimate the dominant frequency of the signal. The distribution at any discrete-time instance ‘k’ and frequency ‘f’ was computed as: [Wang 93]

$$SPWD(k,f)=\sum_p t_{win}(p) \sum_q e^{-i2\pi fq} f_{win}(q) S(k+q+p) S^*(k-q+p)$$

where, t_{win} and f_{win} are the time and frequency smoothening windows, S is the analytical signal computed from the time series and S* is the complex conjugate of S. We used a Blackman window for time smoothening and a Hanning window for frequency smoothening. To test the performance of our SPWD algorithm, we used amplitude and frequency modulated test signal. This signal was chosen because it has characteristics,

in terms of amplitude and frequency changes, similar to those observed during VF episode. The test signal (Figure 2a) was generated using the equation:

$$y(t)=(2+a)\cos(2\pi f_c t + \beta\sin(2\pi f_m t))$$

where, $a=\cos(2\pi 0.3t)$

In the equation above, the carrier frequency (f_c) was set to be equal to 8 Hz and the modulating frequency (f_m) was selected to be equal to 0.5 Hz. These values were chosen based on the observation that the mean dominant frequency during VF is about 8 Hz and that the continuous frequency changes during VF are not abrupt but slow with periods approximately equal to 2 seconds [Patwardhan 00]. The parameter β, which is the index of modulation, determines the maximum deviation in the frequency about the mean carrier frequency. In this case, β was set to 4 and produced a maximum change in frequency of 2 Hz.

The dominant frequency at any instance 'k' in time was computed by multiplying the signal by a 600 ms window centered at the time instance. An analytic signal was used to compute the SPWD. Frequency smoothening was performed by a frequency smoothening window and an FFT was computed. This resulted in the frequency distribution of the signal at a time instance corresponding to the time instance 'k'. Smoothed-Psuedo Wigner Distributions are typically 3-D functions with time and frequency on the x and y-axis, and amplitude on the z-axis. However, since we were interested in the dominant frequency at 'k' we did not compute the frequency distributions at other time-instances within the 600 ms window. The frequency between 5 Hz and 12 Hz where the spectrum had a maximal value was termed as the dominant frequency. Dominant frequency was computed every 40ms for 30 seconds of VF.

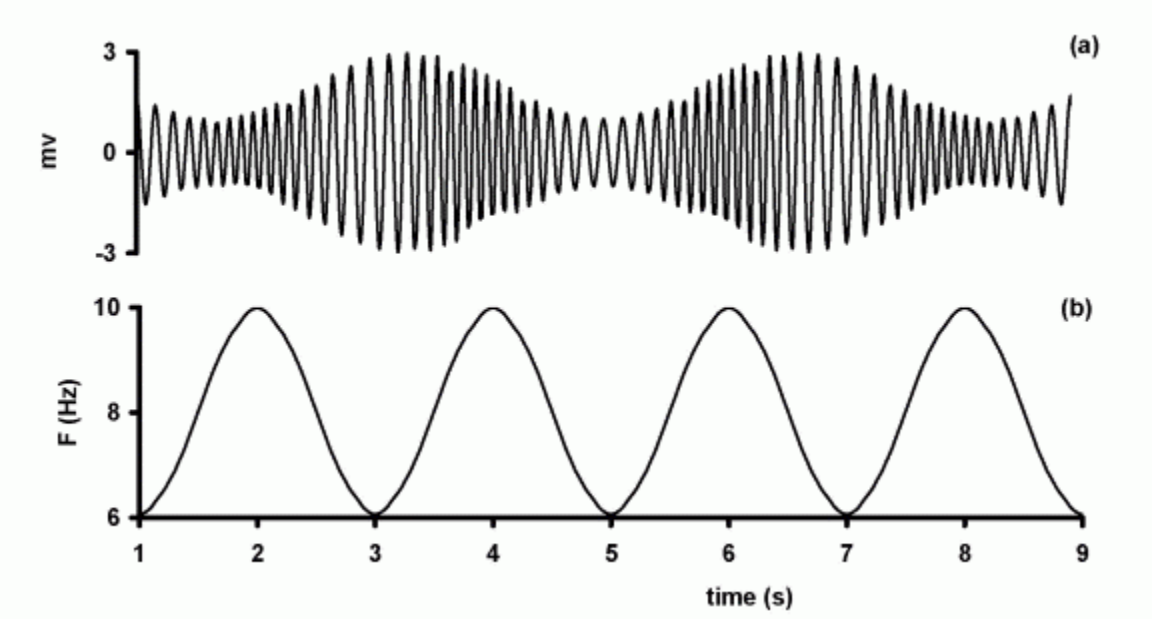

Figure 2. Test signal to verify performance of SPWD.
(a). Amplitude and Frequency modulated test signal. (b). Dominant frequency computed using SPWD of the signal.

Feasibility Study for Estimation of APD Restitution Using Control of DI

Adult rats (Sprague Dawly), 1 to 2 years old, weighting between 200-250 gm were anesthetized with sodium pentobarbital (20 to 30 mg/kg). In order to avoid blockade in coronary vessels (after the heart was explanted), heparin (about 2500 units) was injected via the femoral vein or directly in the ventricles. After waiting for about 5 minutes, so that the animal was under deep surgical anesthesia, the chest was opened. The heart was explanted and a tube inserted into the left ventricle through the aorta. Warm Langendorff solution at 37-39^{o}C was continuously perfused through the cannula in the aorta. The solution consisted of the following (in mM): NaCl 148, KCl 5.4, 0.4, $MgCl_2$ 1.0, $CaCl_2$ 1.8, $NaHCO_3$ 5.8, NaH_2PO_4 and glucose 5.5 [Gray 95a]. The solution was bubbled with a 95% O_2-5% CO_2 (pH 7.4, 37$\pm$0.5 ^{o}C) gas. The heart was placed in a petri dish. To record transmembrane voltage from a single cell, we used custom-made glass microelectrodes that were pulled using a microelectrode puller. Borosilicate glass capillaries with 0.1mm internal diameter were used to make microelectrodes. The microelectrodes were filled with 3M KCl solution. A thin silver wire was inserted into the microelectrode and the other end of the silver wire was connected to an amplifier via a

head stage. The weight of the microelectrode was supported by the silver wire and this arrangement was used as a floating glass microelectrode to obtain trans-membrane voltage recordings. The glass microelectrodes were pulled such that the tip was long and flexible. The micromanipulator was gradually lowered so that the tip of the microelectrode touched the surface of the heart. The offset level of the signal was adjusted to make it zero. The resistance of the electrode was measured using a square wave current injection stimulus generated by the amplifier. Acceptable resistance of the microelectrode was between 10-40 MΩ. With the acceptable resistance, the electrode was further advanced in extremely small steps using the micromanipulator until a transmembrane recording was obtained.

The protocol for collecting data was as follows. The transmembrane voltage was used as input to an analog-to-digital converter of the real-time TMS320C31 Digital Signal Processor kit (Texas Instruments). The sampling frequency was set at 2.8 KHz. The baseline (resting membrane potential) of the signal was adjusted to –70 mv (using offset) so that a set value of –63 mv could be programmed as threshold for detecting APD_{90}, i.e. to indicate that 90% repolarization had occurred. Once 90% repolarization had occurred, a pre-selected value of DI (ms) was obtained from a table of values and a stimulus was delivered after waiting for the time equal to the DI. The stimulus current was delivered between the floating glass microelectrode and the bath, which served as the ground. The stimuli consisted of square pulses 10 ms in width and –10v in amplitude. The stimuli from the digital-to-analog converter (of the TMS320) were fed to a constant current amplifier (A-M systems 3100). Using the 1Volt/volt settings, the output of the A-M systems amplifier was connected between the floating glass microelectrode (also used for recording) and ground. A trial was complete once the desired number of stimuli (equal to the DI intervals in the table) had been delivered or transmembrane recordings were lost. We also recorded a few trials of transmembrane voltage changes when the heart was in sinus rhythm.

Computer Model for Restitution Simulation Study

We used a Luo-Rudy dynamic (LRd) model of cardiac cell to perform the simulations [Luo 94]. The schematic of the LRd cell is shown in Figure 3. This model takes into account the following currents to compute the action potential of a cardiac cell.

a) I_{Na}, Fast Sodium current

b) $I_{Ca,t}=I_{Ca}+I_{Ca,K}+I_{Ca,Na}$, Currents through the L-type Ca^{2+} channel,

c) I_{Kr}, rapidly varying delayed rectifier potassium current,

d) I_{Ks}, slowly varying delayed rectifier potassium current,

e) I_{NaCa}, exchanger current,

f) $Iv= I_{K1}+ I_{Kp} + I_{p(Ca)}+ I_{Na,b} + I_{Ca,b} + I_{NaK}$, Total time-independent current, where,

I_{K1}, Time independent potassium current,

I_{Kp}, Plateau potassium current,

$I_{ns(Ca)}$, Nonspecific Ca^{2+} activated current,

$I_{p(Ca)}$, Sarcolemmal Ca^{2+} current,

$I_{Na,b}$, Na^{2+} background current,

$I_{Ca,b}$, Ca^{2+} background current,

I_{NaK}, Na^{+}-K^{+} pump.

Further, the model also takes into account the intra and extracellular concentrations of Na^{+}, K^{+}, and Ca^{2+}. The Ca^{2+} dynamics of the sarcoplasmic reticulum are also incorporated in the cell model. The simulations were performed in a single cell LRd model and a 2-dimentional sheet of cells where each cell was modeled as an LRd cell.

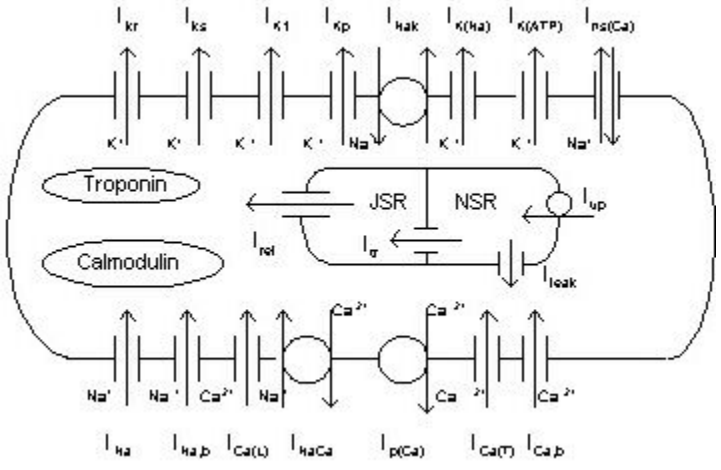

Figure 3. Schematic of a Luo-Rudy dynamic model of a cell.

Simulations for Single Cell

It is known that the APD of the LRd cell decreases progressively for about 10 seconds upon rapid stimulation [Faber 00]. To determine the number of beats it takes for the cell to reach a steady state, the cell was paced constantly at a DI of 0ms, 30ms, 60ms, and 300 ms for about 300 beats so that the APD reached a steady state. During steady state the resting membrane voltage was determined to be about –83mv. Once the steady state for the APD was achieved, the cell was subjected to different patterns of DI, which are described in the results section. Action potential was initiated by delivering a –40μA square pulse of 3 ms duration. As soon as the voltage repolarized to APD_{90} value (-80.7 mv), we waited for a predetermined time that was the desired DI. The APD for the activation that followed this DI was paired with the DI in estimating restitution curves. After the desired DI, another pulse was delivered and an action potential initiated.

The transmembrane voltage of the cell is computed by integrating the differential equation:

$$\frac{\partial V}{\partial t} = -I_{ion} / C$$

where, I_{ion} is the sum of all the ionic currents described above and C is the membrane capacitance. Several of the ionic currents depend on the gating variables (G_i) with change governed by the ordinary differential equation (ODE):

$$\frac{dG_i}{dt} = A_i(1 - G_i) - B_i G_i,$$

The constants A_i and B_i, are rate constants and solely voltage dependent functions. In the integration of the ordinary differential equations, a scheme that was based on the Rush-Larsen method of integration was used [Rush 78]. The Rush-Larsen method is based on the fact that since A_i and B_i change slowly. In such a case, the above differential equation can be re-written as:

$$\frac{dG_i}{dt} = -G_i(A_i + B_i) + A_i$$

For this equation, the steady state solution is a constant, such that,

$dG_i / dt = 0,$ and $G_i(\infty) = A_i /(A_i + B_i)$

The solution to the homogeneous equation is:

$G_i = Ce^{-t(A_i+B_i)}$, in which C is the constant that satisfies the initial condition $G_i = G_i(t=0)$. Therefore, with $A_i's$ and $B_i's$ assumed constant over a time increment Δt, the complete solution to differential equation, with time constant $\tau_i = 1/(A_i + B_i)$ becomes,

$$G_i = G_i(\infty) - [G_i(\infty) - G_i(0)]e^{-\Delta t/\tau_i}$$

Thus, all the ionic currents are computed and the differential equation is integrated with a time step Δk. In order to reduce the computation time without sacrificing on the accuracy of the result, an adaptive time-step was used to integrate depending on the state of the action potential [Qu 99]. If the rate of change of transmembrane voltage (dv/dt) was greater than 5.0 mv/ms, Δt, was fixed at 0.01ms, otherwise it was computed using the equation:

$$\Delta t = \frac{0.01*5}{dv/dt}$$

When the rate of change of voltage was small, as during the resting phase, a maximum time step of 1.0 ms was used to integrate the ODEs. All programs were written in FORTRAN 90 (Lahey Computer Systems).

Simulations for 2-dimentional Sheet of Cells

A 10x10 matrix of cells was used to quantify APD restitution curve of a cell in a 2-dimentional sheet of cells. The conduction between the cells was modeled by the equation:

$$\frac{\partial V}{\partial t} = -I_{ion}/C + D_x \frac{\partial^2 V}{\partial x^2} + D_y \frac{\partial^2 V}{\partial y^2}$$

The first term on the right-hand-side is the same term as in the earlier simulation. The last two terms on the right-hand-side in the equation are the terms from the reaction-diffusion equation. In this equation, V is the transmembrane potential, C is the membrane capacitance, D_x and D_y are the diffusion constants in the x and y direction, associated with the gap junction between the cells and I_{ion} is the sum of all the transmembrane currents for the cell. This equation was integrated iteratively in a three-step process using the operator splitting method [Qu 99]. The method used for

integration is described in brief below. Let Δk be the time-step for integration and 'k' is any time instant. The three integration steps were used as follows:

1. Using the value of 'V' at time instance 'k', the partial differential equation

$$\frac{\partial V}{\partial t} = D_x \frac{\partial^2 V}{\partial x^2} + D_y \frac{\partial^2 V}{\partial y^2}$$

is integrated for a half time step equal to $\Delta k/2$.

2. Using the results for 'V' obtained from step1, the ordinary differential equation

$$\frac{\partial V}{\partial t} = -I_{ion} / C$$

is integrated for time step $\Delta k/2$ using the Euler method. The total ionic current I_{ion} is computed for each cell as described in the previous simulation.

3. Using the value of 'V' in step 2, the partial differential equation,

$$\frac{\partial V}{\partial t} = D_x \frac{\partial^2 V}{\partial x^2} + D_y \frac{\partial^2 V}{\partial y^2}$$

is integrated for a half time step equal to $\Delta k/2$. The procedure is then repeated by returning to step 1 until the simulation has been performed for desired length of physiological time. In practice, Steps 1 and 3 can be combined except for the first and last $\Delta k/2$ time-interval.

The schematic of the arrangement for the 10x10 matrix of cells is shown in Figure 4 below.

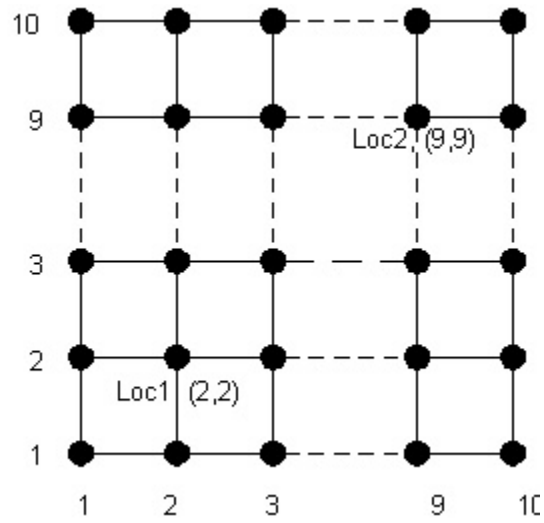

Figure 4. The figure shows a schematic of 10x10 matrix of cells used to perform the restitution simulations.
The cell at Loc1 (2,2) was stimulated and the restitution was measured at the remote location Loc2 (9,9).

In the 10x10 matrix of cells, one corner consisting of 3x3 sub-matrix of cells was stimulated just like in the case of the single cell simulation. Restitution was measured at two locations, Loc1 (2,2) and Loc2 (9,9). Loc1 is one of the cells, which is stimulated directly, whereas Loc 2 was a cell that was away from the stimulus site. The spatial steps Δx and Δy were set equal to 0.02 cm, therefore, distance between Loc1 and Loc2 (being hypotenuse of a triangle with sides of length 7 cells each) was $1.414*7*\Delta x=9.8*\Delta x$. This implies that Loc1 and Loc2 were separated by a distance of about 10 times the distance between adjacent cells in the row or column direction in the matrix. Stimulus strength of -40μA was used for all the simulations to stimulated the cell at location 1. The DI were controlled in a predetermined manner just as in simulations with single cell. The details of the sequences will be described in the results section.

Model for Entrainment of VF

We used a Luo-Rudy [Luo 91] model of the ventricular action potential to perform simulations for entrainment part of our study. This model includes the following currents to compute the action potential:

I_{Na}, Fast sodium current,

I_K, time-dependent potassium current,

I_{K1t}, time-independent potassium current,

I_{si}, Slow-inward current

The model also updates the intracellular concentration, Ca_i. As evident, the LR model of the cell is less detailed than the LRd model used in the restitution study. For the entrainment study we preferred the LR model to the LRd model because of the simplicity of the LR model. Our attempt in this study was to quantify entrainment and therefore the LR model of action potential was sufficient for the study.

Spatial arrangement of the stimulators

The schematic in Figure 5a shows a typical arrangement of stimulators in a 400x400 matrix of cells representing a small piece of tissue of the myocardium. On an average, the length of a myocardial cell is 0.025cm therefore the matrix represents a tissue size of 10cm x 10cm. The solid lines represent schematically, the wire stimulators that were used. The stimulators were 5 cell units high and 320 cell units long. With this arrangement of the stimulators, rows 1 (bottom) through 8 (top) of the stimulators were stimulated in a manner such that a wavefront propagated from bottom to top in the matrix of cells. Each row was spaced from the neighboring row by a length of 32 cells, which is equivalent to 32x0.025 cm=8 mm. We recorded the transmembrane voltages from 18 locations, indicated by red circles in Figure 5. We used the recordings from these locations to quantify entrainment.

After we performed simulations with the arrangement shown in the schematic of Figure 5a, we realized that the entrainment was better in the middle of the matrix as compared to the edges, so we performed simulations with a larger matrix of size 400x800 cells (Figure 5b). In simulations using larger matrix we recorded changes in transmembrane voltages from 240 locations, which covered almost the entire matrix of 400x800 cells. The recording electrodes were arranged in 16 rows by 15 columns format. The rows were named ‘A’ through ‘P’ and the columns were numbered 1 through 15. The electrode in 3^{rd} row and 7^{th} column was thus, ‘C7’. We assessed changes from these locations during stimulation to quantify the area that was entrained. Quantifying cycle length changes over time was the easiest way to determine entrainment. The rate at which each stimulator was turned on determined the target

cycle length, hence, in any cell not directly stimulated by the stimulator, if the cycle length equaled to the target cycle length we concluded that the cell was entrained. After the simulation was complete, the cycle length was computed by identifying the phase 0 of the action potentials and computing the difference between the two times at which consequent phase 0's occurred. Time instance for Phase 0 was determined as the time-instance when the voltage was greater than –80mv and the rate of change of voltage was greater than 20 mv/ms. Once phase 0 instance was identified, no further detection of phase 0 was allowed for another 10 ms.

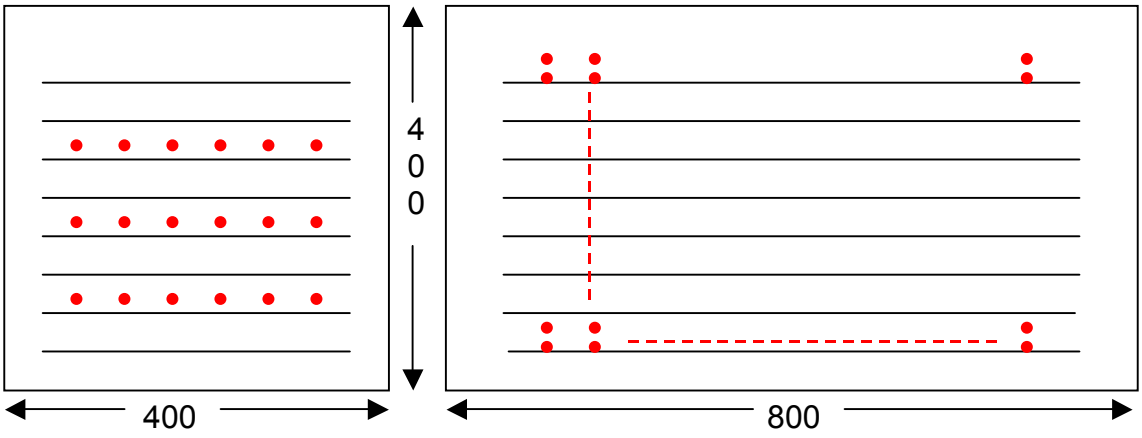

Figure 5. Schematic of the spatial arrangement of the stimulators.
The black lines represent the stimulating wire electrodes. The red circles represent the recording electrode locations. In (a) there were 18 recording electrode. Whereas in (b) there were 16x15=240 recording electrodes. The transmembrane voltages from these locations were stored for the entire length of simulation and then used to determine entrainment

Stimulation process

During simulation, VF was established by an S1-S2 protocol [Starmer 95]. An S1 stimulus consisted of stimulating 20 rows of cells (in all columns) along the lower edge of the matrix. This established a planar wavefront that traveled from bottom to top. When the wavefront traveled about half the matrix (200 rows), a second stimulus S2, perpendicular to the first one was initiated. An S2 stimulus was initiated along the left side of the matrix of cells and was 300 cells wide. S2 was made much wider than S1 so that the core of the rotor that is established, is approximately at the center of the matrix. Within the first 1000 ms of the simulation, VF establishes as the reentrant wavefronts

undergo functional block and multiply. Ventricular fibrillation was allowed to continue in the matrix for 3000 ms. For the remainder of the text, this time instance will be referred to as 0 ms since all the simulations for quantifying entrainment were started from the initial conditions at 3000 ms. Continuous boundary conditions were used on the left and right side of the matrix (so that the left and right side of the matrix were connected). No-flux boundary conditions were set at the top and bottom edge of the matrix.

The first simulations we performed were with line stimulators as shown in the schematic in Figure 5(a) and 5(b). As described earlier, the black lines are the line stimulators 5 cells along row direction and 325 cells along the column direction. The boundary conditions used were continuous along the left and right side of the matrix and no flux on the to and bottom edge of the matrix. These conditions were chosen to allow the entry of native VF wavefronts from the left and right side of the matrix but not from the top or bottom edge of the matrix. The circles in the figure represent one cell from where the transmembrane voltage was recorded during simulations. In Figure 5a, the bottom row of recording electrodes were e11 through e16, left to right. The middle row of electrodes were numbered e21 through e26, left to right and the top row of electrodes are e31 through e36, left to right.

Determination of delay between adjacent stimulators

This parameter is dependent on the conduction velocity determined earlier and the spacing between the adjacent stimulator rows. For the simulations with the 400x400 matrix, we chose a spacing of 32 cells between centers of the adjacent stimulator rows. In the row direction, the stimulators were spread over 325 cells (out of 400 cells) so that they covered about 81% of the length along the rows. Using the conduction velocity estimate determined above (0.643 m/s) for g_{Na}=23.0, the delay between stimulators was set to 10.8 ms. The initial conditions for each simulation were the values of the parameters at 3000 ms of VF. That is, all simulations were started from the initial conditions that existed when a stable VF was established at 3000 ms, therefore, in subsequent results this time instance will be referred to as 0 ms. We used a stimulating current of -400μA which is about 40 times the diastolic threshold for the value of sodium conductance used in our models, yet, much smaller than the current delivered during

defibrillation. Stimulator 1 was for turned on at 0 ms and the pulse width was 0.6 ms. The pulse width was same for all the stimulators. After a delay of 10.8 ms, line stimulator 2 (row 2) was turned on and so on. For the next activation sequence, stimulator 1 was again turned on after an interval equal to the cycle length. To study the performance of this approach, we scanned various cycle lengths as described below.

Under the arrangement of Figure 5(a) we performed multiple simulations to entrain VF. One simulation was performed for 2000 ms where stimulation is not used so that VF continues for the 2000 ms and is termed as 'native VF'. We used time-coherence computed from two electrodes in the direction of intended wavefront travel, as a parameter to determine if the desired capture had occurred during stimulation. The time-coherence during stimulation was compared with time-coherence during native VF. The time-coherence algorithm is explained below.

Estimation of time-coherence

Given two signals *x(t)* and *y(t)*, we can model *x(t)* as a output of *y(t)* passed through a transfer function $h_{yx}(t)$.

$$x(t) = y(t) * h_{yx}(t) + n_x(t)$$

where $n_x(t)$ is the error between the predicted and true value of *x(t)*.

Using a discrete time index k, the above equation can be written as:

$$x(k) = H_{yx}^{T}(k) Y(k) + n_x(k)$$

At each time step, *k*, the transfer function is updated by minimizing the squared error between the estimated *x(k)*, which is denoted by $x_{est}(k)$, and the true value of *x(k)*. In the above equation $H_{yx}^{T}(k)$ represents the transfer function in the discrete time-domain. The LMS algorithm introduced by Widrow [Widrow 85] is used to minimize the error.

The updated transfer function is given by

$H_{yx}(k+1) = H_{yx}(k) + \mu_x n_x(k) Y(k)$

The factor μ_x governs the rate at which the adaptation takes place. The difference between the predicted and the true value of y is estimated as,

$n_x(k) = H_{yx}(k) Y(k) - x(k)$

The square of the error is given by:

$e^2 = (x_{est}(k) - x(k))^2 = (H_{yx}(k) Y(k) - x(k))^2$.

The squared error is minimized at each step of the iteration using the LMS algorithm by Widrow. This minimization gives the adaptation rule:

$H_{yx}(k+1) = H_{yx}(k) + \mu_x (H_{yx}(k) Y(k) - x(k)) Y(k)$

where μ_x is the adaptation constant.

Similarly, series *y(k)* is modeled as a sum of linear operation on *x(k)* plus the error $n_y(k)$ to obtain the adaptation rule,

$H_{xy}(k+1) = H_{xy}(k) + \mu_y (H_{xy}(k) X(k) - y(k)) X(k)$

Thus at each time instance, an estimate of the coherence between the series *x* and *y* is obtained by taking the product of $H_{xy}(f)$ and $H_{yx}(f)$ which is the frequency domain representation of the filters $h_{xy}(k)$ and $h_{yx}(k)$, respectively.

$C_{xy}(k,f) = H_{xy}(f) H_{yx}(f)$

At each index of *k*, the filters and hence the coherence estimate is updated.

The coherence between two electrodes, selected such that the line joining them is perpendicular to the direction of travel of the wavefront, is integrated within a small window (approximately 2 Hz wide) about the pacing cycle length for the stimulation trials. We averaged coherence from twelve pairs of electrodes. This coherence is compared with the coherence computed between the same two electrode sets (as used before) during native VF.

Chapter Four: Results

Assessment of Changes in Dominant Frequency

Validation of time-frequency method

We used a technique based on time-frequency analysis to determine changes in dominant frequencies over 30 sec of VF. In order to validate our analysis technique, we compared dominant frequencies estimated using time frequency analysis with those obtained from the more widely used technique of using differentiated electrograms. The electrogram in Figure 6(a) was differentiated using a 5-point [Cabo 90] derivative computed as:

$$m_k = \frac{-2y_{k-2} - y_{k-1} + y_{k+1} + 2y_{k+2}}{10\Delta t}$$

where, k is the time instant, y_i is the digitized sample, and Δt is the sampling interval. The differentiated signal is shown in Figure 6(b). Using threshold criteria of –0.5mv/ms [KenKnight 95] activation times were marked at the time instances at which the rate of change of voltage (dv/dt) for the electrogram exceeded the threshold. To construct the activation interval time series, activation interval was held constant between the two consecutive activation times used to compute the activation interval. The change in activation interval with time is shown in Figure 6(c). The reciprocal of activation interval is dominant frequency. The change in dominant frequencies with time computed from the activation intervals is shown in Figure 6(d) as a solid line. The figure shows that the dominant frequencies computed using the two methods were similar (r^2=0.8).

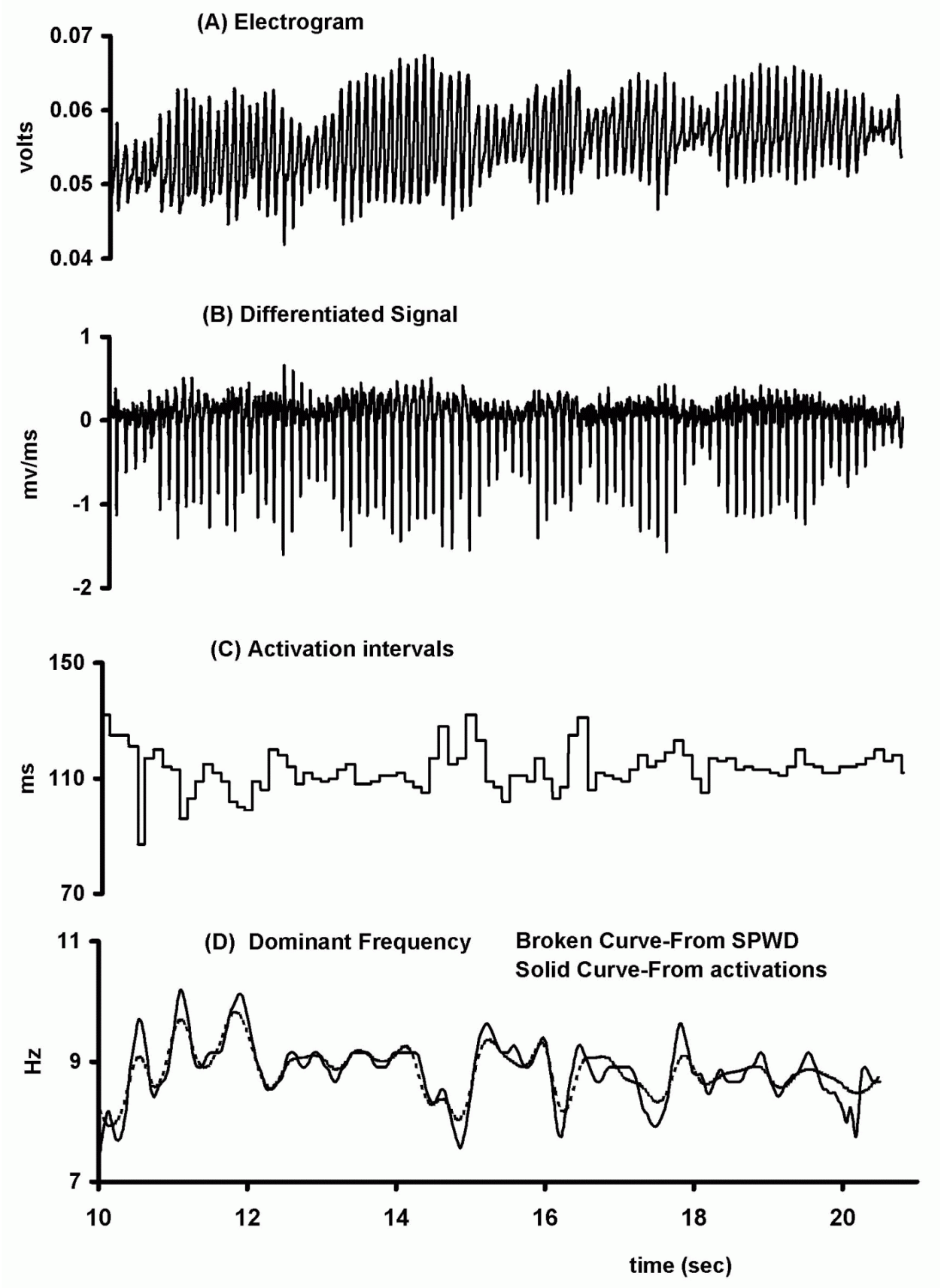
(A) Electrogram
0.07
0.06
0.05
0.04
volts
(B) Differentiated Signal
1
0
-1
-2
mv/ms
(C) Activation intervals
150
110
70
ms
(D) Dominant Frequency
Broken Curve-From SPWD
Solid Curve-From activations
11
9
7
Hz
10
12
14
16
18
20
time (sec)

Figure 6. Comparison of dominant frequency computation using SPWD and activation intervals.
(a). Typical Electrogram. (b). Differentiated electrogram. (c). Activation intervals vs. time computed from differentiated electrogram. (d). Dominant frequency computed from the activation intervals. The broken curve indicates the dominant frequency computed from the electrogram using the Smoothed Pseudo Wigner Distribution. The solid curve represents the dominant frequency computed from the activation intervals in Figure 6(c).

Mean, minimum and maximum dominant frequency

Using our new technique we determined the average mean, maximum and minimum frequencies recorded in each animal. The dominant frequency was determined every 40 ms for 30 sec of VF in every electrode that recorded an electrogram free from excessive noise and artifacts due to poor epicardial contact. For each electrogram, we determined the minimum, mean and the maximum frequencies that were recorded during 30 sec of VF i.e. the minimum, mean and maximum of the 750 estimates of the frequency. The minimum frequencies across all the electrodes in a trial were averaged to give an estimate of the minimum frequency recorded for that trial. The minimum frequencies corresponding to each trial in an animal were averaged to form the average minimum frequency in each animal. Similarly, we computed the average maximum frequencies for all animals. Within a trial, the dominant frequencies at each 40 ms time step during the 30 seconds of VF, across all the electrodes were averaged. In this way, we obtained how the dominant frequency, averaged spatially, changed over 30 seconds of VF of a trial. The mean of this change in dominant frequency over 30 sec was used as an estimate of the average dominant frequency for a trial. Figure 7 shows the mean dominant frequency for each animal. The average minimum and maximum frequencies recorded in each animal are shown as error bars.

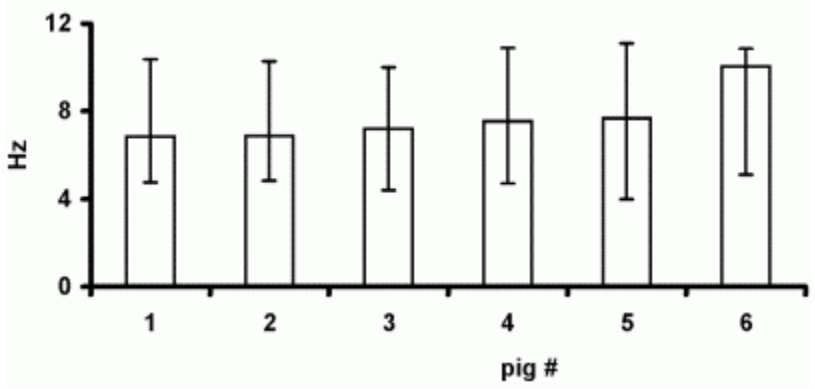

Figure 7. Mean dominant frequency.
The mean dominant frequency recorded in each swine is shown by vertical bars. The error bars indicate the average minimum and maximum frequencies recorded in each animal.

Spatial variation

Standard deviation among dominant frequencies recorded from different electrodes at any time step indicates the degree of variation in activation intervals spatially, i.e. over the ventricular epicardium. To investigate if the spatial variation changed with duration of VF, we compared the spatial standard deviations in dominant frequencies during early part of VF with that during the late part of VF. During the first five seconds of VF, at every time step, we computed the standard deviation of dominant frequencies across all electrodes in a trial and averaged the values of standard deviations obtained for all the trials to get an estimate of spatial standard deviation during early VF for that trial. Similarly, for the last 5 seconds of VF, we computed the standard deviation for each trial. The spatial standard deviations during early VF for all trials within an animal were averaged to form the spatial standard deviation during early VF for each animal, and the spatial standard deviations during late VF for all the trials within an animal were averaged to form the spatial standard deviation during late VF for each animal. Figure 8 shows the spatial standard deviation during early VF (hollow bars) and late VF (filled bars) for all the six animals. Over all the trials, the average spatial standard deviation during early VF (1.08Hz) was significantly higher ($p<0.05$) than the average spatial deviation during late VF (0.8Hz).

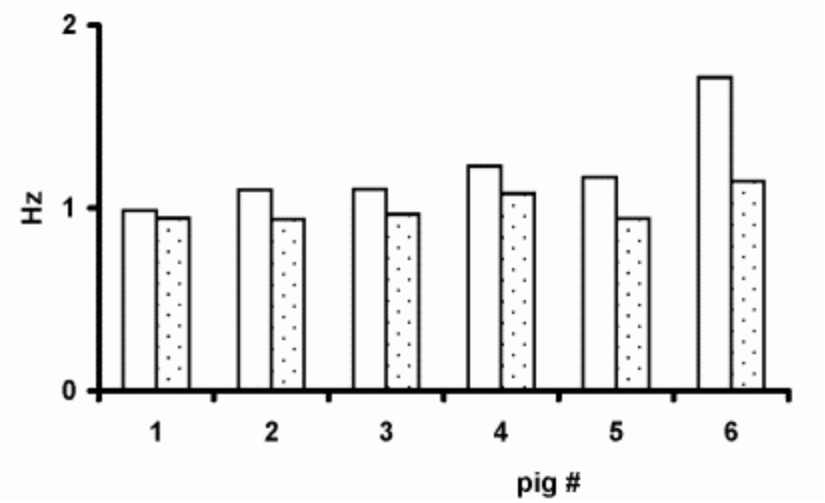

Figure 8. Comparison of spatial standard deviation during early and late VF.
The hollow bars show the average spatial standard deviation during early VF for each animal. The filled bars show the average spatial standard deviation during late VF for each animal. On an average, across all the trials, the spatial standard deviation during early VF (1.08Hz) was significantly higher ($p<0.05$) than that during late VF (0.8Hz).

Temporal variation

The temporal standard deviation in dominant frequencies would indicate the degree to which the dominant frequencies change over time. (Earlier we have quantified this information as the mean, minimum and maximum frequency; here we compare the standard deviation.) For every electrode, the standard deviation from successive estimates of dominant frequencies during the 5 seconds of early VF was computed. The temporal standard deviation thus computed was averaged across all electrodes in a trial and this average was used as the estimate of temporal standard deviation during early VF for that trial. Similarly, we computed the temporal standard deviation during late VF. On an average, over all the trails, the temporal standard deviation during early VF (1.22 Hz) was significantly higher ($p<0.05$) than the standard deviation during the late VF (0.97 Hz). The hollow bars in Figure 9 show the average temporal standard deviation during early VF for each animal, whereas the filled bars indicate the average temporal standard deviation during late VF in each animal.

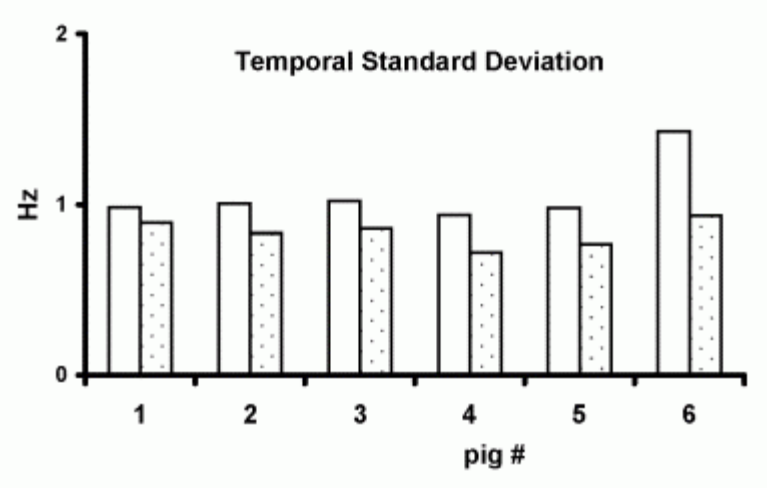

Figure 9. Comparison of temporal standard deviation during early and late VF.
The hollow bars indicate the average temporal standard deviation during early VF, whereas the filled bars indicate the average temporal standard deviation during late VF. The temporal standard deviation during early VF in each animal was higher ($p<0.05$) than that during late VF in each of the six animals.

Distribution of dominant frequencies

Since dominant frequency has been shown to be an indicator of the refractory period of the tissue, distribution of dominant frequencies would be an indicator of the distribution of the refractory period. We quantified the distribution of the dominant frequencies during early and late VF for three cases: (a) entire ventricles, (b) over the apex, and (c) over the base of the ventricles. The electrodes on the heart were grouped into four regions: right apex, right base, left apex and left base. The procedure used to compute the distribution is explained using the group of electrodes on the right apex as an example. For a trial, the histograms of the dominant frequencies was computed for each of the electrodes within the right apex and averaged to form the histograms of dominant frequencies for the trial. Having obtained the frequency histograms for each individual trials, the distributions were averaged to obtain the distribution of dominant frequencies for the right apex. The histograms were computed during both, early and late VF for the right apex. Similarly, the histograms were also computed for the right base, left apex, and the left base. Figure 10 shows the average distribution of dominant frequencies during early VF (dark line) and late VF (broken line) for the four regions as well as the entire ventricle. The average represents the average across all the good

trials. The histogram of dominant frequencies was symmetrical about the mean value during both, the early and late VF. Also, note that the means during late VF were significantly higher ($p<0.05$) than the means during early VF.

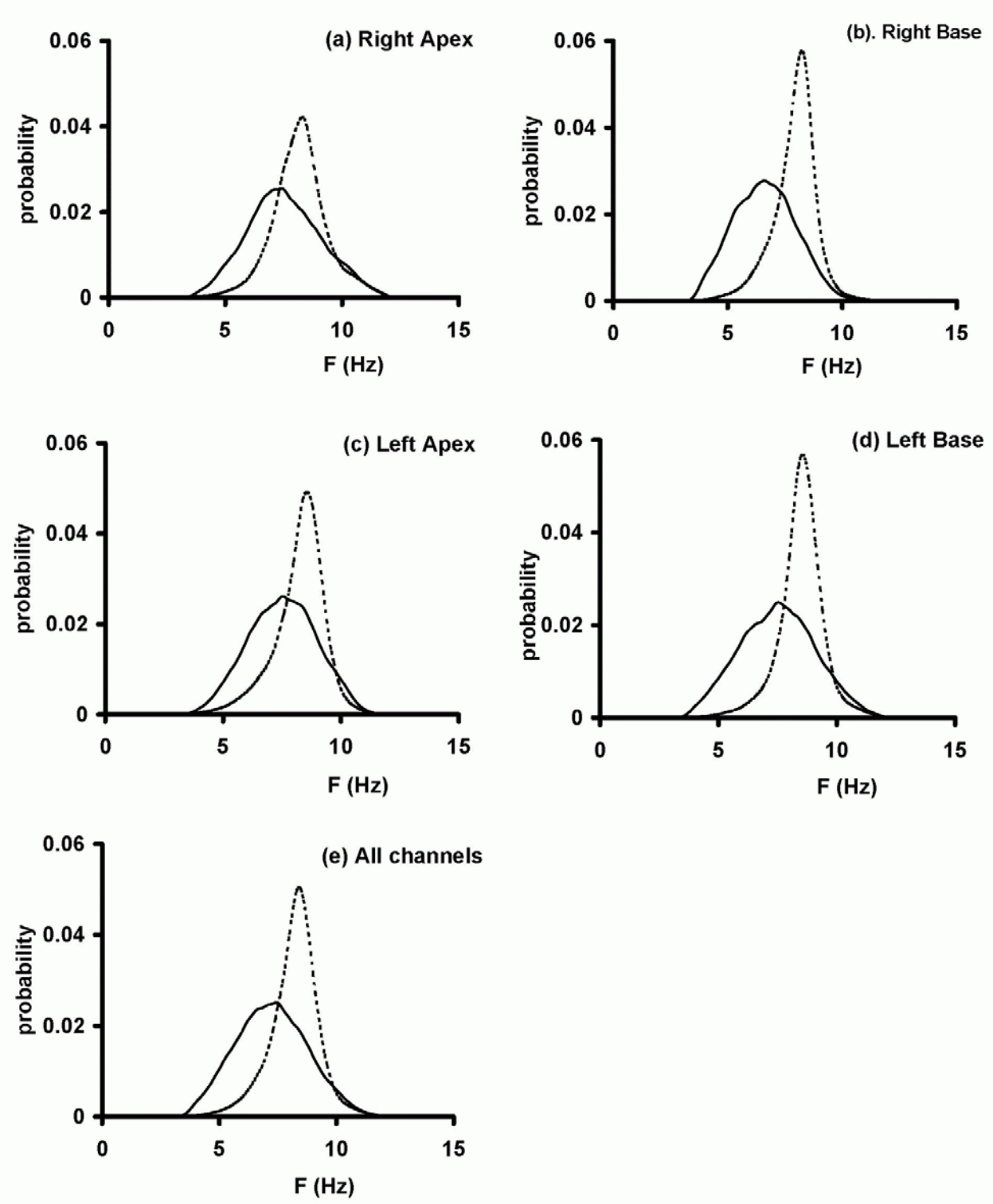

Figure 10. Probability distribution of dominant frequencies.

The solid curve is the distribution of dominant frequencies during early VF and the broken curve is the distribution of dominant frequencies during late VF for (a) right apex, (b) right base, (c) left apex, and (d) left base. Each curve represents an average across all the good trials.

Temporal changes in mean dominant frequency

One of the objectives of this study was to determine if the dominant frequencies recorded in the electrograms showed an increase that we have reported earlier in ECGs recorded in canines [Patwardhan 00]. In the previous study we observed that the dominant frequencies increased during 30 seconds of VF. Within a trial, the average dominant frequency over 5 seconds of early VF (temporal averaging) was computed for each electrogram and these values were averaged across all the electrodes (spatial averaging). This procedure resulted in an estimate of average dominant frequency during early VF for the trial. Similarly, we determined the average dominant frequency during late VF for a trial. The hollow bars in Figure 11 show the average dominant frequencies during the first five seconds of VF and the filled bars show the average dominant frequencies during late VF. We found that dominant frequency during late VF (7.72 Hz) was significantly higher ($p<0.01$) than the dominant frequency during early VF (7.15 Hz). Figure 12 shows a typical change in dominant frequency for an electrogram during 30 seconds of VF. The example shows how the dominant frequencies show a local (in time) variation in dominant frequencies and an increase on an average with time.

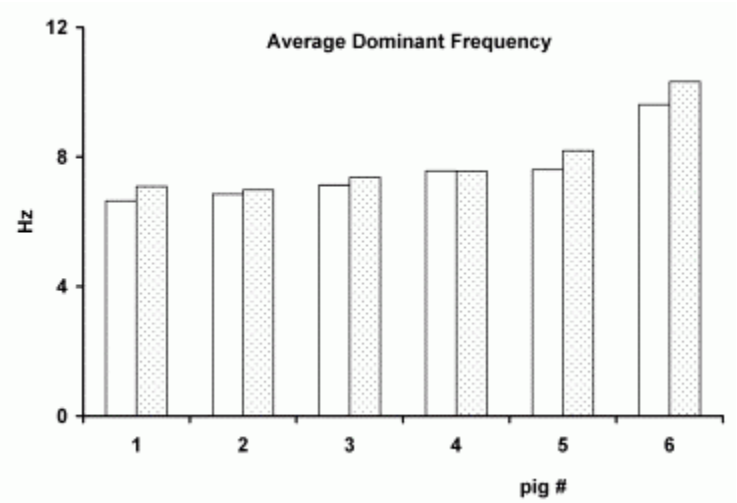

Figure 11. Average dominant frequencies during early and later VF.

The hollow bars indicate the average dominant frequency during early VF i.e. the first 5 seconds of VF, whereas the filled bars indicate the average dominant frequency during the last 5 seconds of VF (late VF). The DF during last 5 sec of VF was significantly higher ($p<0.05$) than the VF during the first 5 sec of VF.

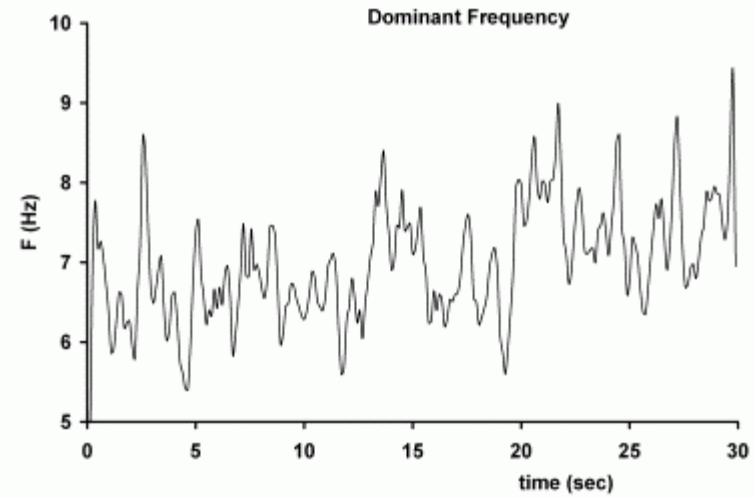

Figure 12. Typical change in dominant frequency recorded in an electrogram during 30 seconds of VF.

Earlier in this section, we demonstrated how our new method based on SPWD was able to detect changes in the dominant frequency on a beat-by-beat basis (Figure 6). In order to validate results obtained using our new method further, we selected three trials at random and compared the dominant frequencies during early and late VF using the new method with those computed using activation intervals obtained by differentiating electrograms. The activations were marked for 5 sec in an electrogram. The activation intervals calculated from these marked activations were averaged to form the mean activation interval. All mean activation intervals, corresponding to each electrode were averaged to form the average activation interval for the trial. The inverse of the mean activation interval is the mean dominant frequency computed using the activation intervals. The mean dominant frequency using the new method was computed as described in the previous paragraph. Table 1 shows that the mean dominant frequencies computed using the two methods were similar. Within each trial, we compared dominant frequencies estimated using differentiated electrograms between early and late VF for statistical significance and found that within a trial, the dominant frequencies during late VF were significantly higher than the dominant frequencies during early VF.

Table 1. Comparison of average dominant frequencies during early and late VF using the SPWD (F_s) and activation times (F_a).

trial		Early VF (Hz)	Late VF (Hz)	p-value (unpaired)
t1	F_a	6.75	7.22	p<0.001
	F_s	6.80	7.20	p<0.001
t2	F_a	7.83	8.04	p<0.001
	F_s	7.76	7.99	p<0.001
t3	F_a	6.50	6.78	p<0.001
	F_s	6.54	6.68	p<0.001

To determine the variation in dominant frequencies within a region of the heart, we compared the dominant frequencies and standard deviations during early and late VF for the four regions of the heart divided as Right and Left, Apex and Base. Table 2 below shows that the increase in dominant frequency and the decrease in spatial and temporal standard deviation in each region was similar to that of the entire heart.

Table 2. Comparison of average dominant frequencies, spatial and temporal standard deviations during early and late VF.

	Early VF	Late VF	Early VF	Late VF	Early VF	Late VF
	Dominant Frequency (Hz)		spatial std (Hz)		temporal std (Hz)	
Left Apex	6.87	6.99	0.88	0.75	0.9	0.72
	p<0.02		p<0.001		p<0.001	
Left Base	6.84	6.96	0.92	0.82	0.87	0.72
	p<0.02		p<0.001		p<0.001	
Right Apex	6.71	6.80	0.87	0.82	0.87	0.78
	p<0.05		p<0.01		p<0.001	
Right Base	6.54	6.66	0.84	0.79	0.82	0.77
	p<0.05		p<0.01		p<0.001	

In order to determine the differences in dominant frequencies between any two adjacent electrodes, we selected two adjacent electrodes within a randomly selected region of the heart. For each trial, the difference in dominant frequencies over 30 seconds was computed and the difference was averaged to form one value of averaged difference per trial. Figure 13 shows a comparison of the averaged differences across all the trials in each of the six pigs. The solid bars are for electrodes in the anterior right base region and the filled bars are for electrodes in the posterior right base region. The figure shows that in any electrode pair, the average differences in dominant frequencies can be quite different from one animal to another. Further, for any two pair of electrodes the averaged differences in one pair can be higher or lower than the other with no consistent pattern.

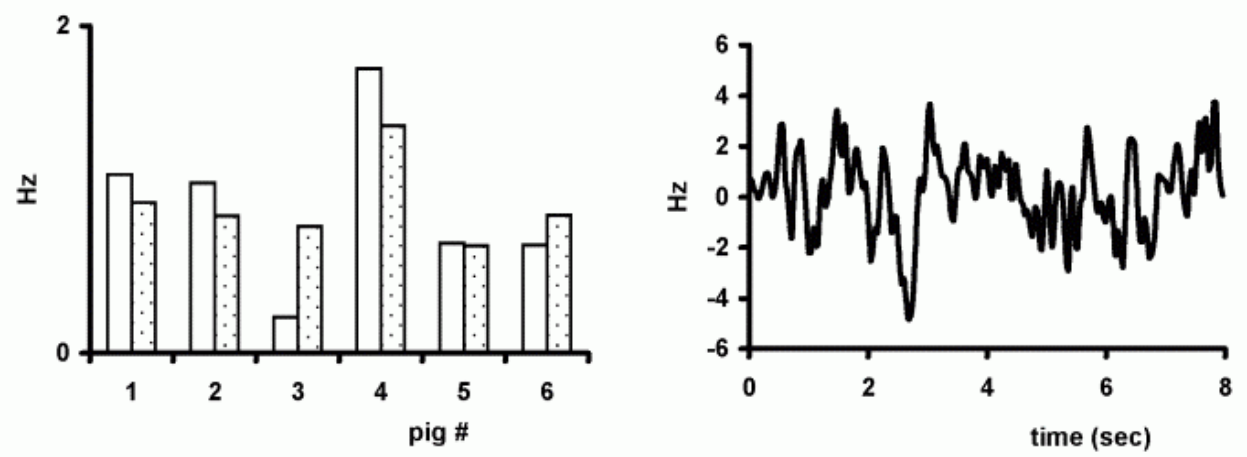

(a) (b)

Figure 13. Average differences in frequencies between adjacent electrodes during early and late VF.
(a). The hollow bars correspond to early VF and the filled bars correspond to late VF.
(b). Typical difference in dominant frequencies between two adjacent electrodes for one trial.

We also compared the average instantaneous frequencies with average initial frequency computed from the first 5 seconds of VF. Average dominant frequency for the first 5 seconds of VF was computed from all the trials. The average dominant frequency at each instance in time (i.e. every 40 ms) after 5 seconds was compared with the initial frequency for all the trials and a p-value computed at each time instance. Figure 14 shows how the p-value changes as VF progresses in time. The figure shows that

average dominant frequencies were higher than the average initial frequency as early as 8 seconds into VF.

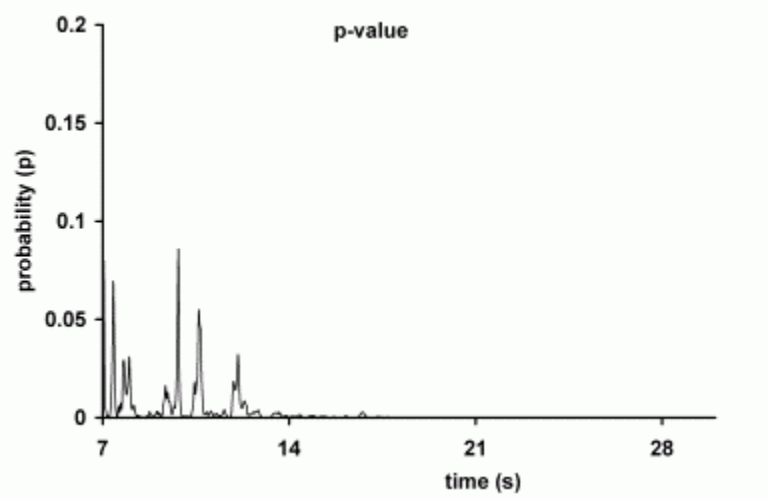

Figure 14. p-value vs. time plot for comparison between dominant frequencies.
The figure shows that the dominant frequencies, as early as 8 sec after VF begins, are significantly higher compared to early VF (first 5 seconds of VF).

Restitution Measurements During Paced Activations

Simulation study

Prior to running the simulations, the LRd cell model was paced for 300 beats at a constant DI of 0, 30, 60 and 300 ms. Figure 15 shows how the APD changes on a beat-by-beat basis during constant DI pacing. Figure 15(a) shows that when the DI was 0 ms, the APD stabilizes faster than any other DI. Therefore, in every simulation, the cell was paced for 250 beats at 0ms DI before subjecting the cell to different sequences of DI. Table 3 shows how the average APD changes as the number of beats increase i.e. at constant pacing.

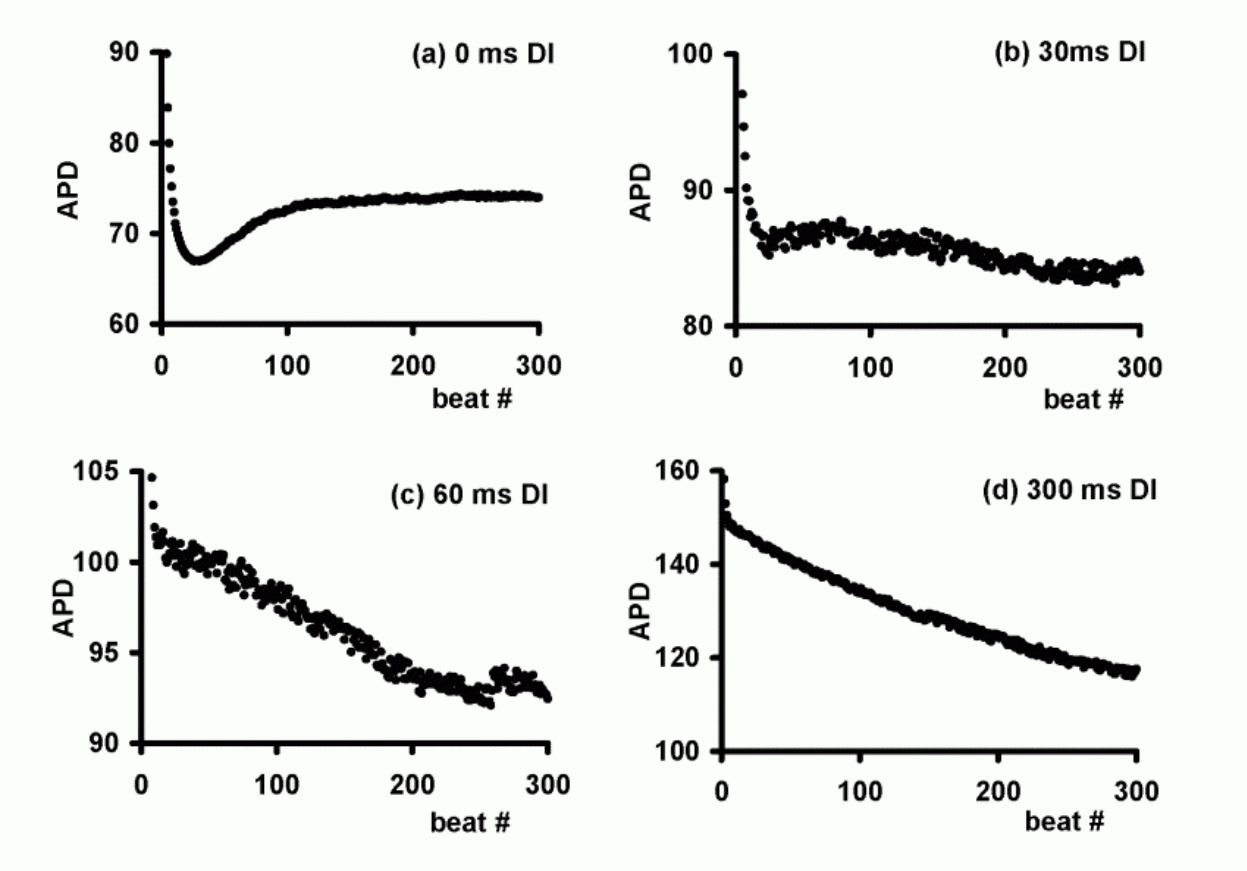

Figure 15. Change in APD when an LRd cell is paced initially at constant DI.
The figure shows how the APD changes when the LRd cell is paced for 300 beats at a constant DI of (a) 0 ms, (b) 30 ms, (c) 60 ms, and (d) 300 ms.

Table 3. Mean APD changes during first 300 beats in LRd cell at various DI.

Mean for beats	DI=0 ms	DI=30 ms	DI=60 ms	DI=300ms
1 to 20	81.61782	97.08375	109.3496	150.0747
70 to 90	71.53571	86.94401	98.84938	136.9771
150 to 170	73.60147	85.7486	95.69215	128.2824
250 to 300	74.09605	84.02773	93.15809	118.187

The cell was paced with a sinusoidally varying DI such that the DI decreased from 60 to 0 ms in 112 beats and then increased again to 60 in another 113 beats as shown in Figure 16(a). As the DI was reduced, the APD decreased as evident by solid diamonds in Figure 16(b). During the following cycle of DI increase, the APD increased again (hollow circles), however, the APD for each corresponding DI was now smaller than the APD during decreasing DI, exhibiting hysteresis of the restitution curve. The restitution curve was divided into 6 ranges of DI as shown in Table 4 below and the slopes of the restitution curves were computed within each section. The maximum slope of the restitution curve was 0.95 and occurred within the range of 10-20 ms of DI. The maximum slope during the increasing DI also occurred during the same range but was smaller (0.73) than that during the increasing DI.

We also changed the steady state pacing DI to 30 ms instead of 0 ms to investigate if the different initial condition would affect the resulting APD. Therefore, instead of 250 beats with 0 ms, the cell was paced at 30 ms DI for 250 beats before subjecting to the sequence of change of DI. Figure 16(c) shows how the APD changes in this case of initial pacing at a constant DI of 30 ms. As in Figure 16(b), hysteresis of the restitution curve was still evident. The results were similar to those in Figure 16(b). A trace of the simulated transmembrane voltage for about 4 seconds is shown in Figure 17. The trace shows the situation when the DI decreased and then increased.

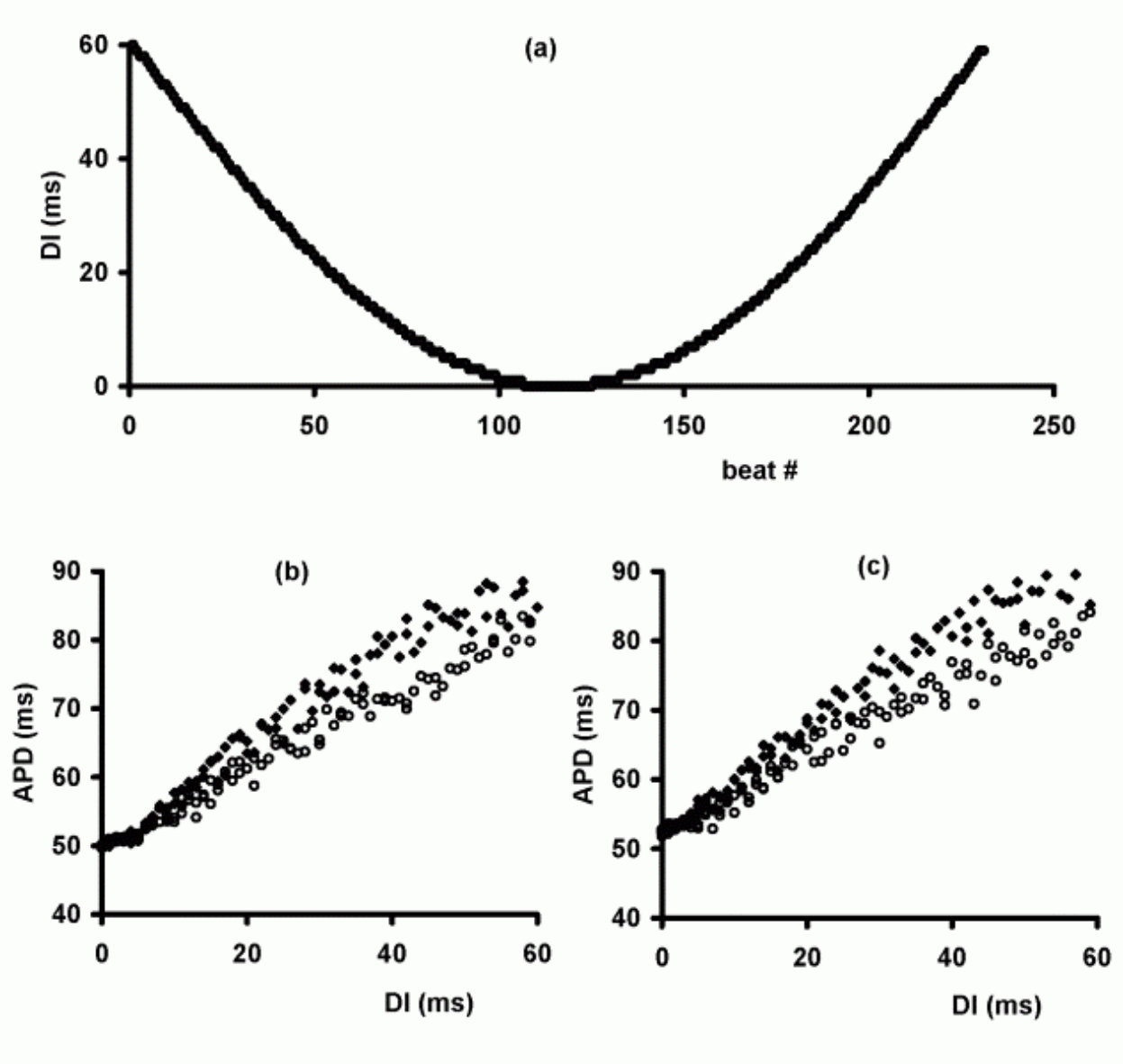

Figure 16. Restitution curve when DI changes from 0 and 60 ms in 115 beats.
(a) The graph shows how DI changes for 230 beats between 0 and 60 ms. Using the average cycle length of 130ms gives a total simulation time of 30 sec. In figure (b) and (c), the solid squares represent the APDs when the DI is decreased from 60ms to 0ms in 113 beats and the hollow circles represent the APDs when the DI is increased from 0ms to 60ms in 113 beats in (a). In (b), the cell was paced at 0ms for 250 beats before subjecting to the sequence shown in (a). In (c), the cell was paced at 30ms DI for 250 beats before subjecting to the sequence in (a).

Table 4. Slopes of restitution curve computed over various ranges of DI.

Range of DI	Decreasing DI	Increasing DI
0 to 10 ms	0.57	0.43
10 to 20 ms	0.95	0.73
20 to 30 ms	0.87	0.55
30 to 40 ms	0.80	0.43
40 to 50 ms	0.46	0.71
50 to 60 ms	0.12	0.52

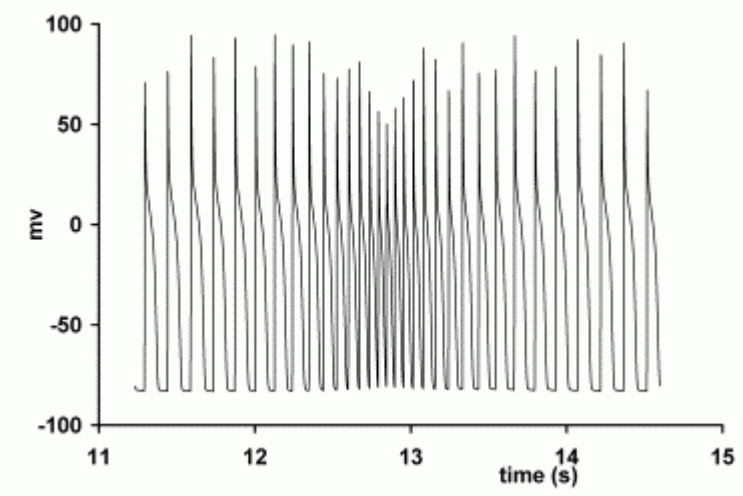

Figure 17. Example of a typical transmembrane voltage vs. time recording.
In this snapshot, the DI decreased for about 2 seconds and then increased for 2 seconds.

In order to determine if the APD decreased continuously when the cell was subjected to several sequences of decreasing and increasing DI, we subjected the cell to two cycles of decreasing and increasing DI. The sequence of DI shown in Figure 16(a) was repeated. Figure 18 shows the restitution curve for this sequence of DIs. For each set of DI increase or decrease, a linear regression line was fitted to the restitution curve. The solid line shows the restitution curve during the first decrease in DI. This is followed by the broken line with long sections, which correspond to the first increase in DI. The broken line with short sections corresponds to the APD when the DI is decreasing again. On an average, the restitution curve due to the second DI decrease is

between the restitution curve due to 1st DI decrease and increase. These observations show that hysteresis is not observed due to continuous shortening of APD due to pacing

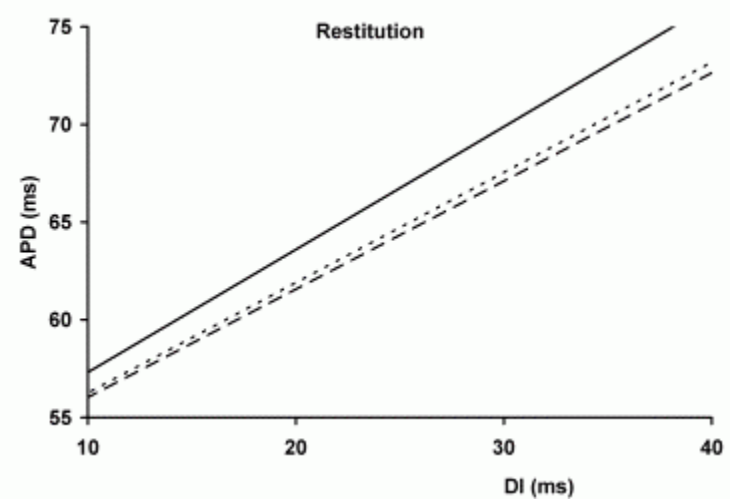

Figure 18. Restitution curves due to a sinusoidally varying DI.
The solid line corresponds to the APD when DI is decreasing. The broken line with long sections corresponds to the increase in DI after the initial decrease. The broken line with short sections is the APD for DI decrease for the second time.

The frequency of DI change was now increased such that the DI decreased from 60 ms to 0 ms in about 57 beats and then increases to 60 ms in the next 57 beats as shown in Figure 19(a). As before, the restitution curve showed hysteresis (Figure 19(b) and Figure 19(c)). The magnitude of hysteresis in this case was smaller than the hysteresis in the previous case.

Figure 20 (a) shows a situation of very rapid change in DI. In this case, the DI was changed from 60 ms to 0 ms in about 14 beats and then increased to 60 ms over the next 14 beats. As seen in Figure 20(b) and 20(c), the restitution curve also showed hysteresis but the magnitude of hysteresis was smaller than the two previous cases.

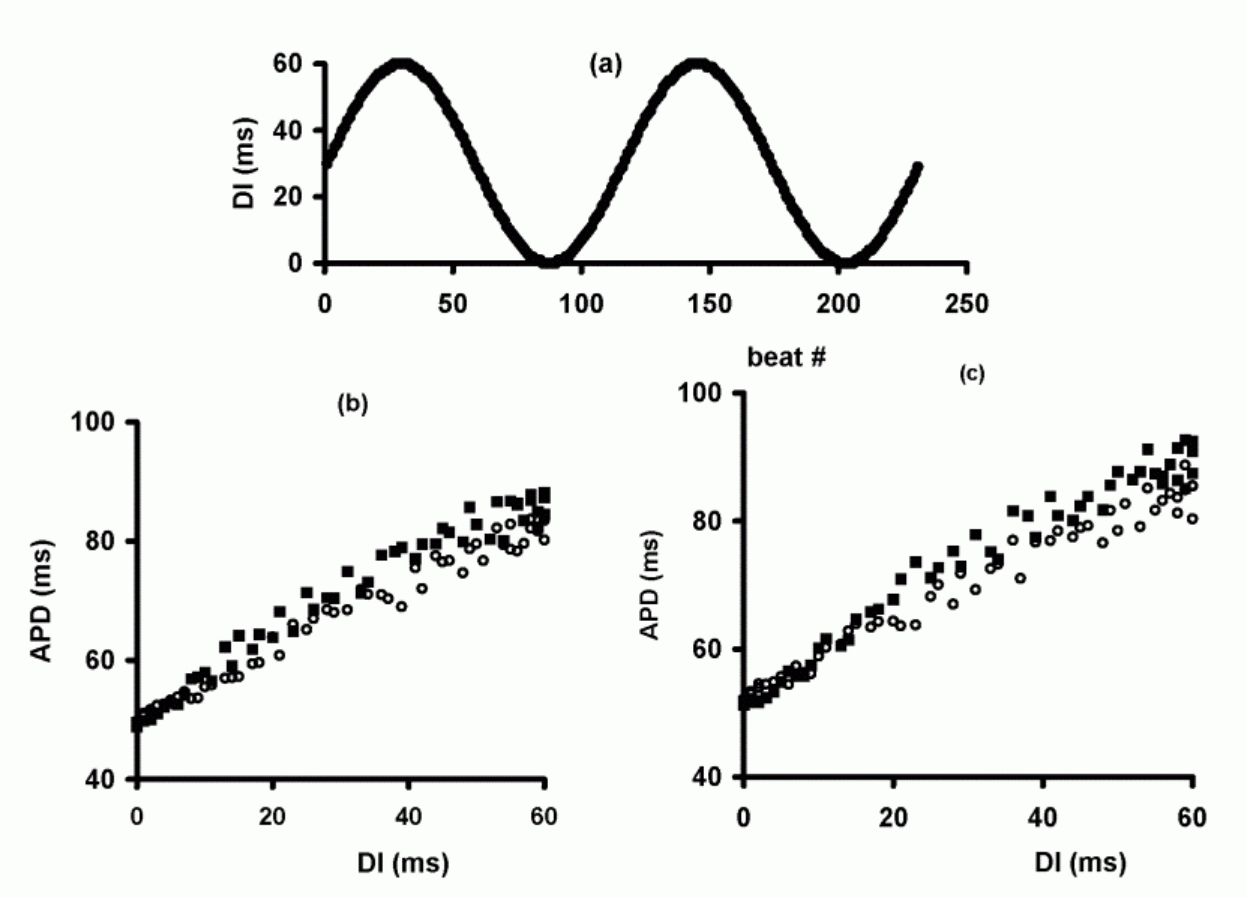

Figure 19. Restitution curve when DI changes from 0 to 60ms in about 57 beats.
In figure (a), the DI changes from 0 to 60ms in about 57 beats. In (b), the cell was paced at 0ms for 250 beats before subjecting to the sequence in (a). In (c), the cell was paced at 30ms DI for 250 beats before subjecting to the sequence in (a).

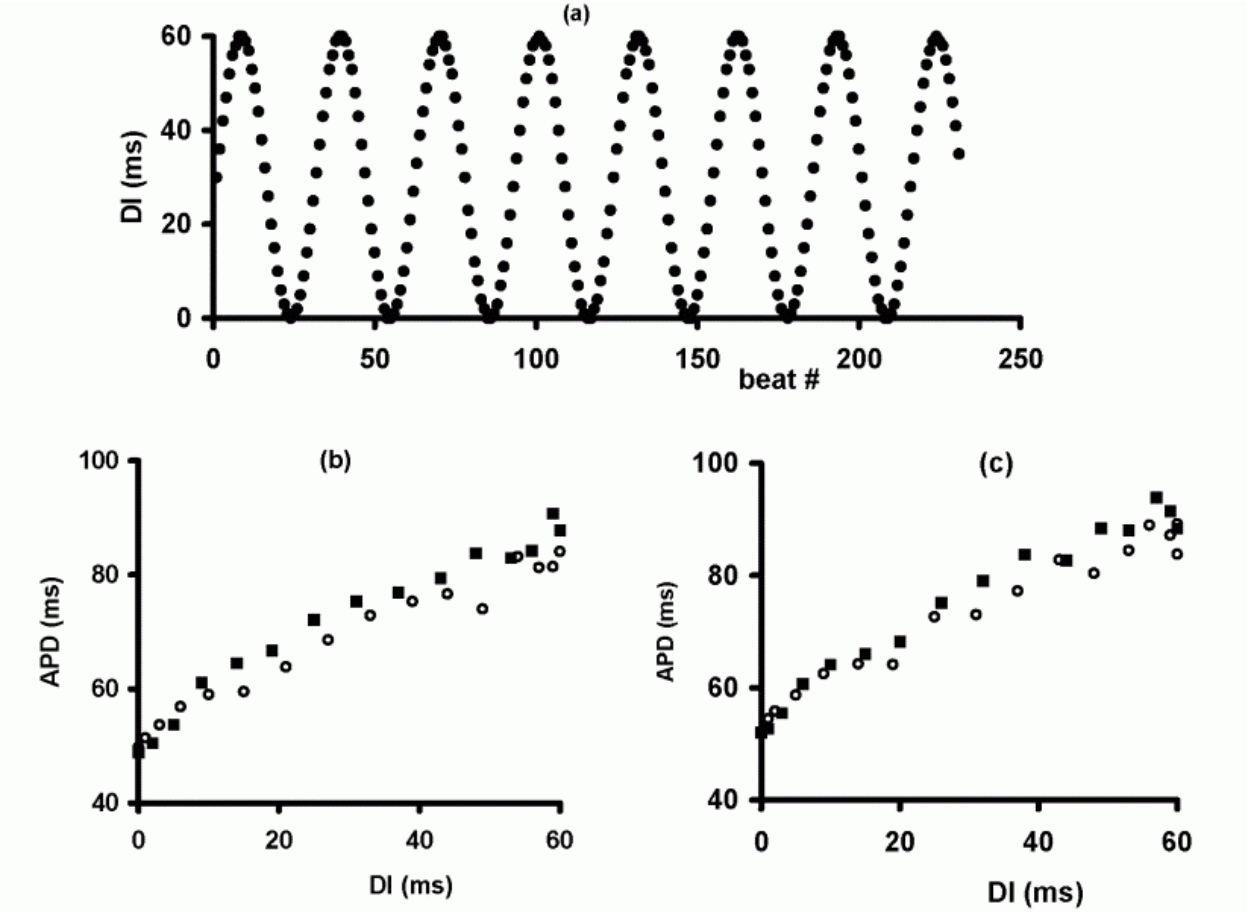

Figure 20. Restitution curve when DI changes from 0 to 60 ms in 14 beats.
(a). The DI was changed very rapidly, The DI changed from 60ms to 0ms in only about 14 beats. In (b), the cell was paced at 0ms for 250 beats before subjecting to the sequence in (a). In (c), the cell was paced at 30ms DI for 250 beats before subjecting to the sequence in (a). The hysteresis is less apparent in this case as compared to the case of slow DI change.

We also stimulated the cell with a sequence of DI that was uniformly distributed between 0 and 60ms as shown in Figure 21(a). Figure 21(b) is a plot of the resulting restitution curve. It appears from Figure 21(b) that there is not one 'curve' but for any DI several values of APD are possible depending upon previous activation history. For a single LRd cell, we also determined the restitution curve using a slightly modified standard protocol. The cell was paced at a constant DI of 300 ms for 21 beats. The 22nd pulse was delivered after a variable DI. The variable DI was gradually reduced from 300 ms down to 0 ms. From 300 ms to 60 ms, the DI was reduced in steps of 20 ms. From

60ms down to 30 ms, the DI was reduced in steps of 3 ms and from 30 ms to 6 ms the DI was reduced in steps of 2 ms. From 6 ms to 0 ms, the DI was reduced in steps of 1 ms. Figure 22 shows the restitution curve determined using the standard protocol. The maximum slope of the restitution was 1.42 and occurred in the range of 0 to 10 ms. The slope of the restitution curve determined using the 0 to 20 ms DI was 1.05, still greater than 1.

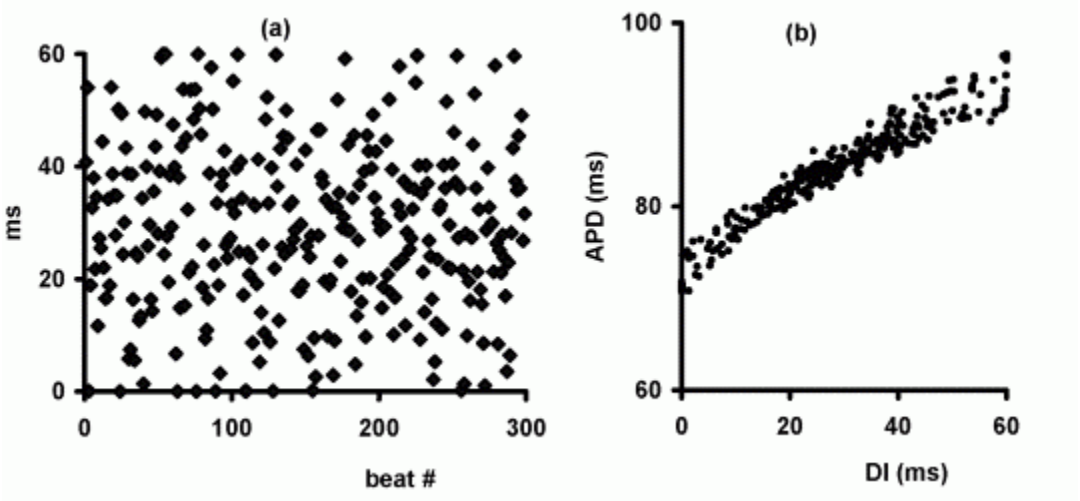

Figure 21. Restitution curve when DI changes randomly.
(a). Random distribution of DI. (b). The APD resulting from each DI. The figure shows that there does not appear to be one restitution curve that relates the APD to a value of DI.

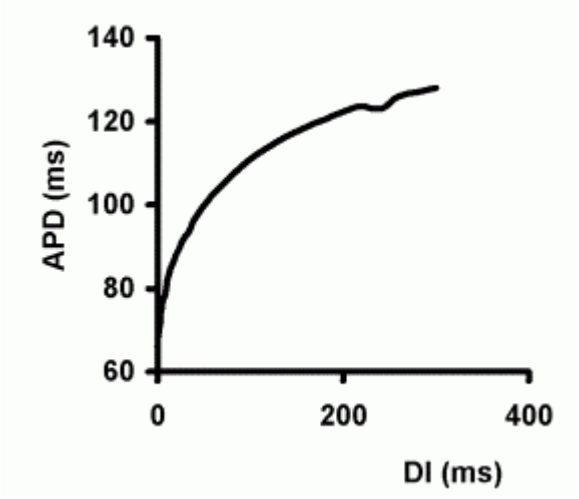

Figure 22. The restitution curve determined by the standard protocol.

Restitution in 2-D matrix of cells

Similar to the simulations with single cell, the cells in the 2-D matrix were stimulated at 0 ms DI for 300 beats and the APD measured on a beat-by-beat basis as shown in Figure 23(a). Figure 23(a) shows the changes in the APD measured at Loc1 (Figure 4), which is a cell that was stimulated. As seen in Figure 23(a), the APD stabilizes by about 150 beats. Figure 23(b) shows the APD changes at Loc2 (Figure 4), which is a cell located 9.8Δx (where Δx is the distance between 2 neighboring cells which are parallel to the edges of the matrix) from the stimulation site. At this site, DI cannot be independently controlled because of the effects of delay due to conduction velocity, and therefore, for each beat we measured the DI as well as the APD. At Loc2 the DI varied between 3 and 5 ms and the APD varied as shown in Figure 23(b). As shown Figure 23(a), the APD becomes stable after about 150 beats, however, the value of APD is shorter than that at Loc1, although the corresponding DIs at Loc2 are longer. This shows that there was less shortening at the stimulus sites as compared to the sites that were away from the stimulus sites.

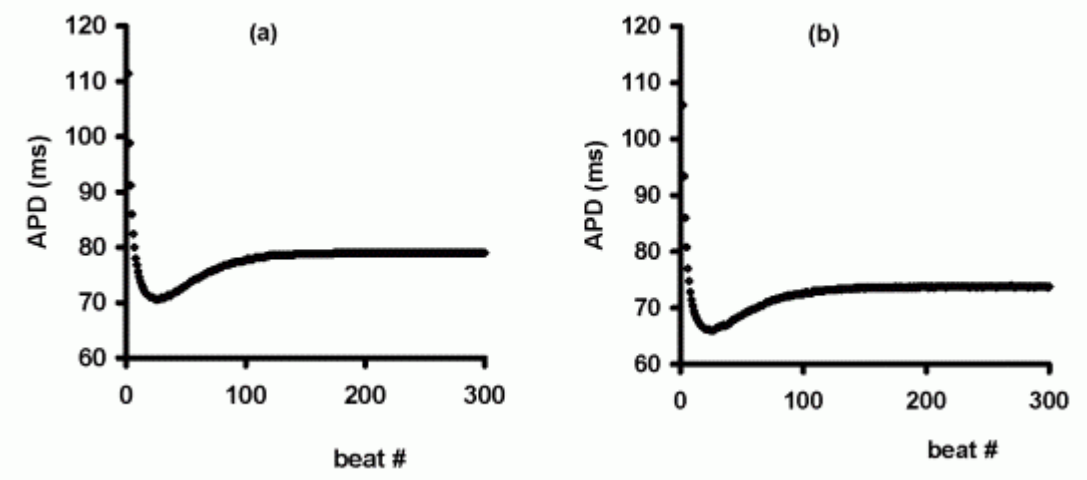

Figure 23. APD changes at constant DI in a 2D LRd matrix at the stimulating cell.
The figure shows how the APD changes with beat number at constant DI in a 2-dimentional matrix, (a) when the recording cell is the same as the stimulating cell (a) and, (b) the recording cell is far away from the stimulating cell. The cell was stimulated while maintaining the DI constant to 0 ms.

We also studied the effect of repeatedly stimulating the matrix of cells at 30 ms. As seen in Figure 24(a), the APD stabilizes after more than 250 beats. Thus, with a longer DI, the APD takes longer to stabilize. As in the case of 0 ms DI (Figure 23a), the

DIs at Loc2 were longer than the DIs at Loc1, however, the APDs at Loc2 were shorter than the APDs at Loc1.

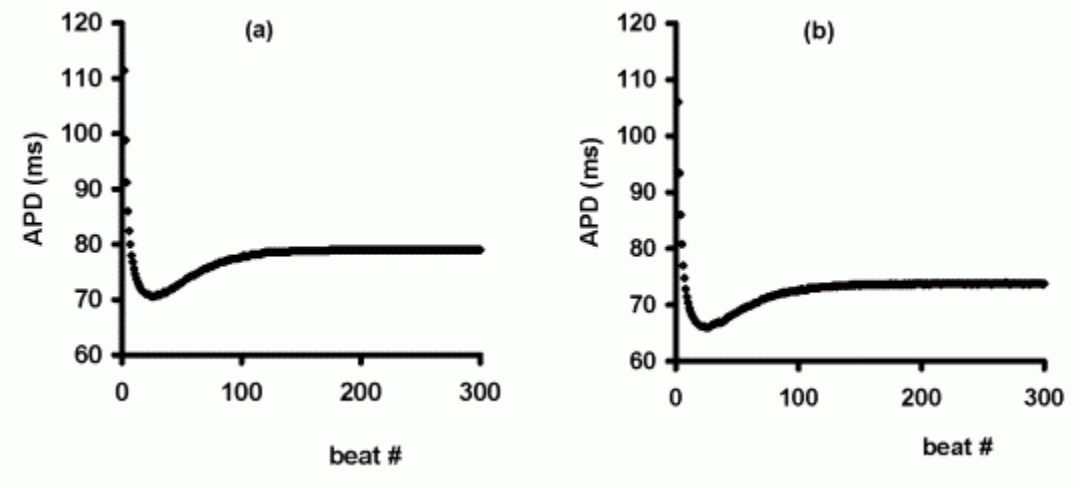

Figure 24. APD changes at constant DI in a 2D LRd matrix away from stimulating cell. The figure shows how the APD changes with beat number at constant DI in a 2-dimentional matrix, when the recording cell is the same as the stimulating cell, figure (a); and the recording cell is far away from the stimulating cell; figure (b). The cell was stimulated while maintaining the DI constant to 30 ms.

Before subjecting the cells to the sequence of DIs, the cells were stimulated at 0 ms DI for 150 beats. Figure 25(a) show the restitution curve at Loc1 when the DIs were increased from 0 to 60 ms in 116 beats (solid squares) and were followed by a DI decrease to 0 ms in another 115 beats (hollow circles). Although the cellular model was similar, these results were remarkably different than those obtained during single-cell stimulation. For DIs between 0 ms and approximately 30 ms, the APDs during increasing DI were larger than the APDs for the corresponding decreasing DIs. This is in contrast to what is observed when a single isolated cell is stimulated. For DIs greater than 30 ms, however, the behavior of the restitution curve is similar to that in the case of a single isolated cell, namely, the APD during increasing DI is smaller than the APD during the decreasing DI when the DI decrease is followed by a DI increase. Figure 25(b) shows the restitution curve at Loc2. The shortest APD measured at Loc2 is the APD corresponding to (an uncontrolled) shorted DI of about 3 ms and is the shortest APD measured at Loc 1 corresponds to a (controlled) shortest DI of 0 ms.

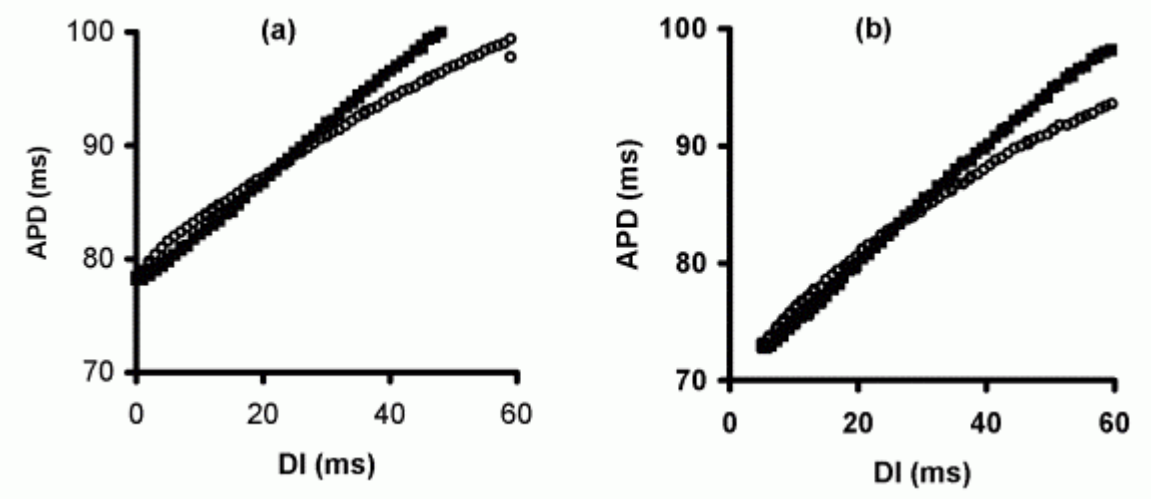

Figure 25. Restitution curves in a 2D matrix when the DI was decreased from 0 to 60 ms in 116 beats.

Restitution curves when the DI was decreased from 0 to 60 ms in 116 beats (solid squares) followed by a decrease in DI from 60 to 0 ms in 115 beats (hollow circles). (a) is for the cell at the stimulus location and (b) is for the cell at a remote location.

We also tested our model for a random variation in DI. The DIs were generated as random variable between 0 and 60 ms with a uniform distribution of DI similar to the one used for single cell. The restitution curve resulting from the stimulation of cells with a random DI is shown in Figure 26(a) and (b). For the DIs that are less than 20ms, the variation in APDs for the same DIs is very small. As the DI's increase, the variation in APDs for the same DI's progressively increases. Figure 26 suggests that there may not be 'one' restitution curve during VF in a connected tissue as seen in a single cell. We further increased the frequency with which the DI changed so that the DI changed from 0 to 70ms in 17 beats (Figure 27) and also varied DI randomly, the results are shown in Figure 28. As in the case of Figure 26 there appear to more than one restitution curves.

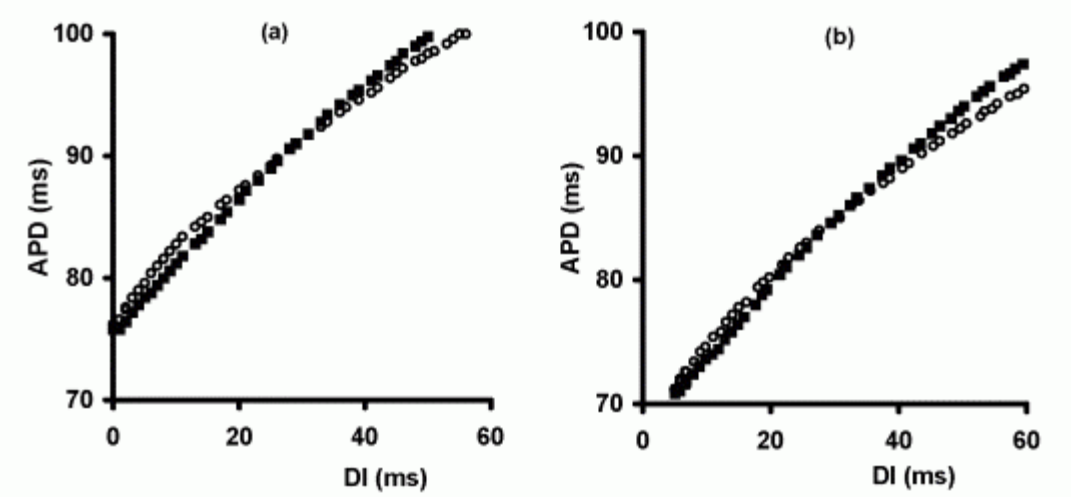

Figure 26. Restitution curves in a 2D matrix when the DI was decreased from 0 to 60 ms in 60 beats.

Restitution curves when the DI was decreased from 0 to 60 ms in 60 beats (solid squares) followed by a decrease in DI from 60 to 0ms in 60 beats (hollow circles). (a) is for the cell at the stimulus location and (b) is for the cell at a remote location.

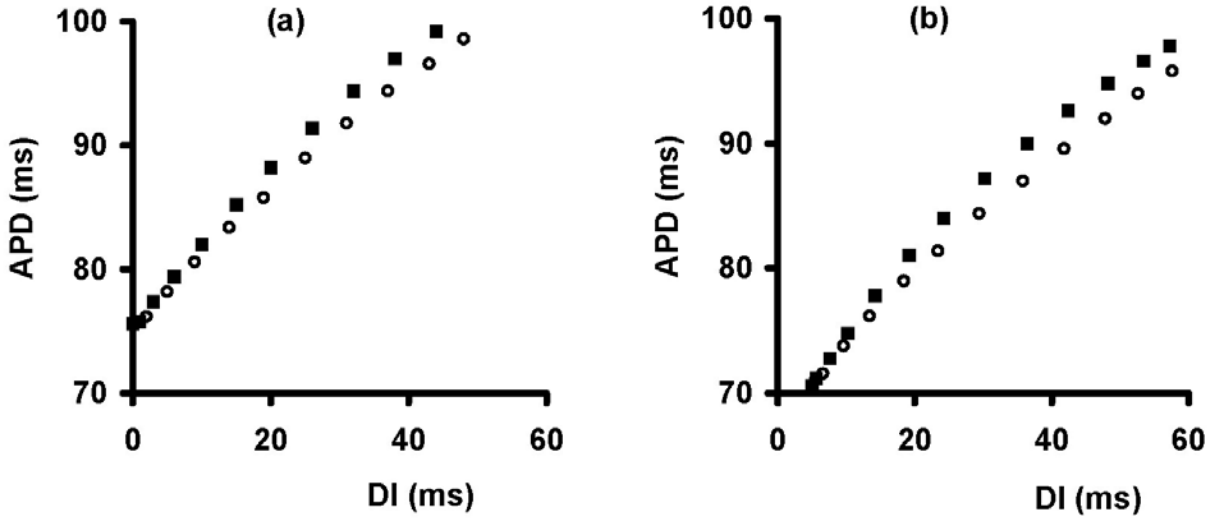

Figure 27. Restitution curves in a 2D matrix when the DI was decreased from 0 to 60 ms in 17 beats.

Restitution curves when the DI was decreased from 0 to 60 ms in 17 beats (solid squares) followed by a decrease in DI from 60 to 0ms in 17 beats (hollow circles). (a) is for the cell at the stimulus location and (b) is for the cell at a remote location.

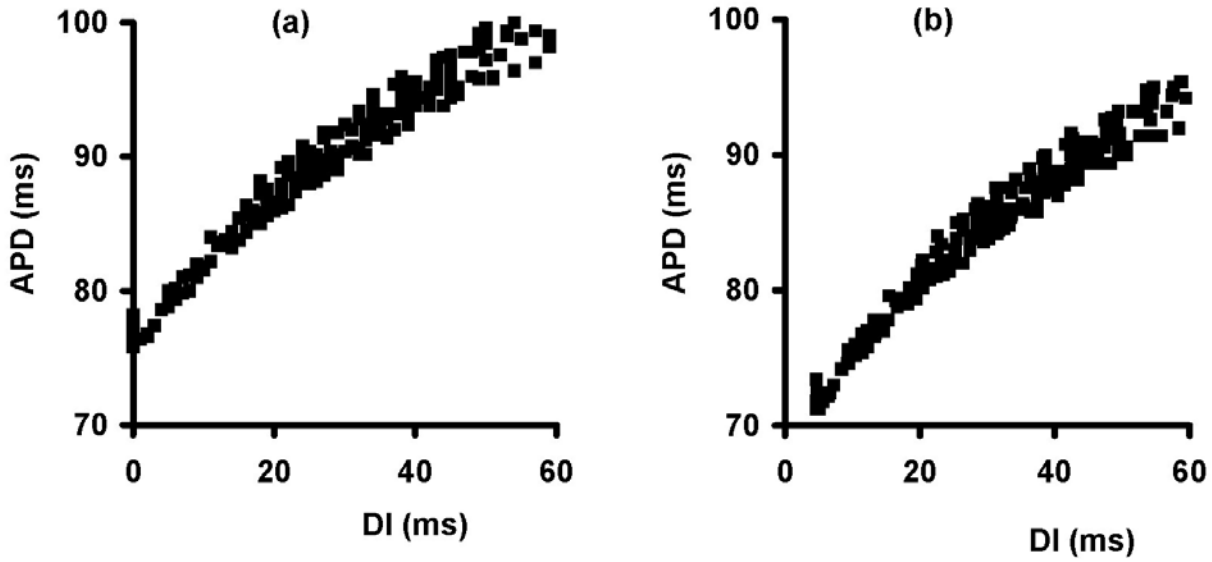

Figure 28. Restitution curves in a 2D matrix when the DI was changed randomly. Restitution curves when the diastolic interval was varied randomly between 0 and 60 ms. The restitution at a stimulus location is shown in (a), and the restitution at Loc2 is shown in (b).

Preliminary results from validation of control of DI procedure

As stated previously we conducted experiments using isolated rat hearts to demonstrate that control of DI procedure can be implemented experimentally. We recorded stable transmembrane recordings in multiple trials, which ranged in duration from a few seconds to ten seconds. Figure 29 shows a small section of stable transmembrane recording between 0 and 2 seconds. When recording, the action potential amplitude was close to 70mv and the APD was almost 90ms; both values being very close to normal values for rat [Clark 93].

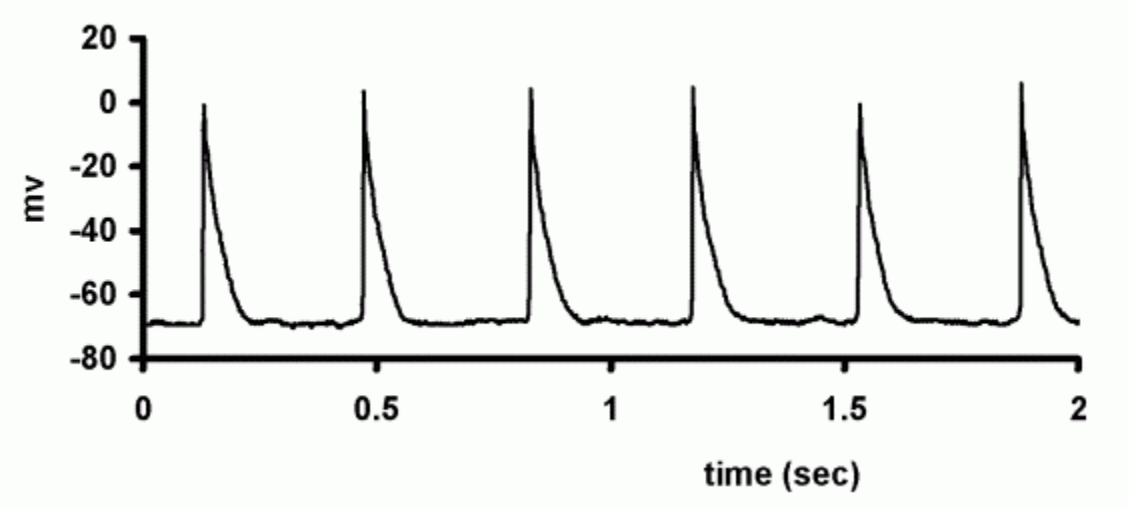

Figure 29. Example of a stable transmembrane recording.

We then used our technique to control DI independently. The offset on the amplifier was adjusted so that the baseline of the transmembrane voltage was about –70mv. The threshold for APD_{90} was set to –65mv so that the intended DI time for each was started as soon as the voltage repolarized to less than –65mv. Figure 30(a) shows a slow variation in DI, such that the DI was intended to reduce from 60ms to 10ms in approximately 10 beats. The resulting DI (due to the delays because of conduction velocity), which we refer to as the physiological DI were computed off-line after the trial was recorded. Figure 30(b) shows how the physiological DI (filled squares) compared with the intended DI (hollow circles). As seen in the figure, the physiological DI is larger than the intended DI. This is due to the delay between the stimulus and the phase-0 of the action potential. Contrary to what was expected based on the restitution function,

the APD increased during the first 116 beats (Figure 30(c)) although the DI were decreasing. Figure 30(d) shows how the delay changes when the intended DI increases. At low DIs (10-20ms), the delay is longer than at longer DIs (50-60ms). Figure 31 (a) shows another case when the DI was changed sinusoidally. In this case, the intended DI was changed from 10 to 48 ms sinusoidally such that there were about 4 cycles of DI variation in 231 beats. As before, we were able to control the DI satisfactorily, except for the delay between the end of stimulus and beginning of phase-0 of the action potential. As before, the delay is longer when the DI is short and the delay is shorter when the DI is long as seen in the Figure 31(b).

We were able to capture the tissue for times ranging from 5 sec to 25 sec. In Figure 32(a) a section of recordings from one of the trials is presented that showed relatively longer stable recording. Prior to the stimulation, a stable transmembrane recording was obtained for about 11 seconds. The transmembrane voltage during this period was about 45 mv in amplitude. This value of action potential amplitude is less than that observed in a rat myocytes by us and other investigators and is most likely a consequence of lower electrode resistance. Although the absolute value of the voltage was somewhat lower, this example illustrates that the technique of controlling the DI independently works satisfactorily. Figure 32 (b) shows the zoomed in capture section from Figure 32 (a).

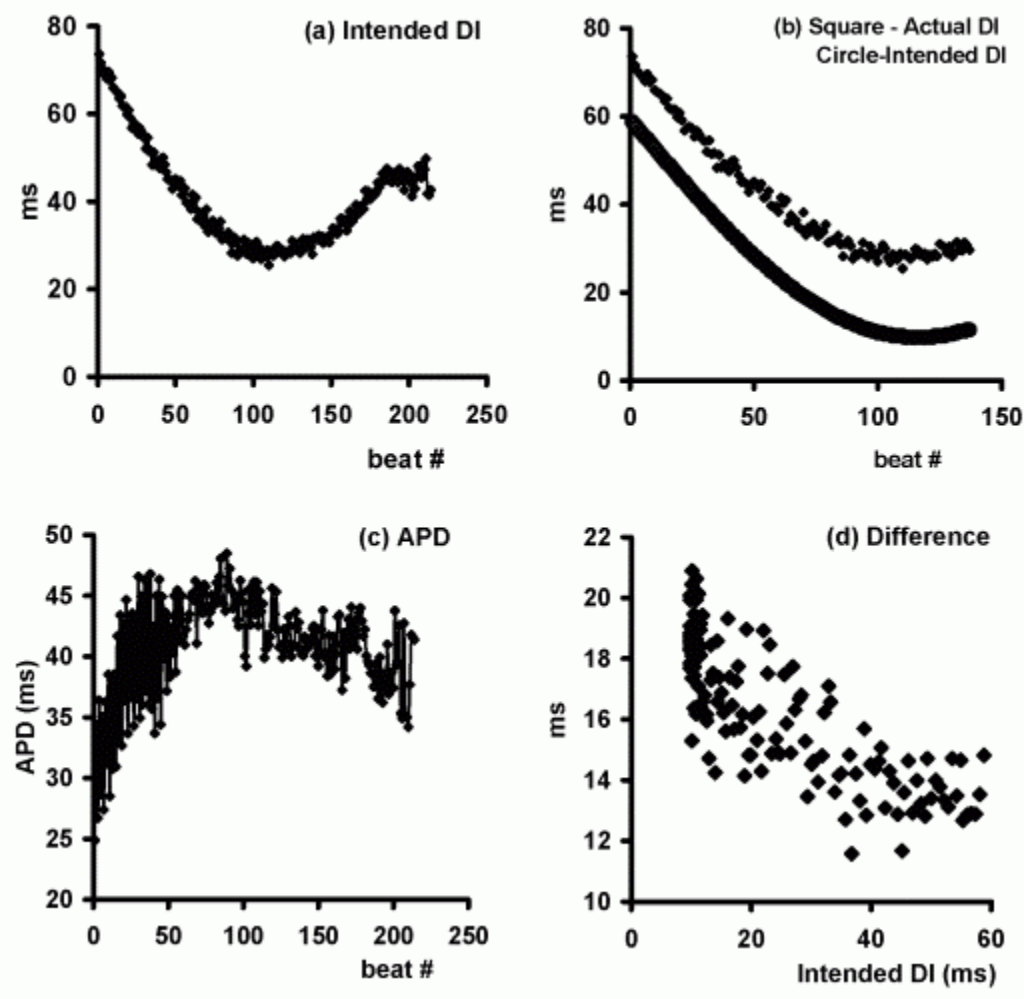

Figure 30. Intended DI and actual DI in rat experiments.
(a). Intended DI for about 220 beats. (b). Actual DI, represented by squares, that was recorded for 150 beats and intended DI, represented by circles. (c) APD recorded for the first 220 beats. (d). Difference between actual DI and intended DI, both plotted in (b).

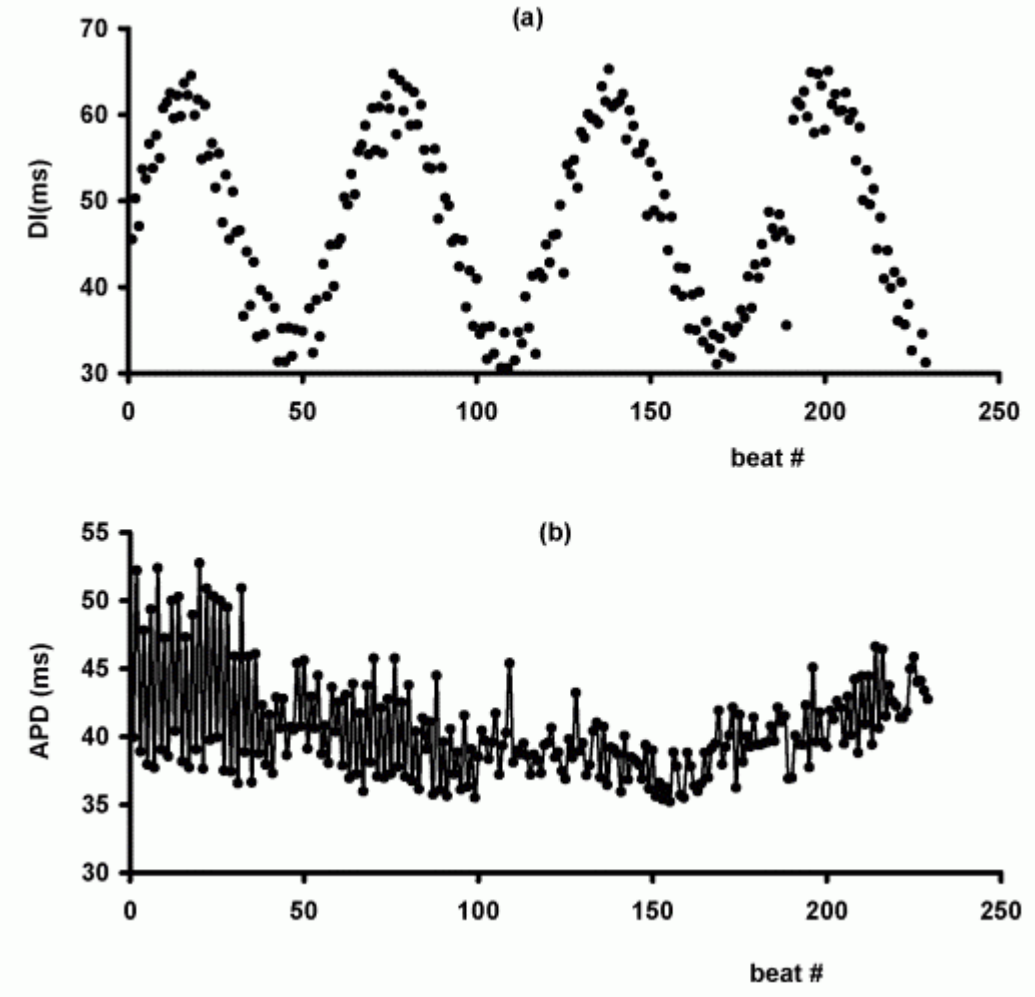

Figure 31. Intended and actual DI in rat experiments for fast change in DI.
(a). The curve with filled squares indicates the actual DI and the curve with hollow circles represents the intended DI. (b). The difference between the actual and intended DI on a beat-by-beat basis.

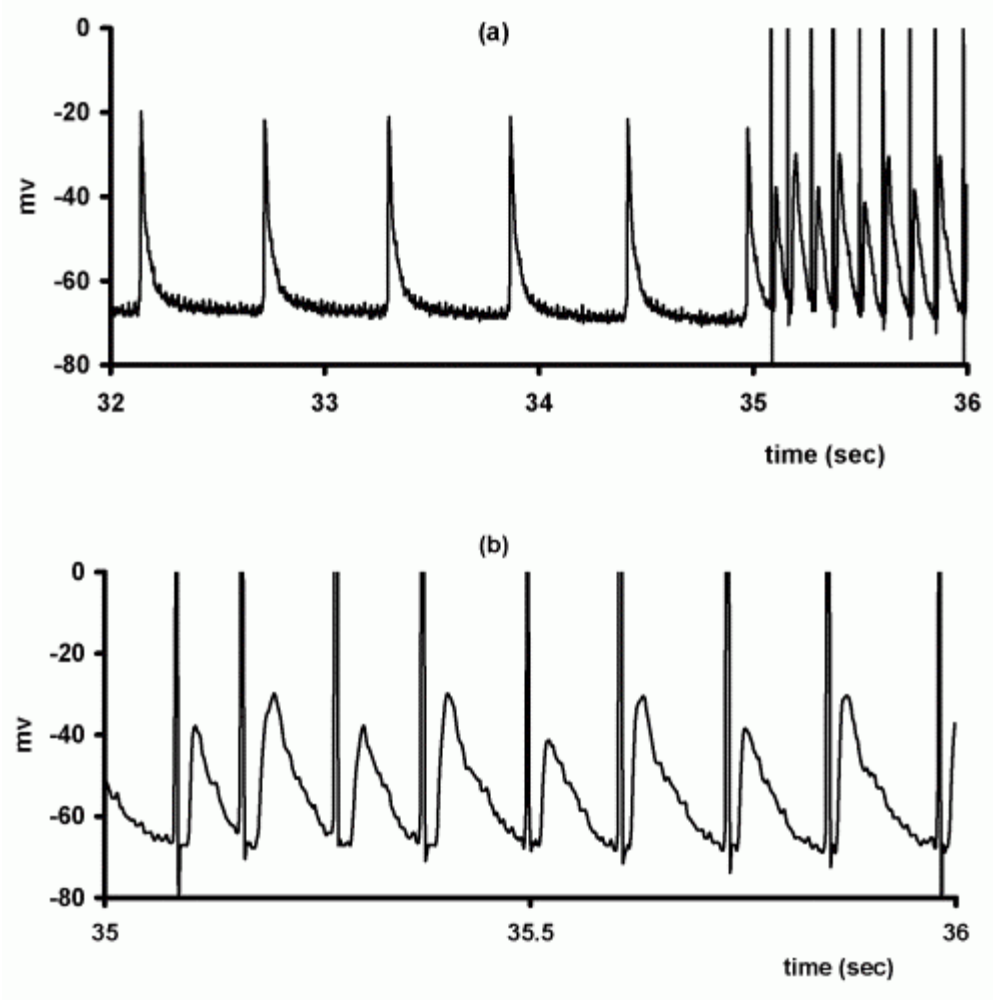

Figure 32. Capture during a trial in rat experiment.
(a). A section of recording showing a trial that illustrates capture by pacing stimuli. (b). Zoomed in display of the last 1-second of the signal in (a).

Entrainment of VF

Determination of parameters that affect entrainment

In order to perform the entrainment simulations we quantified several parameters viz. conduction velocity, diastolic threshold, shortest cycle length during VF without stimulation, and the mean cycle length. Estimates of conduction velocity and diastolic thresholds were determined in small size of matrices (without VF). Our assumption is that the conduction velocity and diastolic threshold values determined under non-VF conditions will be valid for the tissue when VF is simulated. In real VF this is not necessarily the case, but determining conduction velocity and diastolic threshold during VF is a difficult task.

Conduction velocity

Conduction velocity was determined by initiating a planar wavefront in a 50x50 matrix of cells. A patch of 10x50 cells was stimulated so that the wavefront propagated from one end of the matrix to the other. Transmembrane voltages were stored at two cells separated by 25 cells (25*0.025cm=0.625cm) in the direction of travel. The conduction velocities were estimated for various values of g_{Na} because of its dominant effect of rate of change of voltage during the Phase 0 of the action potential. This rate of change of voltage primarily determines the conduction velocity. The estimate of conduction velocity corresponding to g_{Na}=23.0 will be used to determine the delay between the adjacent stimulators.

Table 5. Dependence of conduction velocity on Na^+ conductance.

g_{Na}	CV (m/s)
18.0	0.570
19.0	0.620
20.0	0.628
21.0	0.636
23.0	0.643

Diastolic threshold for pacing stimulus strengths

We estimated the diastolic threshold for simulated tissue for various sized of stimuli. For all simulations, the matrix size was 50x50 cells and the membrane parameters for the LR cell were as shown in Table 6.

Table 6. Summary of parameters used in the LR model.

LR cell parameter	**Value**
C (Capacitance)	1.0μF
g_{Na} (Sodium Conductance)	23.0
g_K (Potassium Conductance)	0.705
g_{Ca} (Calcium Conductance)	0.07
K_o (Extracellular Potassium)	5.4
K_i (Intracellular Potassium)	145.0
Na_0 (Extracellular Sodium)	140.0
Na_i (Intracellular Potassium)	18.0
$\Delta x=\Delta y$	0.025
$D_x=D_y$ (Diffusion constant)	0.001

For a small area of 2x2(=4 cells) in the middle of the 50x50 matrix, we were able to initiate a ring wavefront when all the cells in the area were stimulated with at least -60μA/cm^2. As the stimulus area was increased to 4x4 cells, the minimum current needed to induce a wavefront reduced to -25μA/cm^2. In the simulations that we performed, the stimulus strength was determined by two parameters; area of the cells stimulated and the intensity of current injected into the cells due to the stimulus. These diastolic thresholds were, therefore, used to determine stimulus intensities.

In majority of simulations performed in this part of our study we used stimulators, which were 5 cells (1.25% of the tissue width) wide in the row direction of the 400x400 matrix or the 400x800 matrix. The length along the column direction was 300 cells for the 400x400 matrix and 680 cells for the 400x800 matrix. We also measured the diastolic threshold when the length along the column direction of stimulated tissue was increased from 5 to 40 cells. These 5x40 cells simulated a line-stimulating electrode, which was used primarily in our entrainment simulations. Table 7 summarizes the results from

estimation of diastolic threshold simulations. The table shows the area of the tissue that was stimulated and the minimum current needed to initiate a wavefront from that stimulus.

Table 7. Diastolic threshold values for various areas of LR cell matrix.

	Current ($\mu A/cm^2$)		
	Wavefront Generated		
Area	**(No)**	**(Yes)**	**Wavefront type**
2x2	-55	-60	Ring
4x4	-20	-25	Ring
5x5	-18	-19	Ring
5x40	-10	-11	Planar

Initiation and Establishment of VF in the 400x400 Matrix of Cells

For all the entrainment simulations, we used either a 400x400 or a 400x800 matrix of cells. The first step in our simulations was establishing VF in the matrix by using cross S1-S2 stimulation. In a 400x400 matrix, an S1 stimulus was delivered to an area of 5x400 cells along the lower edge of the matrix. This stimulation resulted in a planar wavefront traveling from bottom to top. After 250 ms when the cells in the matrix had partially recovered, an S2 stimulus, which was delivered to an area of 400x5 cells (perpendicular to S1). The interaction of wavefronts produced by S1-S2 stimuli resulted in a reentrant wavefront in about 500 ms. When simulation was continued further, in about 300 ms, the single reentrant wavefront broke-up into several small wavefronts, thus simulating VF. Continuation of simulation for several seconds beyond this time showed that the reentrant activity simulating VF remained stable.

Determination of shortest APD that is possible in VF

In order for us to determine the range of cycle lengths with which each stimulator (row) needs to be paced, we determined the shortest APD that is observed during non-stimulated VF. Transmembrane voltages were recorded during 2 seconds of simulated VF from 18 electrodes located as described in Figure 5. Using these transmembrane potentials, the APD and DI were determined during VF from which the probability distribution was obtained. The probability distribution curves, estimated by using

normalized smoothed histograms showed that the mean CL was about 100 ms and that the CL were distributed somewhat evenly about the mean value although some skewness toward longer CL was observed. These results also show that using 50 ms as an estimate of shortest possible cycle length was reasonable. To optimize the capture we performed simulations at various pacing cycle lengths greater than 50ms up to the mean cycle length of about 100 ms. The distribution of DI in Figure 33(b) shows the highly asymmetrical distribution with the maximum probability at about 5 ms.

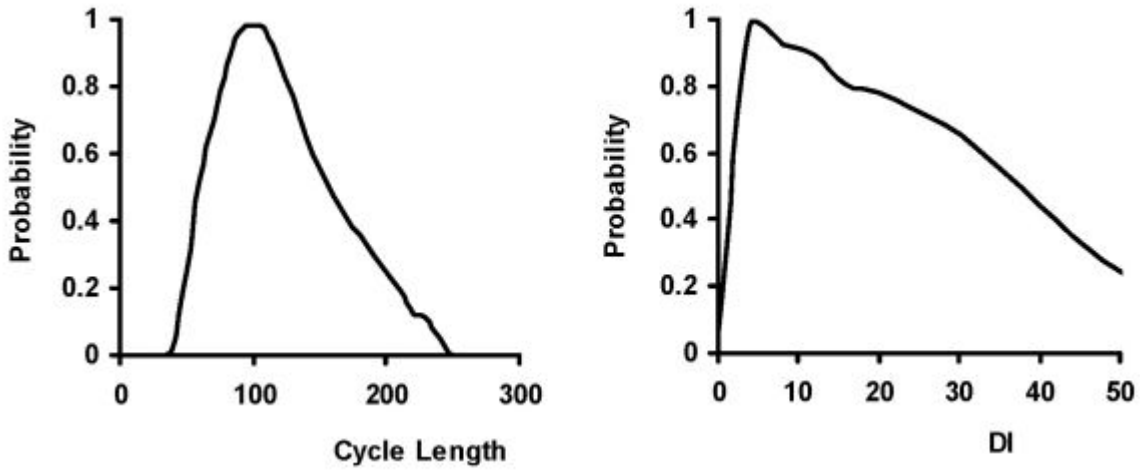

Figure 33. Probability distribution curve for cycle length and diastolic intervals.
(a) Probability distribution of cycle length during 2 seconds of VF. (b) Probability distribution of diastolic intervals during 2 seconds of VF.

Simulation with different cycle lengths

With the spatial arrangement of stimulators described above, we performed stimulation simulations for 2 sec of VF. For the first 500 ms, the cycle length was a constant 55 ms and for the next 1500 ms, the cycle length was 65 ms. We define the latter cycle length as the target cycle length. In different simulations, the target cycle length was changed to 70 ms, 75 ms, 80 ms, 85 ms and 90 ms. The results for variation in cycle lengths that resulted during simulation when the pacing target cycle length was 65ms are shown in Figure 34. These cycle lengths were determined from the 18 recording electrodes described in Figure 5(a). Figure 34 shows broken line for both the 55 ms and the 65 ms (target) cycle length. The cycle lengths that resulted during stimulation are indicated by hollow circles. This figure shows that for target cycle length of 65 ms only two electrodes (e13, e14 in Figure 34(b)) out of the 18 recording

electrodes show capture for time between 4000 and 4500 ms and by changing the target cycle length, it was our goal to maximize the number of electrodes that show capture simultaneously. For example, consider the first electrode e11. The last two cycle lengths, just prior to 5000 ms mark are very close to the target cycle length indicating that capture had taken place. Other electrodes that show capture at the same time instant are e22, e24, and e31. No other electrodes show capture at this time instant indicating that spatio-temporal stimulation was not able to modify the activation patterns during VF. What we learn from this simulation is: at several sites such as e13, e14, e16, e23, e24, e33, e35 and e36, the CL recorded is almost twice that of the target cycle length indicating that alternate stimuli were blocked and did not generate an action potential. This prompted us to increase the target cycle length. Increasing the target cycle length by large quantities would not be helpful because a very long target cycle lengths would allow for captured areas to repolarize and hence allow for the native VF activations to invade again.

We show here the results when the target cycle length was 85 ms. This simulation shows us the best overall capture of all the different cycle lengths. One of the remarkable improvements by increasing the target cycle length is evident in electrode e15 of Figure 35(c). In the simulation with CL 65ms, between time 3500 and 4500ms, electrode e15 shows CLs which are about 130ms which are twice of the target cycle length (Figure 34(c)). Whereas, in the simulation with CL 85ms, between time 3500 and 4500ms, electrode e15 shows CLs which are almost equal to the target cycle length indicating that the site was captured for almost 1000 ms (Figure 35(c)). A side-by-side comparison of the plots in Figure 34(c) and Figure 35(c) is shown in Figure 37. A similar observation is seen in electrodes e16, e31 and e32 in Figure 34 and 35. As we increase the target cycle length to 95ms (Figure 36), the incidence of capture decreases. Later on, we will show that when the matrix size in increased, the stimulation at 95 ms gives better entrainment than the stimulation at 85ms.

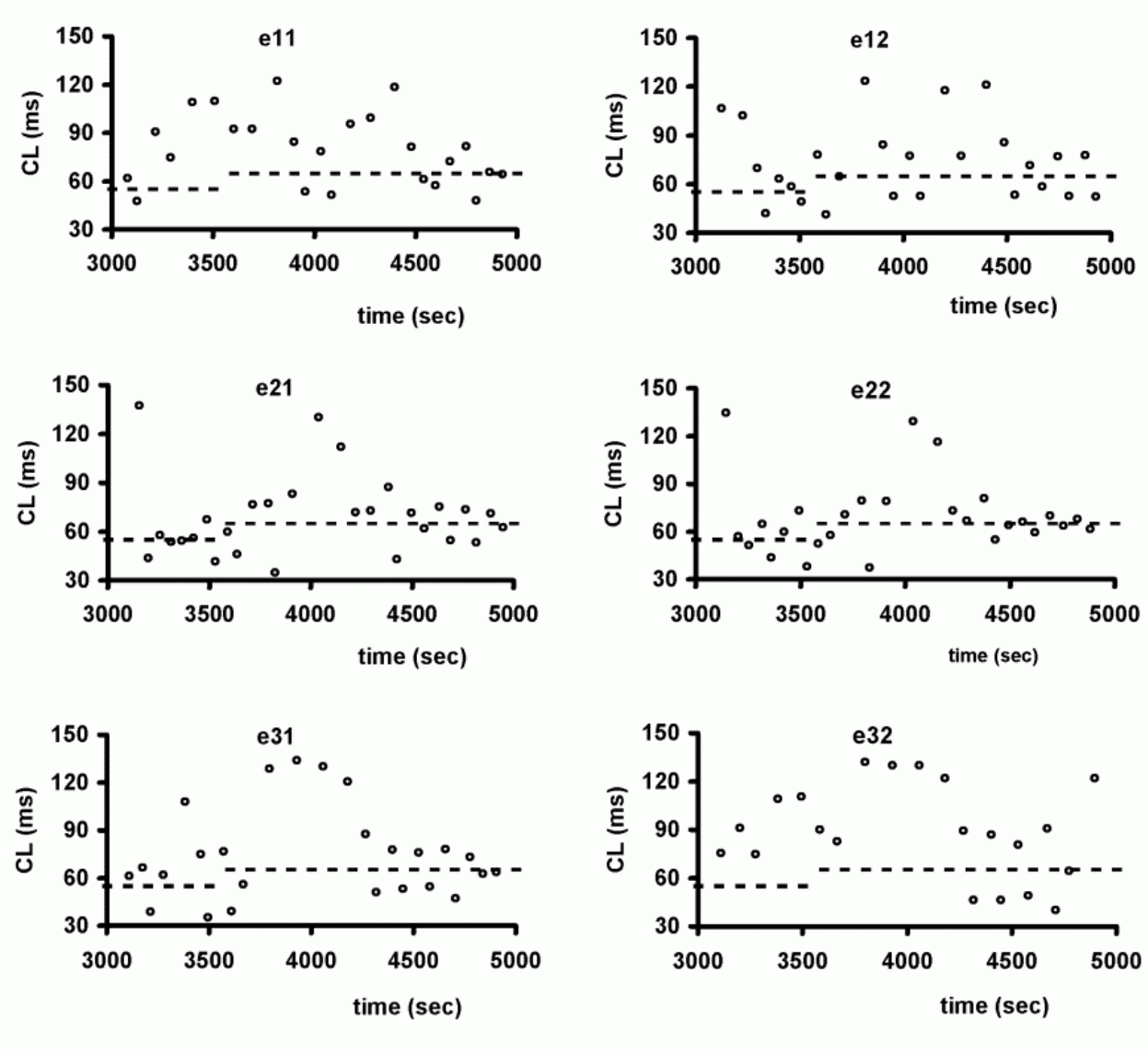

Figure 34a. Cycle lengths for 1st, 6 of 18 electrodes during 65ms target cycle length.

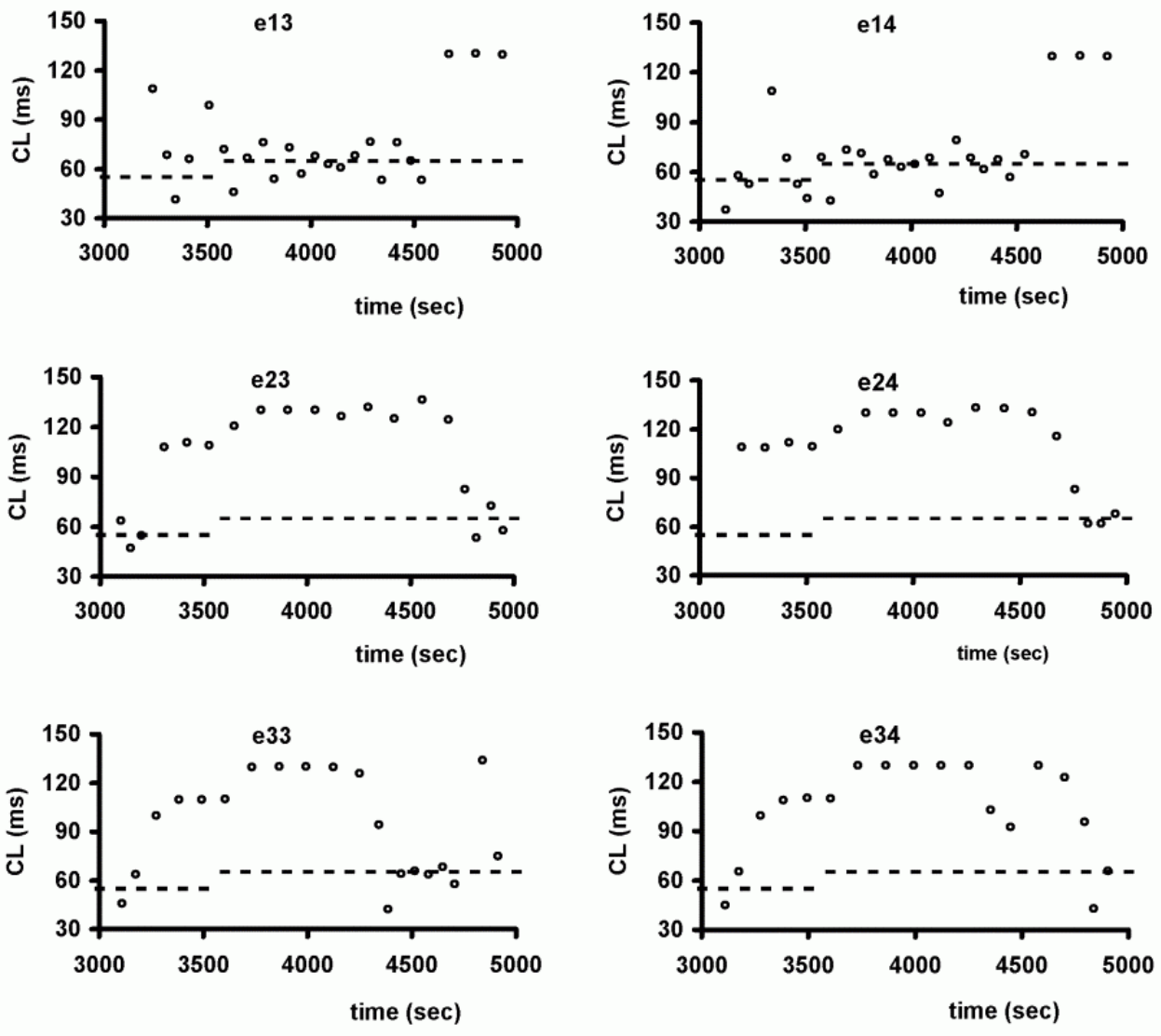

Figure 34b. Cycle lengths for 2nd, 6 of 18 electrodes during 65ms target cycle length.

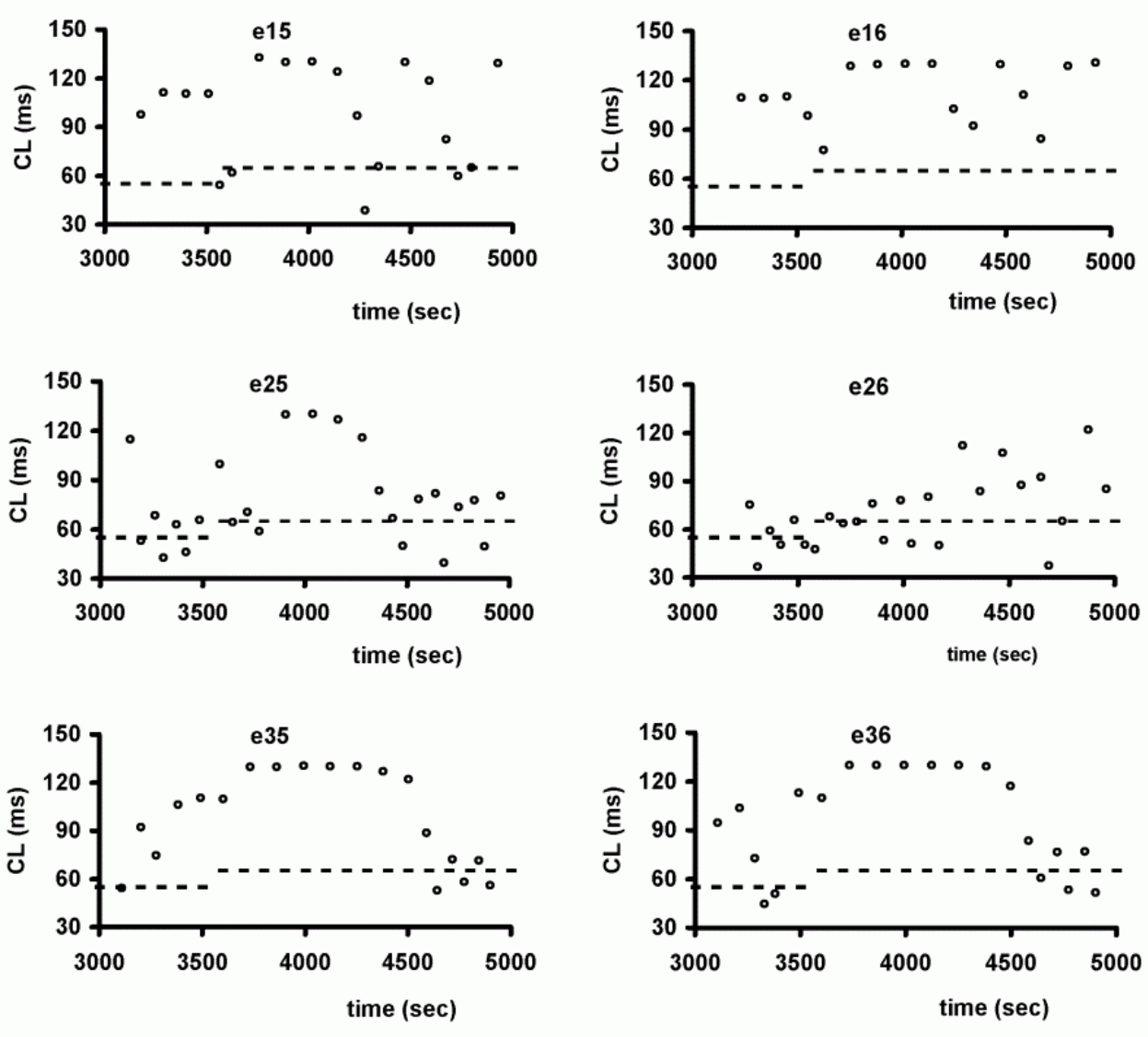

Figure 34c. Cycle lengths for 3rd, 6 of 18 electrodes during 65ms target cycle length.

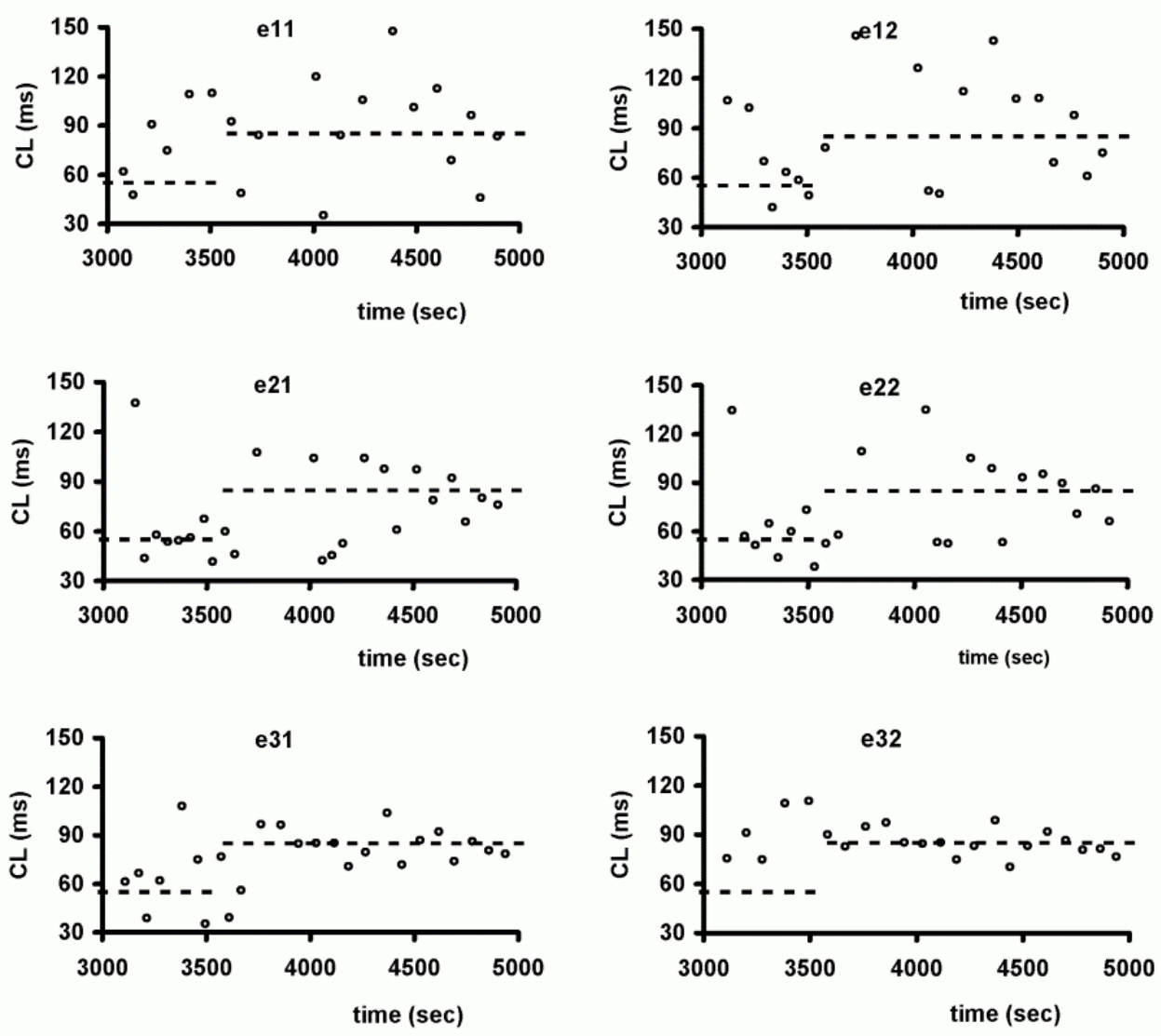

Figure 35a. Cycle lengths for 1st, 6 of 18 electrodes during 85ms target cycle length.

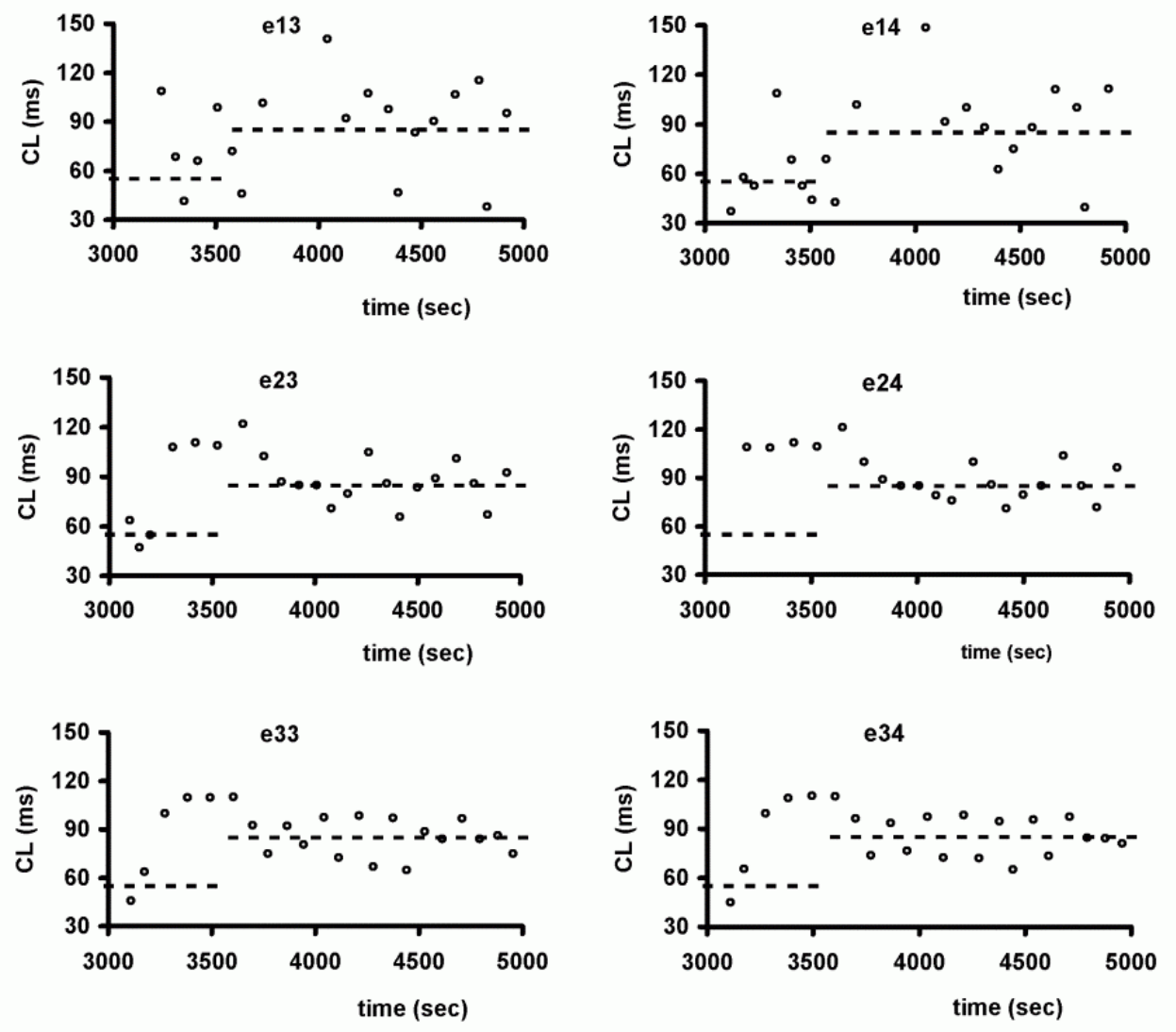

Figure 35b. Cycle lengths for 2nd, 6 of 18 electrodes during 85ms target cycle length.

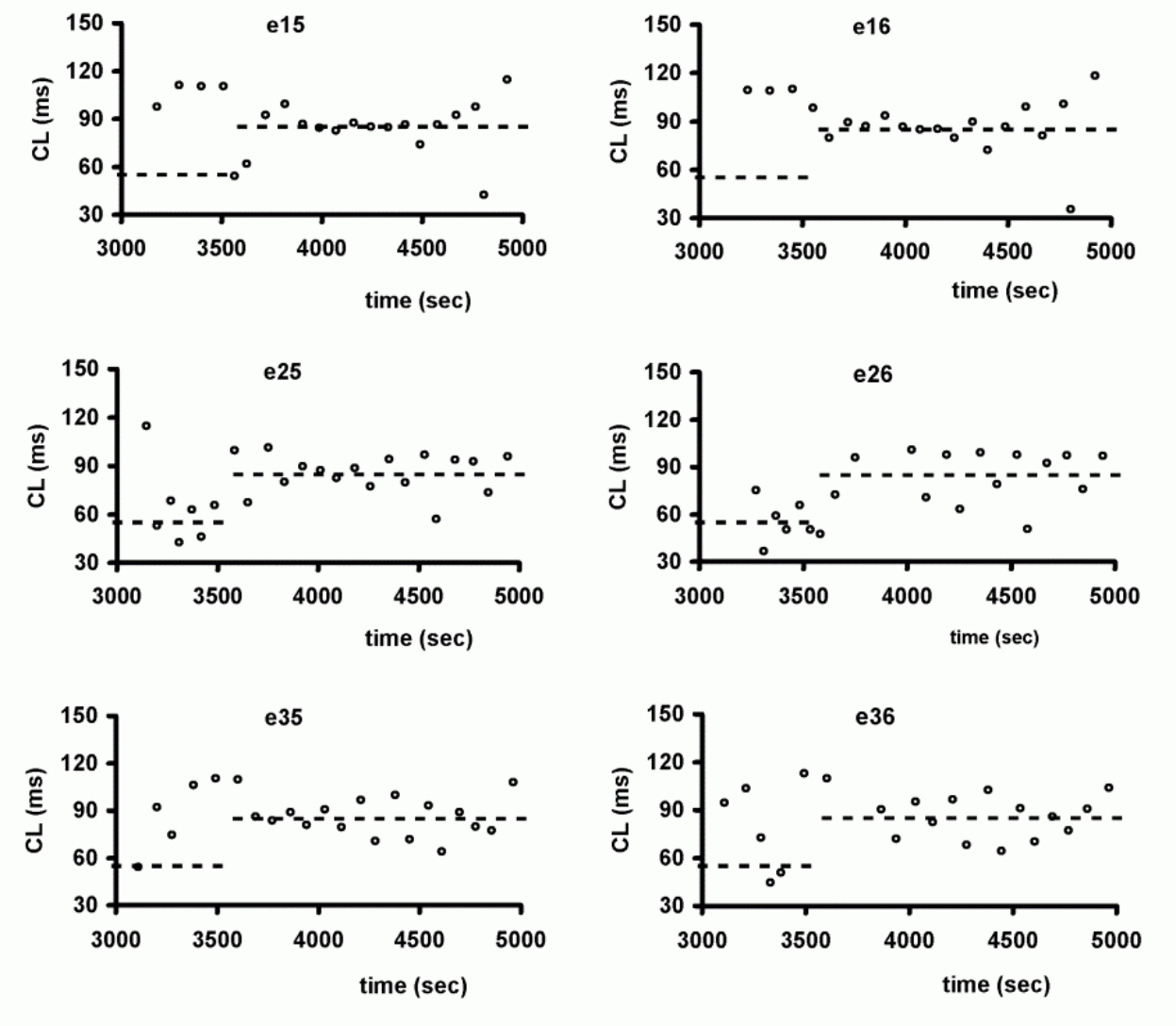

Figure 35c. Cycle lengths for 3rd, 6 of 18 electrodes during 85ms target cycle length.

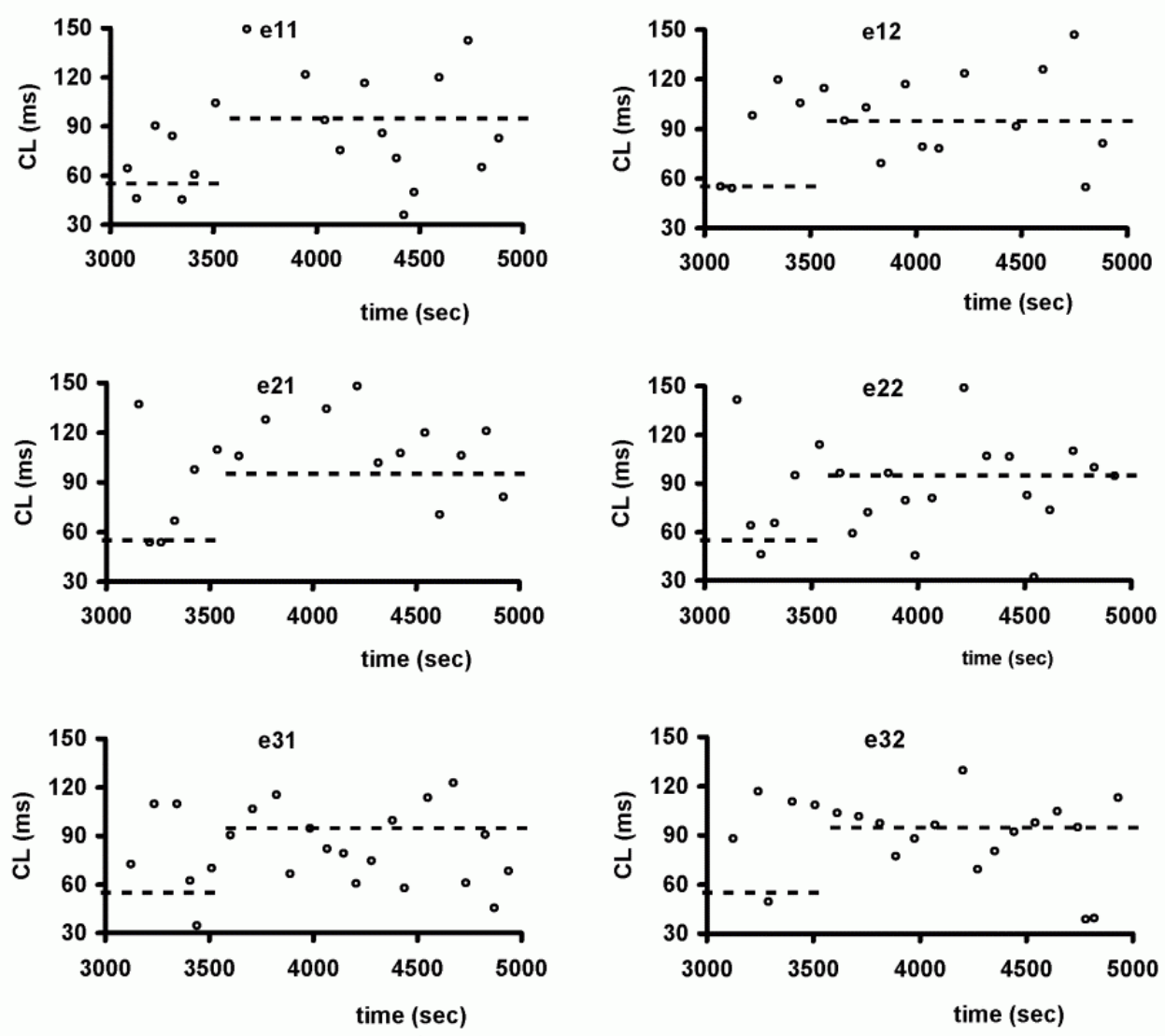

Figure 36a. Cycle lengths for 1st, 6 of 18 electrodes during 95ms target cycle length.

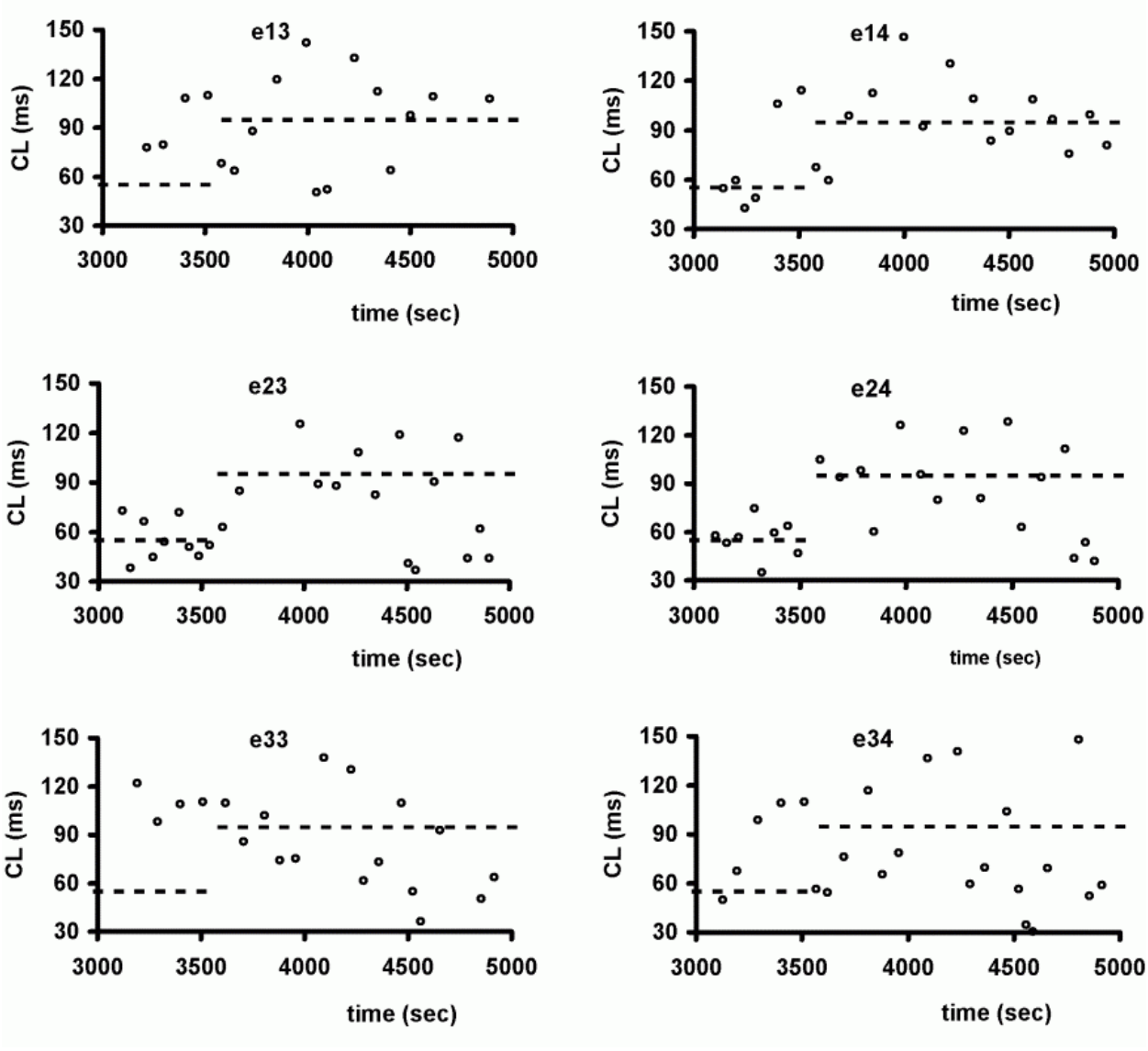

Figure 36b. Cycle lengths for 2nd, 6 of 18 electrodes during 95ms target cycle length.

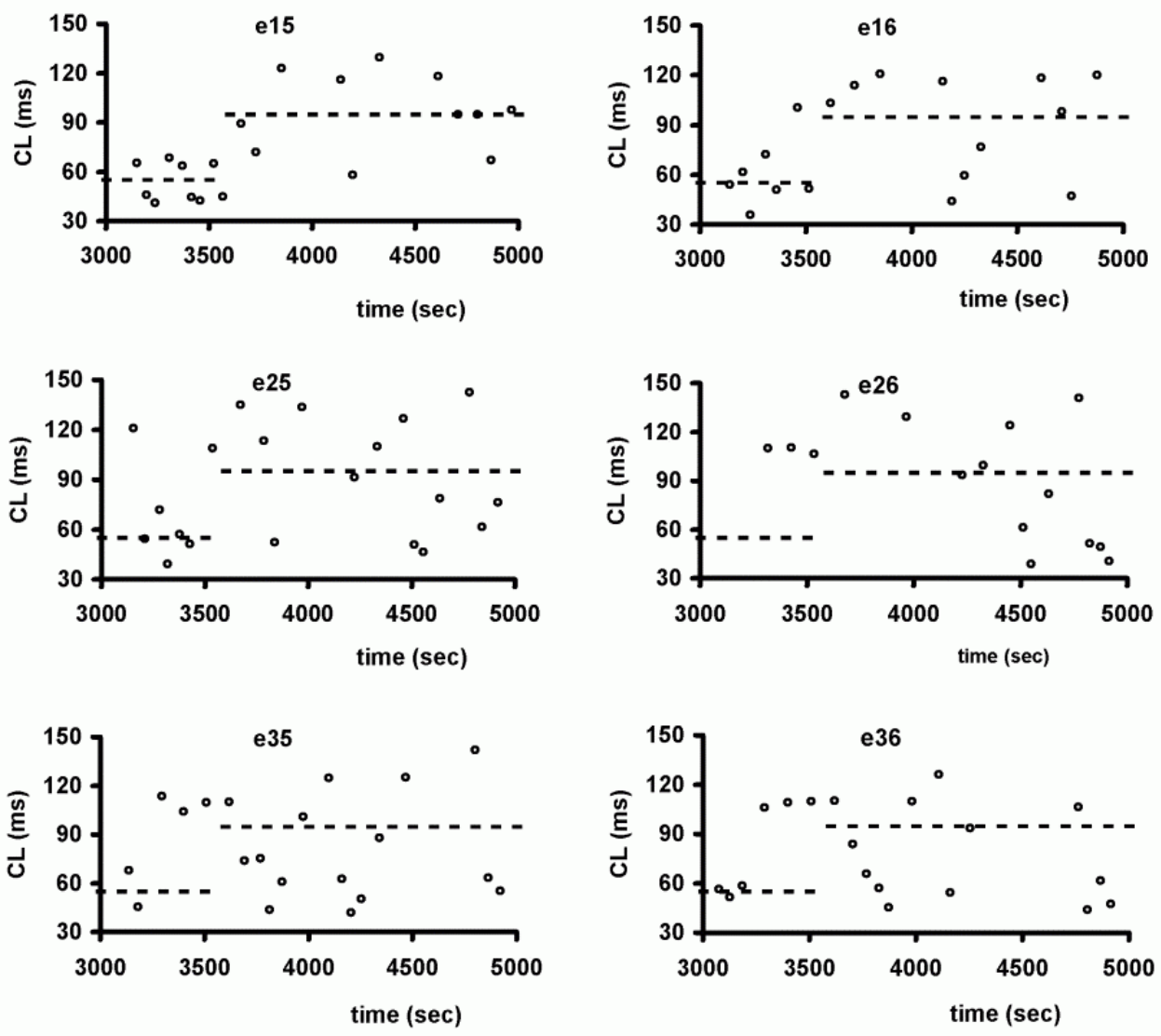

Figure 36c. Cycle lengths for 3rd, 6 of 18 electrodes during 95ms target cycle length.

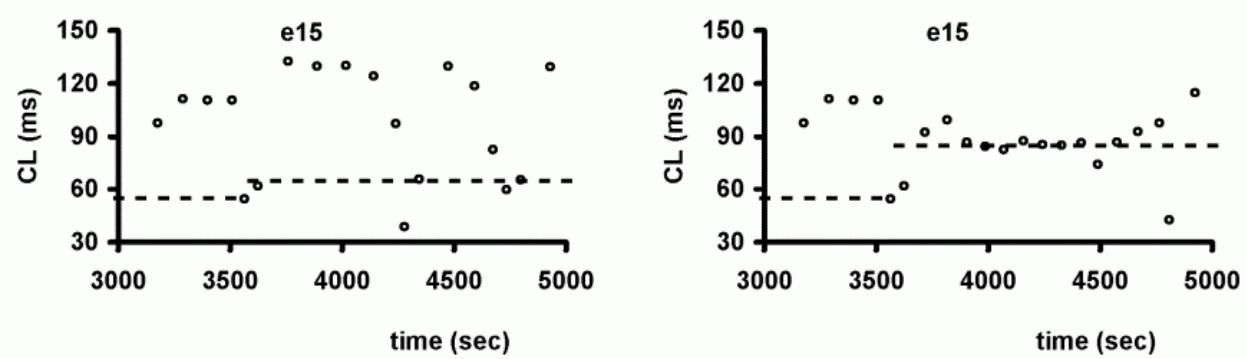

Figure 37. Comparison of actual cycle lengths in one electrode when the target cycle length was 65 ms and 85ms.
Actual measured cycle length at the electrode e15 when the target cycle length was (a). 65ms an when the target cycle length was (b) 85 ms. The CL in (b) between 3500 and 4500 ms was much closer to the target cycle length in (a).

We have included three movies (AVI files) for 1000 ms of VF simulation. Movie 1 is 1000ms of simulated VF without any stimulation. Movie 2 is 1000 ms of simulated VF with 65 ms target cycle length and Movie 3 is 1000 ms of simulated VF with 85 ms target cycle length. White areas in the movie show the depolarized wavefront and black areas in the movie show the repolarized tissue. For the sake of optimizing display performance, the matrix displayed is 200x200 cells; representing every other cell in the original 400x400 matrix. We stored transmembrane voltages from each cell in the matrix every 10 ms. Therefore, for 1000 ms of simulation we have 101 frames. The movie files will display at the rate of 2 frames per second, therefore the total display time for each movie will be 50.5 seconds of real time. As stated before, this display time represents one second simulated VF. The movie shows that the target cycle length of 65 ms was faster than optimal because the stimuli can be seen to occur before the tissue has had a chance to repolarize from activations due to the earlier stimuli. This incomplete recovery resulted in a block and is evident in the movie at 8 sec time instant (Time instances can be seen when playing the movie using the Windows Media Player). Based on these results, we increased the target cycle length in steps of 5 ms and performed more simulations. Movie 3, which is the simulation when the target cycle length is 85 ms, shows that for this target cycle length entrainment was better in the inner areas of the matrix as compared to the outer (left and right) edges of the matrix. Therefore, we

increased the matrix size to 400x800 cells so that we now had 800 columns of cell with 400 rows in each row.

Movie 1

Simulated VF without stimulation.

Movie 2

Simulated VF with stimulation at target cycle length=65ms.

Movie 3

Simulated VF with stimulation at target cycle length=85ms.

Determining optimal parameters for entrainment

We quantified entrainment by the method described as follows. Using the schematic in Figure 5(b) where we used a 400x800 cell matrix, we recorded the change in transmembrane voltage with time at 240 locations for 2000 ms of simulation. From the transmembrane recordings, cycle lengths were determined for 2000 ms at each of the electrodes. In order to quantify capture, we counted the number of times the CL was target cycle length ±10% during the last 500 ms. The following color code indicates the number of cycle lengths which were target cycle length ± 10% ms during the 500 ms time-period:

Black-0 (Minimum)

Blue-1

Green-2

Yellow-3

Orange-4

Red-5 (Maximum)

Within the 500 ms, all the locations which allowed at least three cycles of capture (yellow) were counted and divided by total number of locations.

Effects of Varying the Cycle Length on Entrainment

Using the schematic in Figure 5(b), we recorded transmembrane voltages when the VF continued in the matrix without stimulation. Figure 38 shows the area captured

during VF without stimulation. Black regions indicate that there were 0 cycle lengths which were 95±10 ms during the 500 ms period. During VF without stimulation, only 2 locations out of the 240 locations showed capture (0.8%).

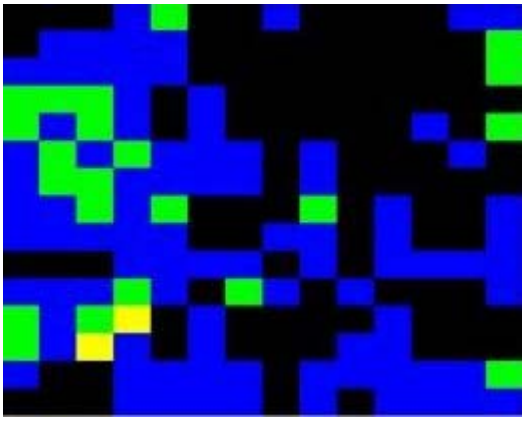

Figure 38. Area captured during VF with no stimulation.

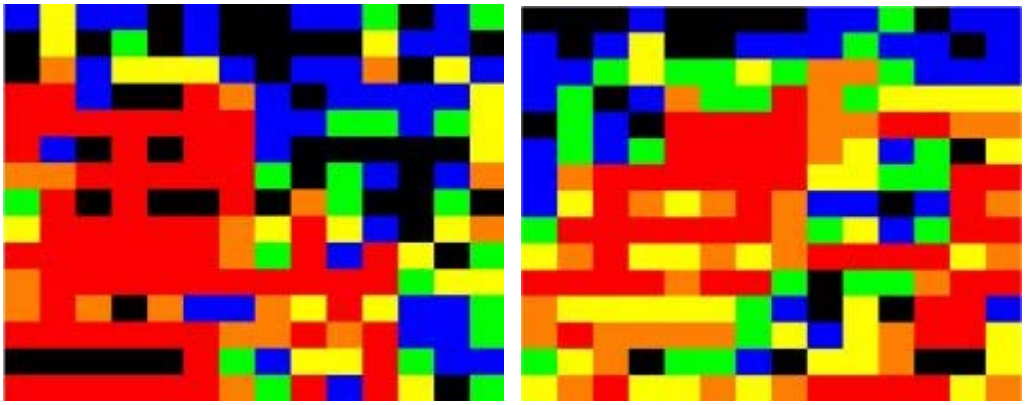

(a) (b)

Figure 39. Area captured during stimulation at target cycle length of 80 and 85ms.
(a) The target cycle length of 80 ms resulted in 43.75% area of capture. (b) The target cycle length of 85ms resulted in 50.8% area of capture.

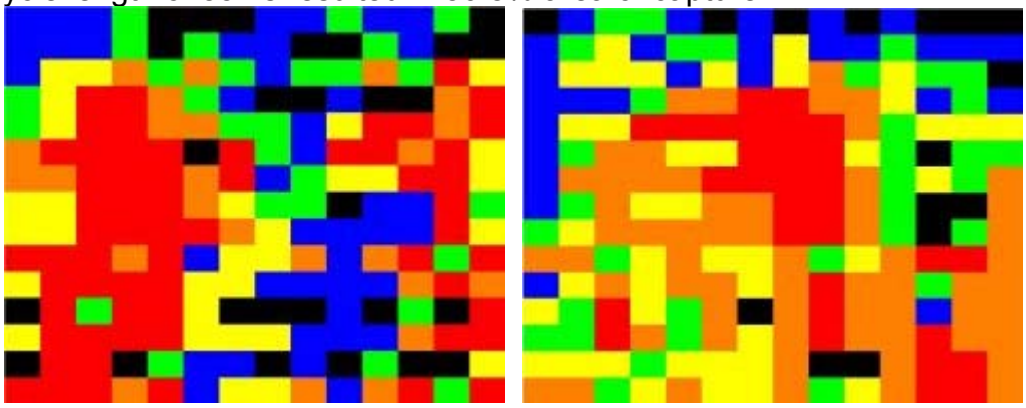

Figure 40. Area captured during stimulation at target cycle length of 90 and 95ms..

(a) The target cycle length was 90 ms and the area captured was 46%. (b) The target cycle length was 95 ms and the area captured was 54%.

Effect of varying distance between the stimulators on entrainment

Another parameter of critical importance that can be varied is the distance between the adjacent stimulators. The distance between the stimulators is determined by how much area is each stimulator able to capture.

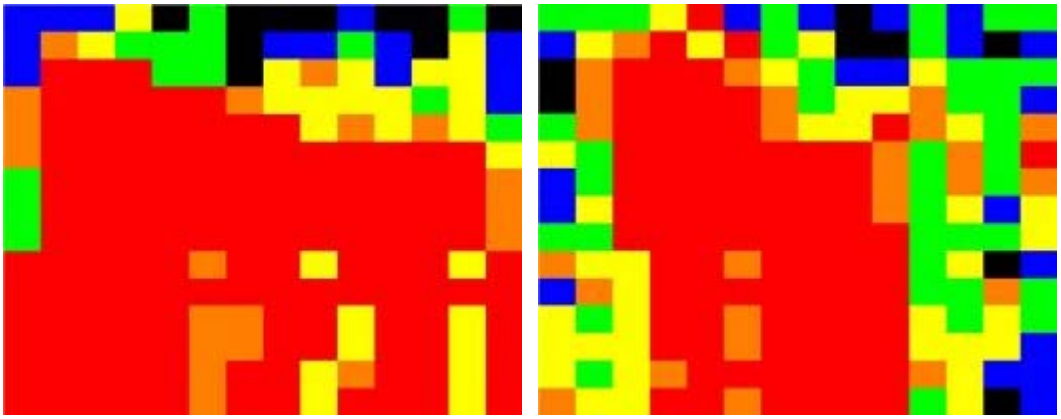

Figure 41. Area captured during stimulation when the separation was 32 and 36 cells. The separation between the stimulator rows was 32 cells in (a) and 36 cells in (b). For both the cases, the cycle length was constant at 95 ms.

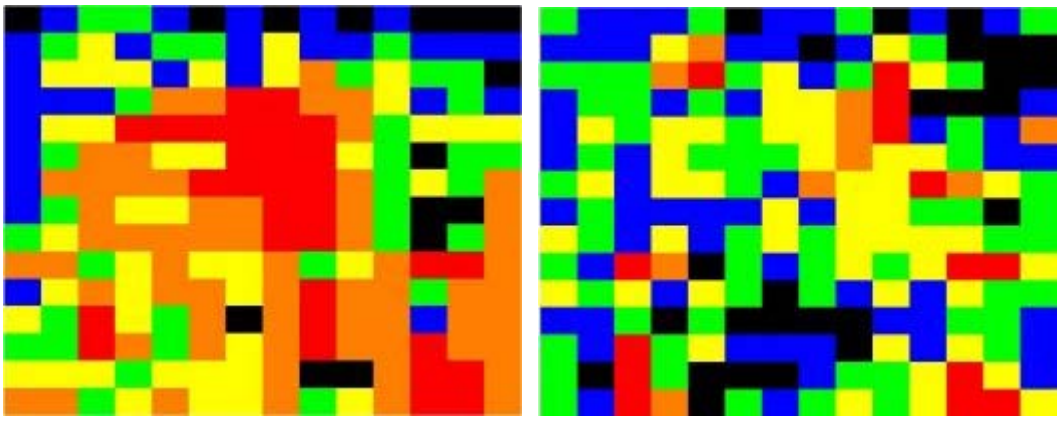

Figure 42. Area captured during stimulation when the separation was 40 and 44 cells. The separation between the stimulator rows was 40 cells in (a). Note that this is the same simulation as in Figure 40(b). The separation between the stimulator rows was 44 cell in (b).

Quantifying capture by coherence

If the entrainment attempt were to be made to time delivery of defibrillation shock, for example, it would be necessary to determine in real-time whether entrainment has occurred so that pacing can be stopped and a defibrillation shock delivered. We propose to use time-coherence in order to determine that entrainment has occurred. In Figure 43a, we have shown plots of transmembrane voltage with time, during VF without stimulation, at two locations. The plot in black is the transmembrane voltage at one location and the plot in blue shows the transmembrane voltage at the other location. The two locations are such that the line joining them is perpendicular to the stimulator rows. In this particular case, the recording locations were separated by 80 cells i.e. 2.24 cm. Time coherence was computed every 40 ms from the two signals and was integrated between the frequencies 11.5Hz and 12.0Hz. These two frequencies limits were chosen because the target cycle length of 85ms corresponds to 11.7 Hz. The coherence is plotted in blue in Figure 43c. Figure 43b shows the plots of transmembrane voltage with time, during VF with stimulation at the same two locations. Time coherence computed between the two signals and integrated between the same two limits mentioned above is shown in red in Figure 43c. The figure shows that time-coherence is considerably higher during stimulation as compared to that during VF, further supporting the hypothesis that entrainment was possible during stimulation at the 85 ms cycle length. In Figure 43b the black trace lags the red trace. This is due to the time delay occurring for the wavefront to reach from the first electrode to the second electrode. The 1:1 correspondence between the two signals in Figure 43b (during stimulation) is apparent. This is expected since we see entrainment.

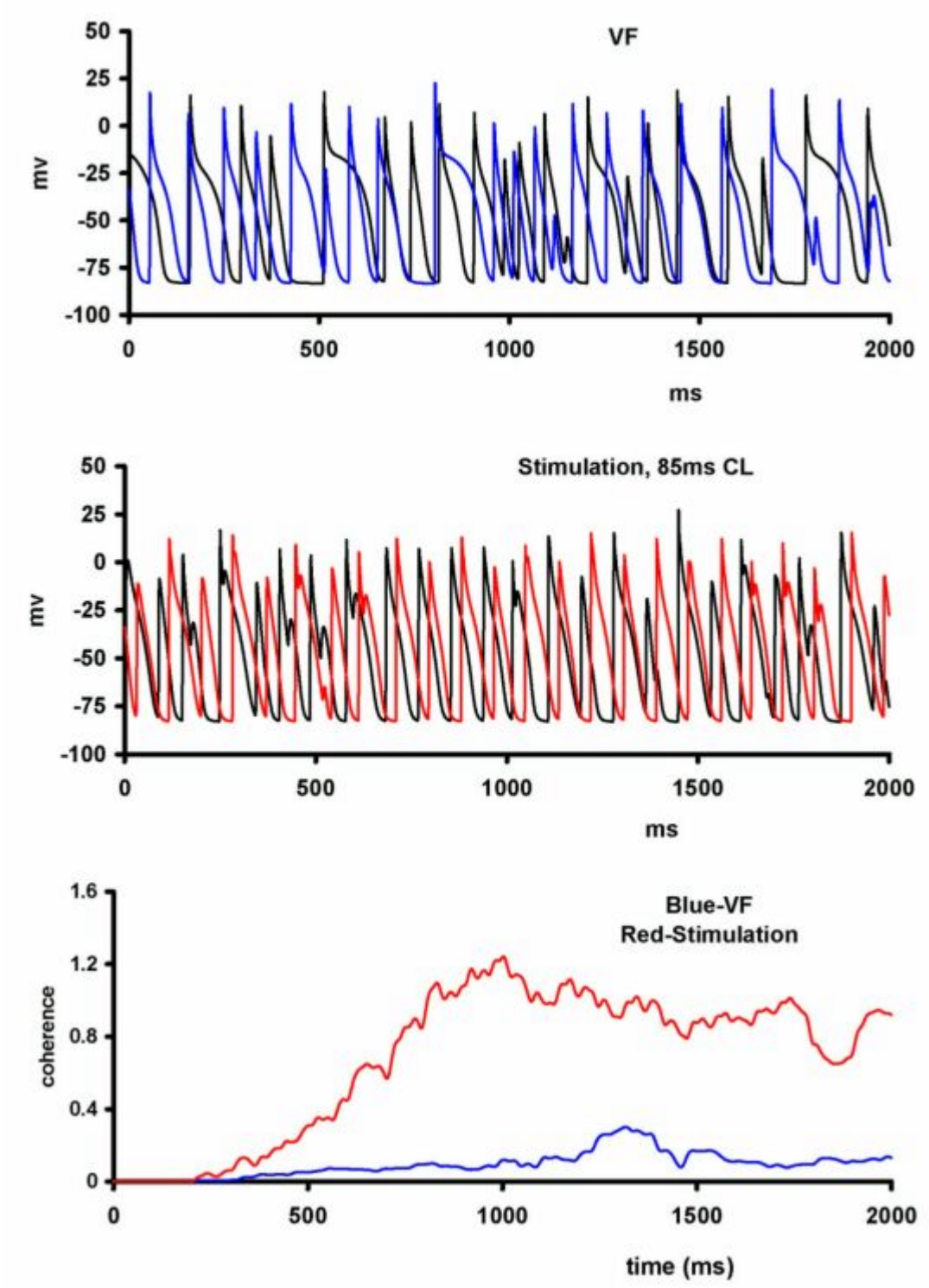

Figure 43. Coherence for capture during stimulation and VF, at one electrode. (a) Transmembrane recording during VF without stimulation at two locations. (b). Transmembrane recordings during stimulation at 85ms target cycle length at the same two locations. (c). The blue curve shows coherence between the two signals in (a) and

the red curve shows the coherence between the two signals in (c). The coherence was integrated between 11.5Hz and 12.0Hz in both the cases.

Figure 44 shows the mean coherence computed as an average of 12 pairs of electrodes. Each pair was selected such that the line joining them was perpendicular to the wavefront. The twelve pairs of electrodes were 'a2-e2', 'a6-e6', 'a10-e10', 'a14-e14', 'e2-i2', 'e6-i6', 'e10-i10', 'e14-i14', 'i2-m2', 'i6-m6', 'i10-m10', and 'i14-m14'. As explained earlier with reference to Figure 5(b), recording electrodes were arranged in a 16 rows x15 column format. The distance separation between the two electrodes in each pair was about 80 cells i.e. 80x0.025cm=2cm. Within two adjacent pairs, the (column) separation was 180 cells i.e. 180x0.025cm=4.5cm. Thus, 'a2-e2' was 4.5 cm away (in column direction) from 'a6-e6'. On an average also, the coherence during stimulation was higher than the coherence during VF without stimulation.

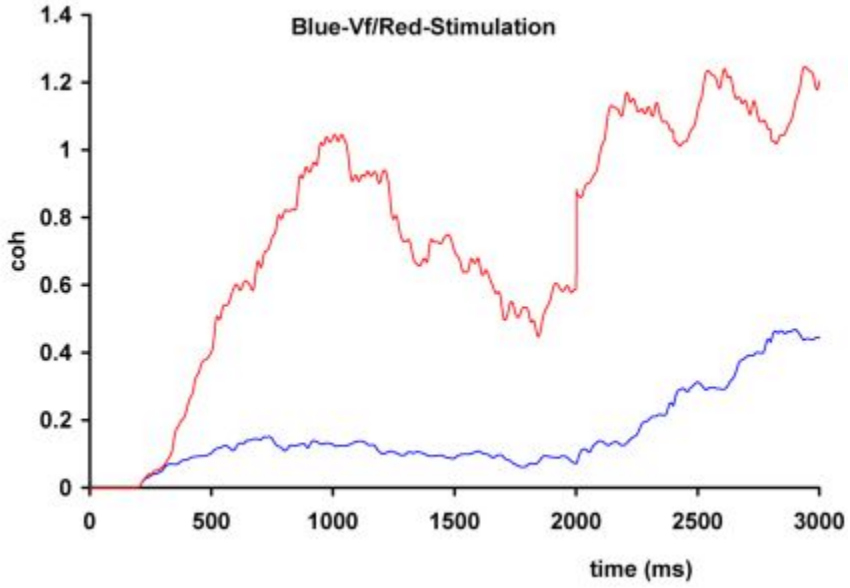

Figure 44. Average coherence during VF and capture during stimulation.
The figure shows average coherence in red for stimulation during VF at 85 ms target cycle length and the blue curve for coherence during VF without stimulation. The coherence was integrated between 11.5 Hz and 12.0 Hz in both the cases.

Chapter Five: Discussion

The main findings of the activation interval study were: (1) dominant frequencies recorded from electrograms increased continuously during the first 30 seconds of VF; (2) dominant frequencies were distributed symmetrically about the mean value during early as well as late VF. Simulation of VF in a matrix, however, indicated that the activation intervals were slightly skewed to the right about the mean value; (3) there was considerable spatial and temporal variation in the dominant frequencies recorded from the epicardial surface.

We previously reported that the dominant frequencies, computed from orthogonal ECGs in dogs, increase continuously during 30 seconds of VF [Patwardhan 00]. Although we expected that the dominant frequencies in the electrograms would also show an increase, it was not clear whether the increase would be observed at multiple epicardial locations. Therefore, in this study, we quantified the changes in dominant frequencies in epicardial electrograms recorded during VF using the technique that we used previously to analyze ECGs [Patwardhan 00]. Changes in dominant frequencies can be important indicators of the underlying mechanisms of VF as suggested recently by several studies [Berenfield 00, Mandapati 98, Wang 98]. Mechanisms of VF, in terms of activation maps, have been extensively studied using a large number of epicardial electrodes [Rogers 99, Hillsley 95, Opthof 91, Misier 95]. However, analyses of activation maps or sequences in these studies have been limited to a duration of few seconds. Analyses was conducted over a duration of few seconds because of the difficult and laborious task of identifying activation times accurately. Marking activation times also has some disadvantages; some activations when differentiated, barely make it to the threshold selected, hence human intervention is necessary to include them or discard them from analysis. A few investigators have studied VF using Fast Fourier Transform (FFT) over longer time periods of data, ranging in duration from one second [Clayton 95] or more [Zatisev 00, Mandapati 98, Wang 98] for quantification of dominant frequencies. The use of relatively longer duration of data may have resulted in lower time resolution in estimation of dominant frequencies in these studies compared to the present study. The poor time resolution in these studies may have lead to significant

averaging of the dominant frequencies. Thus, studies so far have not analyzed changes in dominant frequencies on a finer time-resolution basis and over long durations of VF. Using the method based on Wigner distribution of a signal, we were able to achieve a much finer time localization and resolution to quantify changes in dominant frequencies over 30 sec of VF.

Time-resolution is an important parameter when estimating changes in dominant frequency on a beat-by-beat basis. We have estimated the dominant frequency every 40 ms; the choice of this time-step depends on how fast the frequencies are expected to change. In swines, the dominant frequency is seldom greater than 12 Hz i.e., the fastest activations are separated by at least 1/12=83.33 ms. Since the time-sample duration is about half that of the shortest expected period, our choice of 40 ms was adequate. The choice of a window length of 600 ms is governed by the degree of acceptable time-averaging and frequency resolution. A shorter data-window will allow for a larger time-localization but there will be few activations. A longer data-window will allow for more activations and thus a better estimate of the frequency but with the consequence of averaging changes in frequency over longer time. Thus, a trade-off between the two factors was the deciding factor in selecting a 600 ms window. With an average dominant frequency of 7.5Hz (133 ms activation interval), we would expect about 4 activations within each 600 ms window, which was used to estimate the dominant frequency.

In Figure 6d, the values of dominant frequency computed from the SPWD and the activation intervals are not exactly identical. This is expected because activations can be detected with a time-resolution of 1 ms (sampling frequency 1 KHz), whereas, computation of dominant frequency using SPWD has a smoothing effect due to finite window size.

At any electrode location on the epicardium we found that there was considerable local temporal variation in dominant frequencies. That is, we did not observe frequencies at any locations that remained stable or invariant over extended periods of time (1 sec or more), as observed by Zaitsev et al. [Zatisev 00]. The dominant frequencies at two electrodes, which were neighbors, was seldom identical unlike those observed by Zaitsev el. al. [Zatisev 00]. There are some differences

between Zaitsev et al.'s study and the present study, which might account for the differences in observations. Zatisev et. al. [Zaitsev 00] used an isolated slab of tissue of size 3x3 cm^2 from a sheep's ventricle, whereas we recorded electrograms from the entire heart. It is known that the dynamics of electrical wavefronts can be different depending upon the tissue mass [Kim 97] and therefore might account for the considerable variation observed by us at different electrode locations. Zatisev et. al. have used a much longer segment of data (2.13 sec) to compute the dominant frequencies which would cause averaging in time of variations in the dominant frequencies, whereas, we used a window of only 0.6 seconds giving us an estimate of changes in dominant frequency with a much finer time resolution.

In our findings, the dominant frequencies were symmetrically distributed about the mean value in all four regions of the heart. Since the effective refractory period is known to be correlated with the dominant frequency (inverse of activation interval) [Opthof 98], and activation interval, AI=DI+ERP, variations in activation intervals suggest that diastolic intervals may occur randomly about a mean diastolic interval. This assumption of random distribution of DI is consistent with the observed correlation between AI and ERP. Consistent with these interpretations, transmembrane voltage recordings made during VF by Omichi et. al. [Omichi 00] also show the presence of a DI during VF in contrast with previous hypothesis that there is no DI during VF.

We observed that the average spatial and temporal standard deviation during early VF was significantly higher than that during late VF. The spatial standard deviation decreased from 1.08 Hz to 0.8 Hz whereas the temporal standard deviation decreased from 1.22 Hz to 0.97 Hz from early to late VF. A possible reason for this decrease in variance might be a decrease in the number of wavefronts as VF progresses, as suggested by a recent study [Pierpont 00]. Our observations of the decrease in standard deviation with increasing duration of VF is also consistent with other observations that the reentrant circuits become more common, larger, live longer and drift slowly during the first 40 seconds of VF [Rogers 99]. Further, if the standard deviation is considered as an indicator of the evolution of organization of VF, then our results are consistent with the findings of Bayly et. al. [Bayly 93] that the spatial

correlation length decreases in approximately the first 3 sec of VF and then increases up to a minute after which it decreases again.

We found that dominant frequency of VF computed from electrograms increased during the first 30 seconds of VF. This increase was found in all except two trials in six animals. In one of the two trials, the frequencies increased for only about 15 seconds and then decreased. We also found that the increase was not linear; the dominant frequency increased rapidly for about 15-20 seconds and thereafter the increase was slow. The increase in frequency that we found is consistent with our previous findings [Patwardhan 00] and two others [Martin 86, Clayton 95]. Clayton et. al., have reported their observations from VF recorded in humans whereas Martin et. al. have reported their observations in dogs. Our observations deviate from other studies in that the dominant frequency of VF decreases as VF progresses [Huang 98] or that the dominant frequency remains constant for about 70 sec of VF [Carlisle 90]. An increase in frequency during VF means an average decrease in activation interval. The activation interval is a combination of APD and DI. A gradual decrease in APD during the first 30 seconds of VF (not attributed to Ischemia [Weiss 82]) could be a possible reason for shortening of activation interval. It has been previously reported that cardiac cells exhibit APD shortening when paced rapidly [Otani 97]. Experimental [Wang 88] and simulation studies [Faber 00] suggest that during rapid pacing, APD can shorten due to I_{Ks} dynamics. One of the possible reasons for decrease in APD is incomplete deactivation of activation gate X_s [Viswanathan 99], and hence an increase in the slow delayed rectifier potassium current (I_{ks}). This observation by Viswanathan et. al. which was in simulations, is further supported by experimental findings of rapid increase of I_{ks} during fast heart rates [Jurkiewics 93]. An additional mechanism that may also contribute to the shortening of APD is the presence of hysteresis in restitution. Our modeling studies show that the APD restitution curve exhibits hysteresis. In a situation of long DI followed by short DI followed by long DI during VF, the APD produced by the second long DI could be shorter than the APD produced by the first long DI (although the two DIs might be the same). If we hypothesize that there is no specific pattern for the occurrence of short and long DI, and that there are about equal number of long and short DI so that the decrease in APD caused by one is not completely compensated by the other, then

hysteresis of the restitution curve could also explain the continuous shortening of APD until the ischemic effects occur and the excitability of the cells decreases.

In the study quantifying restitution during VF, we measured the APD restitution curve of a cardiac cell by independently controlling the DI. Our primary result is that restitution curve determined from a single cell simulated using the LRd model, and to some extent in connected cells also simulated using LRd model, exhibits hysteresis. Using a standard protocol, in the single cell we found that the maximal slope of the restitution curve was greater than one. When we used our new protocol of independent control of DI to determine the restitution curve, the maximal slope was less than one in both, the single LRd cell as well as a sheet of 2-D LRd connected cells. The inconsistency in determining the maximal slope of restitution curve is evident from several studies published recently. The slope of the restitution curve was found to be less than one when determined by the standard protocol [Gilmour 99, Koller 98]. The same parameter was found to be greater than one when measured by fixed pacing at short cycle length [Koller 98]. Simulation studies using LR model in a single cell have also revealed the maximal slope of restitution curve to be less than one [Qu 99]. These results, including ours, clearly demonstrate that the maximal slope of a restitution curve is dependent upon the method used to formulate the restitution curve.

The hysteresis in the restitution curve was more prominent when the DI intervals were changing slowly. The hysteresis can be attributed to the memory properties of the cardiac cell. As explained by Otani et. al., [Otani 97], memory is a quantitative measure which reflects the proportion of time, within a few time constants prior to any time instance, for which the membrane was in a depolarized state. In other words, the depolarized state of the membrane contributes positively to the memory term and the repolarization contributes negatively. When the diastolic intervals are decreasing from 10 ms to 0 ms, at any time instance say 4 ms, the history (past 4 or 5) of diastolic intervals is such that the diastolic intervals are longer as compared to the same time instant when the diastolic intervals are increasing. Thus, during the increasing diastolic intervals, the memory quantity is more as compared to that during the decreasing diastolic intervals. This results in the APD to be shorter for same DI when the diastolic intervals are increasing as compared to when the diastolic intervals are decreasing.

In view of the hysteresis behavior of the restitution curve, we consider the question of how VF is maintained. During VF, how fast any cell is repeatedly activated depends on two factors:

(1) The availability of the depolarizing charge, and

(2) The refractory period of the cell.

At any cell, an action potential will be produced if there is depolarizing charge available from the neighboring cells and the cell is not in a refractory period. The time to availability of depolarizing charge determines the DI of the cell. If all the cells were to fire as soon as they repolarized, the APD of the cells would eventually remain constant as the APD cannot decrease beyond a certain point, and the dominant frequencies recorded from this location would remain constant. However, our experiments clearly demonstrate that the dominant frequency at any location varies continuously between a low and high value. What this observation indicates is that DI may also change from long to short continuously in any cell; in other words, the DI also changes randomly.

In this study we first determined the restitution curve using our new method in a single LRd cell as well as the 2-D matrix of connected LRd cells. The LRd cell has an inherent characteristic that the APD decreases continuously for the first few hundred beats when paced at a constant DI. The inherent characteristics of the cell required that we pace the cell a few hundred times in order to eliminate the APD changes not related to the DI. It is seen that for pacing at a constant DI of 300ms, which is a long DI, the APD reduces very slowly, whereas, for pacing at a constant DI of 0 ms the APD decreased more rapidly. A possible explanation for this shortening of APD is the memory effect of the cell. At short DI intervals, as discussed above, the cell remains depolarized for a longer time and hence, the APD shortens faster due to the memory effect. On the other hand, the memory effect leading to APD shortening is small when DI are long, and hence the APD continues to shorten even after 300 beats at a constant pacing of 300ms DI.

During stimulation, the action potential was slightly smaller during the beats when DI was between 0 and 10 ms. Smaller action potential amplitudes for short DI is consistent with what other investigators [Otani 97, Gilmour 97] have reported. Just as memory has an effect on the APD, it also affects the action potential amplitude [Otani

97]. This could probably explain the shortening of the action potential amplitude observed in Figure 17.

An interesting observation during our simulations was that during pacing at a constant DI of 0 ms, the steady-state APD was about 72 ms whereas, when the cell was subjected to the decreasing sequence of DI from 60 to 0 ms in about 116 beats (or faster) the APD at 0 ms DI was substantially lower than 72 ms and was about 50 ms. The mechanisms for this decrease are unclear because if shortening of APD is a function of time as well as the history of DIs, then the constant pacing at 0 DI beyond 250 beats should have produced further shortening of the APD beyond the steady-state value of 72 ms.

We observed hysteresis of the restitution curve when the DI was decreased and then increased. When we stimulated the cell in a sequence of decreasing DI (1^{st} decrease), increasing DI (1^{st} increase), decreasing DI (2^{nd} decrease) and increasing DI (2^{nd} increase), in that order, we found that the restitution curve due to the 2^{nd} decrease was above the restitution curve due to the 1^{st} increase and below the restitution curve due to the 1^{st} decrease. Further, the restitution curve due to the 2^{nd} increase was between the restitution curve due to the 2^{nd} decrease and 1^{st} increase. This observation indicates that the variability in the APD at any given DI decreases with time, that is, the hysteresis becomes flatter. Therefore, the APD shortening due to memory effect may have limits. In other words, it is likely that during VF, the APD shortens continuously due to the memory effect for a few tens of seconds but it cannot happen for a longer duration. If the shortening of APD with time due to memory effect is true, then this interpretation is consistent with our observations that the cycle periods during the first 30 seconds of VF shorten continuously.

Restitution in a single cell is due to the incomplete recovery from active, time-dependent membrane gates, which control the time-dependent currents. In multi-cellular preparations, the axial current flow between cells also comes into play and influences the restitution curve [Laurita 97]. The study by Laurita et. al. also demonstrated that the voltage gradients, during premature stimulation in a connected tissue, are much larger when the DIs are small than when the DIs are long. Due to these reasons, we measured the hysteresis of restitution in a matrix of LRd cells. The steady-state APD

measured at Loc1 (stimulus sites) was about 5 ms smaller than the steady-state APD measured at Loc2 for either 0 ms or 30 ms constant DI pacing. A possible reason for this might be due to the increased axial current at the site of pacing. Further, the hysteresis of the restitution was not as prominent as in the case of a single cell.

The main objective and results from our preliminary rat experiments were to demonstrate that it is possible to implement our protocol in tissue and independently control the DI in real-time. These results support further experiments that could be performed in species such as canines or swines, which are used extensively to study the VF phenomenon. Our studies were meant to be preliminary and proof of concept type, however, the initial results that we obtained when we controlled the DI independently as in our simulations, showed that APD did not decrease with decreasing DI or increase with increasing DI. Although we are aware of the fact that these were preliminary results from initial studies, this rather dramatic observation that the APD and DI do not seem to follow the expected relationship as predicted by the restitution function warrants further investigation of this issue and supports future studies that use the new stimulation protocol.

The entrainment of VF studies that we conducted using a computer model of a cardiac tissue show that at least in simulations, entrainment of VF is possible. Two parameters, which seem to be of more importance than others in determining entrainment, are the conduction velocity and the DI. In our study we have assumed conduction velocity to be constant through the tissue as well as during the time duration of VF. In an actual tissue, conduction velocity is larger in the longitudinal direction than in the transverse direction. Conduction velocity also tends to be higher in the base region than that in the apex region [Ujhelyi 99]. Conduction velocity also exhibits restitution; for diastolic intervals less than about 40 ms, conduction velocity decreases rapidly with decreasing diastolic intervals [Qu 99]. It is not very clear as to the range or distribution (in a statistical sense) of the DIs that occur during VF but results of our simulation (Figure 33b) and indirect evidence [Koller 98] suggest that DIs about 10-15 ms in duration exist during VF. Estimating conduction velocity in real-time is a difficult task and therefore, varying the delay between adjacent stimulator lines continuously to accommodate for the change in conduction velocity is difficult. However, our results

suggest that it may not be necessary to 'fine tune' the estimated delay between stimulators to accommodate the changes in conduction velocity due to restitution. Once some degree of entrainment is obtained, then continual pacing at constant cycle lengths should minimize the effects due to restitution of CV.

The distribution curve for cycle lengths during VF in Figure 33 is almost symmetrical about the mean, except for a small skew towards higher cycle length. This observation matches with distribution of dominant frequencies that is included in Figure 10. The distribution plot of DI in Figure 33b suggests that in the computer model, diastolic intervals that are 20 ms or longer occur quite often. This does not seem to be the case during VF observed experimentally. This is one of the limitations of using simulated VF. Tissue thickness may be a reason for such differences, our simulations were essentially conducted in a monolayer tissue, which is quite different from even the thinnest portions of the right ventricles. Further studies utilizing three-dimensional models should provide better results in terms of distribution of the DI.

Before we implemented the simulations we hypothesized that we would pace at a cycle length, which would be the smallest observed cycle length during VF. Therefore we analyzed the cycle lengths during our simulations of VF in the model and found that the shortest sustainable CL was about 55 ms. Therefore, we experimented by setting the cycle length of stimulators at 55 ms through 65ms. We found that at such short cycle lengths it was difficult to sustain capture as revealed by the CL vs. time plots at electrodes e24, e25, e34 and e35 in Figure 34. These plots reveal that alternate stimulator pulse was blocked. This is most likely because of the fact that the APD was not short enough (less than 55ms or 65 ms) so as to allow an action potential to occur. Therefore, we increased the CL further and found much better entrainment at CL of 85 ms as compared to CLs which were higher or lower than 85 ms. Since we used continuous boundary conditions along the left and right edge of the matrix, the simulation matrix of 400 column formed a cylinder with circumference of tissue equal to 10 cm. Therefore, at longer stimulation cycle lengths, wavefronts from the side of the matrix likely invaded the entrained area thereby decreasing the total entrained area. This is evident by observing the animation in Movie 2, which clearly shows entrained areas as well as the wavefronts invading the tissue from the left and right sides.

The observation that in the 400x400 matrix of cells, continuous boundary conditions result in wavefronts from the left and right side of the matrix are detrimental to the entrainment prompted us to increase the stimulation area. However, since it is not possible to increase the stimulation area without increasing the total matrix size, we increased the matrix size to 400x800 cells. In Figure 39 through 42, the red area indicates that 5 cycles of entrainment was observed in the tissue. To qualify a tissue area as entrained, we used the criteria that at least 3 out of the maximum possible 5 cycles in the 500ms period showed the CL at target cycle length. Using this criteria, the CL at 95 ms seems to be the best since the capture was almost 58%. However, if we used a criteria that entrainment occurred when all the five cycles showed values close to target cycle length, then, the target cycle length of 80ms and 85ms seem to be better. We varied the distance between the stimulators, from 0.8 cm to 1.1 cm. As the stimulators were moved closer to each other the entrainment became better. These results suggest that in order to achieve reasonable degree of entrainment, the electrode rows should be spaced about 1 cm away from each other.

Successful entrainment during stimulation is also revealed by the time-coherence computed during stimulation and during VF without stimulation. As the trace in Figure 43(c) illustrates, the time-coherence is high during stimulation and low during VF. The traces in the middle plot of Figure 43 just before the 1000ms mark show a good correlation between the two waveforms, thereby explaining the high coherence. Occasionally, the traces in Figure 43(a) appear correlated as well but this is probably due to one limitation of using the LR model that wavelengths of the wavefronts in the matrix are much longer than those observed in real-VF.

Entrainment of VF is important because of several reasons. As discussed earlier in the background section, the spatial existence of excitable gap and its evolution with time is not known. Proof of entrainment will lend support to the idea that excitable gap does exist during VF and that advantage can be taken of the excitable gap. Another implication of successful entrainment has direct implications towards more efficient defibrillation. One hypothesis related to defibrillation suggests that if there is more uniform activation within the region of the heart that receives the lowest potential gradients during a defibrillation shock, then that shock has higher probability of success

than the one that follows less uniform activation. Several studies have been reported where pharmacologic intervention makes the VF less fractionated [Hillsley 95, Kim 99] . In one of the studies that we have reported earlier, we found that just prior to the defibrillation shock, coherence computed between two orthogonal ECGs was higher for those trials that in which the shock successfully terminated VF than for those trials where defibrillation shock was unsuccessful [Patwardhan 00]. For a given electrode configuration, it is easy to determine regions in the heart that receive the lowest potential gradient. Therefore in the future even if we are able to entrain this small part of the myocardium that receives low potential gradient using distributed pacing, it is possible that we could increase the efficacy of defibrillation. Thus entrainment provides a means to test this hypothesis rather than the approach where one looks for uniformity and then gives a shock. Ultimately, one may even think of terminating VF altogether using distributed pacing without the necessity of a defibrillation shock.

References

[Akiyama 81] Akiyama T. Intracellular recording of in-situ ventricular cells during ventricular fibrillation. Am. J. Physiol. Vol. 240(4), pp. H465-71, 1981.

[Allessie 91] Allessie M, Kirchof C, Scheffer GJ, Chorro F, and Brugada J. Regional control of atrial fibrillation by rapid pacing in conscious dogs. Circulation. Vol. 84(4), pp.1689-1697, 1991.

[Bayly 93] Bayly PV, Jonhson EE, Wolf PD, Greenside HS, Smith WM, and Ideker RE. A quantitative measurement of spatial order in ventricular fibrillation. J. Cardiovasc. Electrophysiol., Vol. 4(5), pp. 533-546, 1993.

[Berenfield 98] Berenfeld O, and Jalife J. Purkinje-muscle reentry as a mechanism of polymorphic ventricular arrhythmia in a 3-D model of the ventricle. Circ. Res. Vol. 82(10), pp. 1063-77, 1998.

[Berenfeld 00] Berenfeld O, Mandapati R, Dixit S, Skanes AC, Chen J, Mansour M, and Jalife J. Spatially distributed dominant excitation frequencies reveal hidden organization in atrial fibrillation in the Langendorff-perfused sheep heart. J Cardiovasc Electrophysiol, Vol. 11(8):869-79, 2000.

[Bonneux 94] Bonneux L, Barendregt JJ, Meeter K, et al. Estimating clinical morbidity due to ischemic heart disease and congestive heart failure: The future rise of heart failure. Am. J. Public Health. Vol. 84(1), pp. 20-28, 1994.

[Boyette 80] Boyette MR, and Jewell BR. Analysis of the effects of change in rate and rhythm upon the electrical activity in the heart. Prog Biophys Mol Biol., Vol. 36, pp. 1-52, 1980.

[Cabo 90] Cabo C, Wharton JM, Wolf PD, Ideker RE, and Smith WM. Activation in unipolar electrograms: a frequency analysis. IEEE Trans Biomed Engg., Vol. 37(5), pp. 500-508, 1990.

[Cao 99] Cao JM, Qu Z, Kim YH, Wu TJ, Garfinkel A, Weiss JN, Karagueuzian HS, and Chen PS. Spatiotemporal heterogeneity in the induction of ventricular fibrillation by rapid pacing. Importance of Cardiac Restitution Properties. Circ Res., Vol. 84(11), pp. 1318-1331, 1999.

[Capucci 99] Capucci A, Ravelli F, Nollo G, Montenero AS, Biffi M, and Villani GQ. Capture window in human atrial fibrillation: evidence of an excitable gap. J Cardiovasc Electrophysiology. Vol. 10(3), 319-27, 1999.

[Carlisle 90] Carlisle EJ, Allen JD, Kernohan WG, Anderson J, and Adgey AA. Fourier analysis of ventricular fibrillation of varied aetiology. Eur Heart J., Vol. 11(2):173-181, 1990.

[Chialvo 90] Chialvo DR, Michaels DC, and Jalife J. Supernormal excitability as a mechanism of chaotic dynamics of activation in cardiac Purkinje fibers. Circ Res., Vol. 66(2), pp. 525-545, 1990.

[Choi 01] Choi BR, Liu T, and Salama G. The distribution of refractory periods influences the dynamics of ventricular fibrillation. Circ Res. Vol. 88(5), pp. e49-e58, 2001.

[Clark 93] Clark RB, Bouchard RA, Salinas-Stefanon S, Sanchez-Chapula J, and Giles WR. Heterogeneity of action potential waveforms and potassium currents in rat ventricle. Cardiovasc. Res. Vol. 27, pp. 1795-1799.

[Clayton 95] Clayton RH, Murray A, Campbell RW. Analysis of the body surface ECG measured in independent leads during ventricular fibrillation in humans. Pacing Clin Electrophysiol. Vol.18(10), pp.1876-1881, 1995.

[Davidenko 93] Davidenko JM. Sprial Wave Activity: A possible common mechanism for polymorphic and monomorphic ventricular tachycardias. J Cardiocasc Electrophysiol. Vol. 4, pp. 730-746, 1993.

[Dorian 96] Dorian P, Penkoske PA, and Witkowski FX. Order in disorder: Effect of barium on ventricular fibrillation. Can J Cardiol. Vol. 12 (4), pp. 399-406, 1996.

[Dorian 97] Dorian P, and Newman D. Tedisamil increases coherence during ventricular fibrillation and decreases defibrillation energy requirements. Cardiovasc. Res. Vol. 33(2), pp. 485-94, 1997.

[Duytschaever 01]. Duytschaver M, Mast M, Killian M, Blaauw Y, Wijffels M, and Allessie M. Methods for determining the refractory period and excitable gap during persistent atrial fibrillation in the goat. Circulation. Vol. 104, pp. 957-962, 2001.

[Eckardt 00] Eckardt L, Haverkamp W, Johna R. Bocker D. Deng CM, Breithhardt G, and Borggrefe M. Arrhythmias in Heart Failure: Current concepts of mechanisms and therapy. J. Cardiovasc. Electrophysiol. Vol. 11, pp. 106-117, 2000.

[Elharrar 84] Elharrar V, and Surawicz B. Cycle length effect on restitution of action potential duration in dog cardiac fibers. Am. J. Physiol. Vol. 244 (Heart Circ. Physiol.13), pp. H782-H792, 1983.

[Faber 00] Faber GM, and Rudy Y. Action potential and contractility changes in $[Na^+]_i$ overloaded cardiac myocyte: a simulation study. Biophysical Journal, Vol. 78, pp. 2392-2404, 2000.

[Fendelander 97] Fendelander L, Hsia PW, and Damiano RJ. Spatial coherence: a new method of quantifying myocardial electrical organization using multichannel epicardial electrograms. J. Electrocardiology. Vol. 30(1), pp. 9-19, 1997.

[Franz 88] Franz MR, Swerdlow CD, Liem B, and Schaefer J. Cycle length dependence of human action potential duration in vivo. J Clin Invest., Vol. 82, pp. 972-979, 1988.

[Gilmour 97] Gilmour RF Jr., Otani NF, and Watanabe MA. Memory and complex dynamics in cardiac purkinje fibers. Am. J. Physiol. 272 (Heart Circ. Physiol. 4): H1826-H1832, 1997.

[Gray 95a] Gray RA, Jalife J, Panfilov A, Baxter WT, Cabo C, Davidenko JM, and Pertsov AM. Nonstationary vortex like reentrant activity as a mechanism of polymorphic ventricular tachycardia in the isolated rabbit heart. Circulation. Vol. 91(9), pp. 2454-2469, 1995.

[Gray 95b] Gray RA, Jalife J, Panfilov AV, Baxter WT, Cabo C, Davidenko JM, Pertsov AM. Mechanisms of Cardiac Fibrillation. Science. Vol. 270(17), pp. 1222-1225, 1995.

[Gray 98] Gray RA, Pertsov AM, and Jalife J. Spatial and temporal organization during cardiac fibrillation. Nature. Vol. 392, pp. 75-78, 1998.

[Guevara 84] Guevara MR, Ward G, Shrier A, and Glass L. Electrical alternans and period doubling bifurcations. IEEE Comp Cardiology. pp 167-170, 1984.

[Higgins 00] Higgins SL, Herre JM, Epstein AE, Greer SG, Friedman PL, Gleva ML, Porterfield JG, Chapman FW, Finkel E, Schmitt PW, Nova RC, and Greene HL. A comparison for biphasic and monophasic shocks for external defibrillation. Physio-Control Biphasic investigators. Prehospital emergency care. Vol. 4, pp. 305-313. 2000.

[Hillsley 95] Hillsley RE, Bollacker KD, Simpson EV, Rollins DL, Yarger MD, Wolf PD, Smith WM, and Ideker RE. Alteration of ventricular fibrillation by propranolol and isprotrenelol detected by epicardial mapping of 506 electrodes. J. Cardiovasc. Electrophysiol. Vol. 6, pp. 471-485, 1995.

[Hsia 96] Hsia PW, Fendelander L, Harrington G, Damiano RJ. Defibrillation success is associated with myocardial organization. Spatial coherence as a new method of quantifying the electrical organization of the heart. J. Electrocardiol. Vol. 29. (Suppl), pp.189-197, 1996.

[Huang 98] Huang J, Rogers JM, KenKnight BH, Rollins DL, Smith WM, and Ideker RE. Evolution of the organization of epicardial activation patterns during ventricular fibrillation. J Cardiovasc Electrophysiol. Vol. 9(12), pp. 1291-1304, 1998.

[Janse 95] Janse MJ, Wilms-Schopman FJG, and Coronel R. Ventricular fibrillation is not always due to multiple wavelet reentry. J Cardiovasc Electrophysiol. Vol. 6, pp. 512-521, 1995.

[Karma 94] Karma A. Electrical alternans and spiral wave breakup in cardiac tissue. Chaos. Vol. 4, pp 461-472, 1998.

[KenKnight 95] KenKnight BH, Bayly PV, Gerstle RJ, Rollins DL, Wolf PD, Smith WM, Ideker RE. Regional capture of fibrillating ventricular myocardium. Evidence of an excitable gap. Circ. Res. Vol. 77(4), pp. 849-55, 1995.

[Kim 96]. Kim KB, Rodefeld MD, Schuessler RB, Cox JL, and Boineau JP. Relationship between local atrial fibrillation intervals and refractory period in isolated canine atrium. Circulation, Vol. 94(11), pp.2961-2957, 1996.

[Kim 97] Kim YH, Garfinkel A, Ikeda T, Wu TJ, Athill CA, Weiss JN, Karagueuzian HS, and Chen PS. Spatio-temporal complexity of ventricular fibrillation revealed by tissue mass reduction in isolated swine right ventricle. Further evidence for the quasi-periodic route to chaos hypothesis. J. Clin. Invest, Vol. 100, pp. 2486-2500, 1997.

[Kim 99] Kim YH, Yashima M, Wu TJ, Doshi R, Chen PS, and Karagueuzian HS. Mechanism of procainamide-induced prevention of spontaneous wavebreak during ventricular fibrillation. Insight into maintenance of fibrillation wavefronts. Circ. Vol. 100, pp. 666-674, 1999.

[Kirchoff 93] Kirchhof C, Chorro F, Scheffer GJ, Brugada J, Konings K, Zetelaki Z, and Allessie M. Regional entrainment of atrial fibrillation studied by high-resolution mapping in open-chest dogs. Circulation. Vol. 88(2): 736-49, 1993.

[Koller 98] Koller ML, Riccio ML, and Gilmour RF Jr. Dynamic restitution of action potential duration during electrical alternans and ventricular fibrillation. Am. J. Physiol. 274 (Heart Circ. Physiol. 44): H1635-H1842, 1998.

[Kuo 83]. Kuo CS, Munakata K, Reddy CP, and Surawicz B. Characteristics and possible mechanism of ventricular arrhythmia dependent on the dispersion of action potential durations. Circulation, Vol. 67, pp. 1356-1367, 1983.

[Kwan 98] Kwan YY, Fan W, Hough D, Lee JJ, Fishbein MC, Karagueuezian HS, and Chen PS. The effects of procainamide on the characteristics of functional reentry in canine ventricular fibrillation. Circ, Vol. 97, pp. 1828-1836, 1998.

[Lammers 86] Lammers WJEP, Allesie MA, Rensma PL et. al. The use of fibrillation cycle length to determine spatial dispersion in electrophysiological properties and to characterize the underlying mechanism of fibrillation. New Trends in Arrhythmia. Vol. 2, pp.109-112, 1986.

[Lee 96] Lee JJ, Kamjoo K, Hough D, Hwang C, Fan W, Fishbein MC, Bonometti C, Ikeda T, Karagueuzian HS, and Chen PS. Reentrant wavefronts in wigger's stage II ventricular fibrillation: characteristics and mechanisms of termination and spontaneous regeneration. Circ Res., Vol. 78, pp. 660-675, 1996.

[Lee 01] Lee MH, Qu Z, Fishbein GA, Lamp ST, Chang EH, Ohara T, Voroshilovsky O, Kil JR, Hamzei AR, Wang NC, Lin SF, Weiss JN, Garfinkel A, Karagueuzian HS, and Chen PS. Patterns of wave break during ventricular fibrillation in isolated swine right ventricle. Am. J. Physiol. (Heart Circ. Physiol) . Vol. 281(1), pp. H253-65, 2001.

[Luo 91] Luo CH, and Rudy Y. A model of the ventricular cardiac action potential: depolarization, repolarization, and their interaction. Circ. Res. Vol. 68, pp. 1501-1526, 1991.

[Luo 94] Luo CH, and Rudy Y. A dynamical model of the cardiac ventricular action potential. I. Simulations of ionic currents and concentration changes. Circ. Res. Vol. 74, pp. 1071-1096, 1994.

[Mandapati 98] Mandapati R, Asano Y, Baxter WT, Gray R, Davidenko J, and Jalife J. Quantification of effects of global Ischemia on dynamics of ventricular fibrillation in isolated rabbit heart. Circulation. Vol. 98, pp. 1688-1696, 1998.

[Martin 86] Martin G, Cosin J, Such M, Hernandez A, and Llamas P. Relation between power spectrum time course during ventricular fibrillation and electromechanical dissociation. Effects of coronary perfusion and nifedipine. Eur Heart J. Vol. 7(7), pp. 560-569, 1986

[Misier 95] Misier A, Opthof T, van Hemel NM, Vermulen JT, de Bakker JMT, Defauw JJAM, van Capelle FJL, and Janse MJ. Dispersion of refractoriness in non-infarcted myocardium of patients with ventricular tachycardia or ventricular fibrillation after myocardial infarction. Circulation. Vol. 91(10), pp.2566-2572, 1995.

[Moe 64]. Moe GK, Rheinboldt WC, and Abildskov JA. A computer model of atrial fibrillation. Am. Heart J. Vol. 67, pp. 200-220, 1964.

[Murakawa 97] Murakawa Y, Yamashita T, Kansese Y, and Omata M. Can a class III antiarrhythmic drug improve electrical defibrillation efficacy during ventricular fibrillation ? J. Am. Coll. Cardiol. Vol. 29(3), pp. 688-92, 1997.

[Newton 01]. Newtown JC, Huang J, Rogers JM, Rollins D, Walcott GP, Smith WS, and Ideker RE. Pacing during ventricular fibrillation: Factors influencing the ability to capture. J. Cardiovasc. Electrophysiol. Vol. 12, pp.76-84, 2001.

[Nolasco 68] Nolasco JB, and Dahlem RW. A graphic method for the study of alternation in cardiac action potentials. J. Appl. Physiol. Vol. 25, pp.191-196, 1968.

[Omichi 00] Omichi C, Lee MH, Ohara T, Naik AM, Wang NC, Karagueuzian HS, and Chen PS. Comparing cardiac action potentials recorded with metal and glass microelectrodes. Am. J. Physiology, Vol. 279, H3113-H3117, 2000.

[Opthof 91] Opthof T, Misier ARR, Coronel R, Vermulen JT, Verberne HJ, Frank RGJ, Moulijn AC, van Capelle FJL, and Janse MJ. Dispersion of refractoriness in canine ventricular myocardium: effects of sympathetic stimulation. Circ Res. 1991; 68: 1204-1215.

[Otani 97] Otani NF, and Gilmour RF. Memory models for the electrical properties of local cardiac systems. J. Theor. Biol., Vol. 187, pp. 409-436, 1997.

[Pandozi 97] Pandozi C, Bianconi L, Villani M, Castro A, Altamura G, Toscano S, Jesi AP, Gentilucci G, Ammirati F, Lo Bianco F, and Santini M. Local capture by atrial pacing in spontaneous chronic atrial fibrillation. Circulation 1997 May 20, 95(10);2416-22.

[Panfilov 98] Panfilov AV. Spiral breakup as a model of ventricular fibrillation. Chaos. Vol. 8, pp 57-64, 1998.

[Patwardhan 00] Patwardhan AR, Moghe SA, Wang K, and Leonelli FM. Frequency modulation in ECGs during ventricular fibrillation. Am. J. Physiology, Vol. 279, pp. H825-H835, 2000.

[Pierpont 00] Pierpont GL, Chugh SS, Hauck JA, and Gornick CC. Endocardial activation during ventricular fibrillation in normal and failing canine hearts. Am J Physiol Heart Circ Physiol, Vol. 279(4):H1737-47, 2000.

[Qu 97] Qu Z, Weiss JN, and Garfinkel A. Spatio-temporal chaos in simulated ring of cardiac cells. Phys Rev Lett. Vol. 78, pp. 1387-1390, 1997.

[Qu 99] Qu Z, Weiss JN, and Garfinkel A. Cardiac electrical restitution properties and stability of reentrant spiral waves: a simulation study. Am. J. Physiology, Vol. 276 (Heart Circ. Physiol. 45), pp. H269-283, 1999.

[Riccio 99] Riccio ML, Koller ML, and Gilmour RF Jr. Electrical Restitution and spatiotemporal organization during ventricular fibrillation. Circ. Res. Vol. 4, pp. 955-963, 1999.

[Rogers 99] Rogers JM, Huang J, Smith WM, and Ideker RE. Incidence, evolution, and spatial distribution of functional reentry during ventricular fibrillation in pigs. Circ. Res., Vol. 84, 945-954, 1999.

[Rush 78] Rush S, and Larsen H. A practical guide for solving dynamic membrane equation. IEEE Trans. on Biomedical Engineering, Vol. 25(4), 1978.

[Shaw 97b] Shaw RM, and Rudy Y. Electrophysiologic effects of acute myocardial ischemia: a theoretical study of altered cell excitability and action potential duration. Cardiovasc. Res. Vol. 35, pp. 256-272, 1997.

[Starmer 95] Starmer CF, Tomato DN, Reedy RS, Gilbert YI, Star bin J, Grant AO, and Kinky VI. Proarrhythmic response to potassium channel blockade. Numerical Studies of Polymorphic Tachyarrhythmias. Circulation. Vol. 92, pp. 595-605, 1995.

[Ujhelyi 99] Ujhelyi MR, Sims JJ, and Miller AW. Induction of electrical heterogeneity impairs ventricular defibrillation: an effect specific to regional conduction velocity slowing. Circulation. Vol. 100(25), pp. 2534-40, 1999.

[Valderrabano 01] Valderrabano M, Lee MH, Ohara T, Lai AC, Fishbein MC, Lin SF, Karagueuzian HS, and Chen PS. Dynamics of intramural and transmural reentry during ventricular fibrillation in isolated swine ventricles. Circ Res., Vol. 88(8):839-48, 2001.

[Wang 93] Wang TP et. al., Use of smoothed pseudo Wigner distribution in classifying hormonal time series. Proc. IEEE Int. Conf. on Systems, Man and Cybernetics, vol. 3, pp. 1130-1131, 1993.

[Wang 98] Wang L Li YC, Yong CA, and Kilpatrick D. Fast Fourier transform analysis of ventricular fibrillation intervals to predict ventricular refractoriness and its spatial dispersion. PACE., vol. 21(12), pp. 2588-95, 1998.

[Weiss 82] Weiss J, and Shine KI. $[K^+]_o$ accumulation and electrophysiological alterations during early myocardial ischemia. Am J Physiol. Vol. 243 (Heart Circ. Physiol 12), pp. H318-H327, 1982.

[Widrow 85] Widrow B, and Streans S. Adaptive Signal Processing. Prentice Hall, Inc. NJ, 1995.

[Witkowski 98] Witkowski FX, Leon LJ, Penkoske PA, Giles WR, Spano ML, Ditto WL, and Winfree AT. Spatiotemporal evolution of ventricular fibrillation. Nature, Vol. 392, 5, pp. 78-82, 1998.

[Zaitsev 00] Zaitsev AV, Berenfeld O, Mironov SF, Jalife J, and Pertsov AM. Distribution of excitation frequencies on the epicardial and endocardial surfaces of fibrillating ventricular wall of the sheep heart. Circ Res. Vol. 86(4):408-17, 2000.

[Zhou 92] Zhou X, Guse P, Wolf PD, Rollins DL, Smith WM, and Ideker RE. Existence of both fast and slow channel activity during the early stages of ventricular fibrillation. Circ. Res. Vol. 70(4), pp. 773-86, 1992.

Vita

Sachin Moghe was born on Dec 21,1971 in Bombay, India. He graduated from Bombay University with an undergraduate in Electrical Engineering in 1993. From 1993 to 1995, he worked as a Service Engineer in the Medical Engineering Division of SIEMENS, Bombay. From 1995 to 1997, he attended the University of Kentucky and was awarded a Masters in Biomedical Engineering. Since May 2001, he has been working as an Imaging Scientist at Bio-Imaging Research, Inc Lincolnshire, IL.